D E P A R T M E N T O F M A T H E M A T I C S

SHOCKED FLOW IN NOZZLES

J.R. WIXCEY

NUMERICAL ANALYSIS REPORT 1/89

U N I V E R S I T Y O F R E A D I N G

SHOCKED FLOW IN NOZZLES

J. R. WIXCEY

NUMERICAL ANALYSIS REPORT 1/89

Department of Mathematics

P.O. Box 220

University of Reading

Whiteknights

Reading

RG6 2AX

United Kingdom

This work forms part of the research programme of the Institute of Computational Fluid Dynamics at the Universities of Oxford and Reading and has been supported by the S.E.R.C.

CONTENTS

ABSTRACT

This report gives a detailed study of quasi one-dimensional shock flow in a de-Laval nozzle. By definition of the compressible flow we may obtain graphs relating the flow variables and then, by considering an algebraic parameterization, the variation of the variables with respect to the distance along the nozzle axis. An adaptive finite element method is formulated from a stationary principle for the approximate solution of a quasi one-dimensional nozzle shock flow and two solution algorithms are compared, differing only in the procedure for the definition of the initial approximation to the flow.

ACKNOWLEDGEMENTS

I am grateful to Dr. M.J. Baines and Dr. D. Porter for their guidance in this work.

I acknowledge an S.E.R.C. research studentship.

INTRODUCTION

The subject of continuous quasi one-dimensional duct flow has been extensively studied in [4], [5] and [6]. The principles used in the previous work are now extended to the consideration of quasi one-dimensional shock flow in a de-Laval nozzle.

In Section One the properties and equations of motion of a one-dimensional compressible flow are presented. The concept of a shock front is introduced and the appropriate jump conditions are stated. The properties of the compressible flow on traversing the shock front are then discussed.

In Section Two the quasi one-dimensional approximation to continuous duct flow is reviewed [3]. A discussion of the conditions affecting de-Laval nozzle flow, in terms of both the inlet and outlet pressures and also the mass flow boundary conditions in quasi one-dimensional flow, then follows. The theory is subsequently extended to give the definition of the quasi one-dimensional approximation to a nozzle shock flow and graphs relating the flow variables may then be obtained ([3] and [4]).

In Section Three a particular quasi one-dimensional nozzle shock flow is defined, which includes the definition of the range of conditions that may produce such a flow. An algebraic parameterization [4] is then used to determine the variation of each variable in the flow in terms of the distance along the nozzle axis, in particular the behaviour on traversal of the shock front.

In Section Four a stationary principle is stated which generates the conditions defining quasi one-dimensional shock flow in a nozzle. This principle is then used to formulate an adaptive finite element method for the approximate solution of the fluid speed in a shock flow. The first solution algorithm presented is a direct extension of that employed for the approximate solution of a continuous nozzle flow [6]. On comparison of the numerical results obtained with the exact solution inaccuracies in the representation of regions of the continuous flow and in quantities associated with the shock front require the algorithm to be modified by re-defining the procedure used to obtain the initial approximation to a shock flow.

SECTION ONE : A ONE-DIMENSIONAL COMPRESSIBLE FLOW

In this section the properties of a one-dimensional compressible flow are presented together with the associated equations of motion. The concept of a shock front is introduced and the appropriate jump conditions are stated. The properties of the compressible flow on traversing the shock front are then discussed.

1.1 THE COMPRESSIBLE FLOW

Air at moderate temperatures may be modelled by the polytropic gas and thus is adiabatic. For present purposes it can be assumed that the flow is inviscid and steady; it is therefore characterized by streamlines. The fluid satisfies the law of Boyle and Gay-Lussac

$$p\,\nu = (R_o/m)\,T\ , \tag{1.1}$$

where p represents pressure, T temperature and ν is the specific volume defined by $\nu = 1/\rho$, where ρ is the density. The thermodynamic constants R_o, the universal gas constant, and m, the molecular weight of the gas, are specified (see [1]) by

$$R_o = 8.31\ \text{Jmol}^{-1}\text{K}^{-1}$$

and

$$m = 28.96 \times 10^{-2}\ . \tag{1.2}$$

The one-dimensional flow is of necessity irrotational and thus by assuming the flow to be homentropic, i.e. constant entropy, S, in the flow field except at discontinuities, then it must also be homenergic,

i.e. the total energy

$$h = \aleph + (v^2/2) \ , \tag{1.3}$$

where v denotes the velocity and $\aleph$ the enthalpy, is constant in the flow field. The fluid motion is governed by the conservation equations of fluid dynamics, which under these circumstances are

$$\text{CONSERVATION OF MASS} : \quad \frac{d}{dx}(\rho\, v) = 0 \ , \tag{1.4}$$

$$\text{CONSERVATION OF MOMENTUM} : \quad h = \text{constant} \tag{1.5}$$

and

$$\text{CONSERVATION OF ENERGY} : \quad \eta = \text{constant} \ , \tag{1.6}$$

where $\eta = \eta(S)$, together with the appropriate entropic equation of state

$$p = \eta\, \rho^{\gamma} \ , \tag{1.7}$$

where γ is the adiabatic exponent associated with the fluid and in the case of air flow (see [1]) it takes the approximate value

$$\gamma = 1.4 \ . \tag{1.8}$$

Additional flow variables associated with the flow are mass flow, Q, where

$$Q = \rho\, v \ , \tag{1.9}$$

and flow stress, P, defined by

$$P = p + \rho v^2 \ . \tag{1.10}$$

The air flow may be either subsonic or supersonic, the definitive quantity being the critical fluid speed, C_*, (see [2])

$$\begin{aligned} v < C_* &: \text{ SUBSONIC FLOW} \\ v > C_* &: \text{ SUPERSONIC FLOW} \ . \end{aligned} \tag{1.11}$$

The magnitude of the critical speed is dependent on the limit speed in the flow, v_L, and the adiabatic exponent (1.8) and occurs where the fluid speed equals the local sound speed. It takes the value (see [2])

$$C_* = v_L \left[\frac{\gamma - 1}{\gamma + 1} \right]^{1/2} \ , \tag{1.12}$$

where

$$v_L = (2\,h)^{1/2} \ . \tag{1.13}$$

1.2 A SHOCK FRONT IN ONE-DIMENSIONAL FLOW

In the analysis so far we have assumed the fluid to be adiabatic, neglecting heat conduction, and thus that the thermodynamic processes in the fluid are reversible; as reflected by the conservation of energy equation (1.6). The forces in the fluid are presumed to be due to the pressure variations alone (1.7) with the effect of friction playing no part.

The effect of irreversible thermodynamic processes, caused by friction and heat conduction, have been neglected because they are associated with large temperature and velocity gradients and we have assumed these to be small. It has been found experimentally that the occurence of large gradients in the thermodynamic variables is confined to within narrow 'transition zones' in the flow. The irreversible process may therefore be modelled mathematically on an inviscid basis by a sudden jump discontinuity across a sharply defined surface in the fluid (see [2]).

We now restrict our attention to a particular form of discontinuity known as a shock front which is stationary in the flow field and is therefore crossed by the fluid. The consideration of one-dimensional flow, in the x-direction only, means that the shock front may be thought of as a plane perpendicular to the x-axis and hence the fluid may be assumed to cross the shock front normally. Notationally all mathematical quantities associated with the 'front side' of the shock, through which fluid enters, will be denoted '+' and those associated with the 'back side' '-'.

Therefore we state that in the continuous flow the mathematical assumption of adiabaticity is justified and the conservation equations (1.4) - (1.6) are valid. An irreversible process in the fluid, if it occurs, is modelled mathematically by a jump discontinuity across which jump conditions must be derived for the mass, momentum and energy balance.

In the present case of a stationary shock front, across which the flow is normal, the jump conditions are (see [2] and [3])

MASS BALANCE : $\rho_+ v_+ = \rho_- v_- = Q$, (1.14)

MOMENTUM BALANCE : $\rho_+ v_+^2 + p_+ = \rho_- v_-^2 + p_- = P$, (1.15)

ENERGY BALANCE : $\frac{v_+^2}{2} + \aleph_+ = \frac{v_-^2}{2} + \aleph_- = h$, (1.16)

i.e. the mass flow, flow stress and total energy are conserved across the shock front. The conditions (1.14) and (1.15) are valid for any fluid irrespective of its equation of state. Condition (1.16) reflects the thermodynamics of the fluid and can be seen to have the form of Bernouilli's law although of course the enthalpy function, because of its dependence on the density which is discontinuous across the shock front, will itself be discontinuous. The irreversible character of the process is evident in the statement that the entropy cannot decrease over the shock front, so that

$$\eta_+ \leq \eta_- \ , \tag{1.17}$$

which is added to the jump conditions (1.14) - (1.16). Equality of this condition corresponds to a theoretical zero shock.

The conditions (1.14) - (1.16) allow several properties of the flow variables, on traversing the shock front, to be inferred. In the case of a polytropic gas it may be established from explicit formulae (see [2]) that the shock front is compressive so that

$$\rho_+ < \rho_- \ . \tag{1.18}$$

The magnitude of the compression is defined by

$$C_{shk} = \rho_- / \rho_+ \ , \tag{1.19}$$

which, in the case of air flow modelled by the polytropic gas, is restricted to the range (see [2])

$$1/6 < C_{shk} < 6 \ . \tag{1.20}$$

Then from (1.14) and (1.15), by using the definition of mass flow rate (1.9), we may obtain (see [2])

$$Q \ (v_- - v_+) = p_+ - p_- \tag{1.21}$$

and also

$$Q^2 = - \ [\ (p_- - p_+) \ / \ (\ 1/\rho_- - 1/\rho_+ \ ) \ ] \ . \tag{1.22}$$

The flow being in the x-direction only it is obvious that the fluid speeds on either side of the shock front and also the mass flow rate will be of the same sign; therefore from (1.21) the pressure across the shock front may be seen to change in the opposite sense to the fluid speed, and from (1.22) the density will change in the same sense as the pressure. Hence, by (1.18), across the shock front

$$v_- < v_+$$

and (1.23)

$$p_- > p_+ \ .$$

In a similar manner, from (1.1), we find, by using (1.7), that

$$\frac{T_-}{T_+} = \frac{\eta_-}{\eta_+}\frac{\rho_-^{\gamma-1}}{\rho_+^{\gamma-1}} , \tag{1.24}$$

and therefore, again using (1.18) and now also (1.17), we may conclude that

$$T_- > T_+ . \tag{1.25}$$

The fluid speed on either side of the shock front is related by Prandtl's relationship (see [2])

$$v_+ v_- = c_*^2 , \tag{1.26}$$

where c_* is the critical fluid speed defined by (1.12). Therefore from (1.23a) we may deduce that

$$v_+ > c_* \quad \text{and} \quad v_- < c_* , \tag{1.27}$$

i.e. the fluid speed at the 'front side' of the shock is supersonic, from definition (1.11), whilst at the 'back side' it is subsonic.

Finally we introduce the quantity known as shock strength. In the case of a polytropic gas (see [2]) this may be defined in the following ways

EXCESS PRESSURE RATIO : $\dfrac{p_- - p_+}{p_+}$, (1.28)

CONDENSATION : $\dfrac{\rho_- - \rho_+}{\rho_-}$, (1.29)

FLUID SPEED PARAMETER : $\left| \dfrac{v_- - v_+}{c_*} \right|$, (1.30)

and as the measure of the shock strength in the present work we shall employ the excess pressure ratio (1.28).

SECTION TWO : QUASI ONE-DIMENSIONAL FLOW

In this section a quasi one-dimensional approximation to continuous duct flow is introduced (see [3] and presented in [4]). A discussion of the conditions affecting the flow behaviour in quasi one-dimensional flow through a de-Laval nozzle, with special reference to shock flow, is then presented. The quasi one-dimensional theory is subsequently extended to give an approximation to shock flow in such a nozzle and relationships between the flow variables may then be obtained (see [3]).

2.1 QUASI ONE-DIMENSIONAL CONTINUOUS DUCT FLOW

We confine analysis for the time being to a continuous air flow, with the fluid having the properties of §1.1, through an axi-symmetric duct; the particular ducts of interest are converging or diverging cone sections and the de-Laval nozzle (these are illustrated in [4]).

The duct is supposed to be slowly varying so that, to a first approximation, the motion is one-dimensional in the x-direction only. The flow must be irrotational and by assuming it to be homentropic it must therefore be homenergic; each of the streamlines in the flow field are thus defined by the constant total energy and entropy values in the flow. Hence the streamlines are indistinguishable and any one of them may be thought of as a streamline along the duct axis that is representative of the flow (see [4]).

The appropriate conservation of mass equation in quasi one-dimensional duct flow is (see [3] or [4])

$$\frac{d}{dx}(Q\,A) = 0 \,, \tag{2.1}$$

where $A = A(x)$ is the local cross-sectional area of the duct and $Q = Q(x)$ is the local mass flow rate defined by (1.9). The complete solution of the flow, in which all of the flow variables are recovered, is possible by using the total energy equation (1.3). Quasi one-dimensional continuous duct flow is therefore completely defined by (1.5), (1.6) and the conservation of mass equation (2.1) with (1.9); the appropriate equation of state being (1.7).

A particular duct flow may be considered on satisfying the mass conservation equation (2.1) in the following manner (see [3] and [4])

$$Q(x) = \frac{C\,A_e}{A(x)} \,, \tag{2.2}$$

where C is the entry mass flow rate to the streamline along the duct axis and A_e is the entry cross-sectional area of the duct. The flow boundaries then become a pair of points at the inlet and outlet duct locations on the central streamline and the boundary conditions (see [3] and [4]) are the assignment of mass flow at entry, Q_e

$$Q_e = C \,, \tag{2.3}$$

and at outlet, Q_o

$$Q_o = \frac{C\,A_e}{A_o} \,, \tag{2.4}$$

where A_o is the duct outlet cross-sectional area.

2.2 THE FLOW BEHAVIOUR IN A DE-LAVAL NOZZLE

We now consider specifically quasi one-dimensional flow through a de-Laval nozzle. It will be assumed that the flow enters the nozzle subsonically; to then enable discussion of the flow that may subsequently occur we must first define the maximum throat mass flow rate, Q_T, that may be attained in a nozzle flow

$$Q_T = \frac{C\, A_e}{A_T} , \tag{2.5}$$

where A_T is the corresponding minimum cross-sectional area of the nozzle at this point. The discussion is clarified by refering to a graph, which will now be derived, of the relationship between the physical conditions that determine a nozzle flow, the inlet and outlet pressures, and the boundary values of mass flow rate in quasi one-dimensional flow.

In [1] algebraic relations have been derived for an ideal gas between the fluid speed and other flow variables that hold for a fluid particle as it moves on a streamline, defined by constant values of total energy and entropy, in any flow field. The graphs of the relationship between any pair of flow variables in any motion on the streamline may then be obtained by prescribing a uniformly increasing range of fluid speed values from zero to the limit speed defined by (1.13) (see [4]).

Recall that quasi one-dimensional nozzle flow is represented by a central streamline along the duct axis. The inter-variable graphs for a fluid particle moving on this streamline, and hence for the approximation to the nozzle flow, then manifest themselves as segments

of each of the full relation graphs, applicable to motion on a general streamline, defined by (1.5) and (1.6). In the present case we are in interested in particular in the pressure vs mass flow rate graph, i.e. $p(Q,h,\eta)$, which is illustrated for typical flow constants in FIG.1 (this is taken from [3] and is also presented in [4]). Note the critical value of the mass flow rate, Q_*, on the graph, corresponding to the critical fluid speed (1.12).

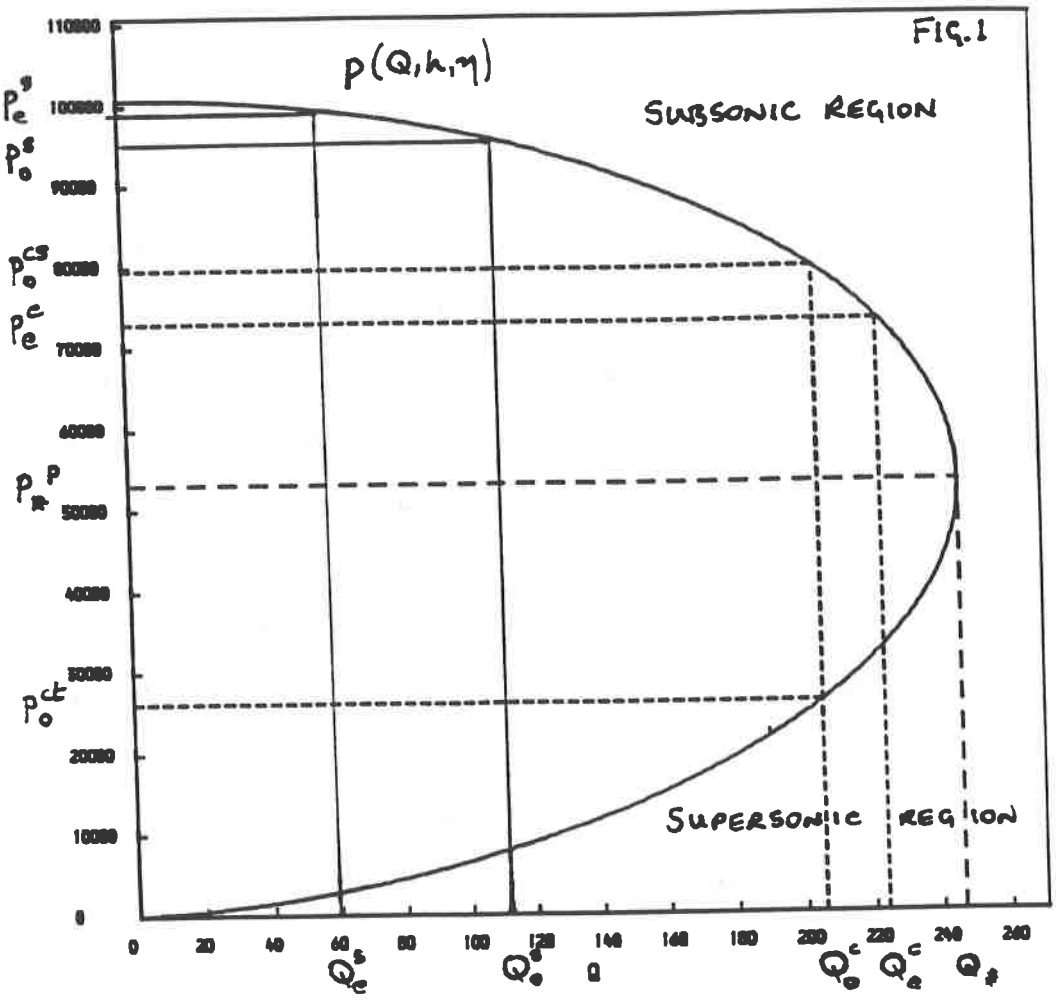

If the entry mass flow rate, Q_e^s, to a particular nozzle is assigned such that the mass flow rate at the throat (2.5) is less than the critical value, Q_*, then the flow will remain subsonic in the complete nozzle (see [4]). Ordinates placed at Q_e^s and at the outlet boundary value, Q_o^s, will determine the corresponding pressure conditions , p_e^s and p_o^s, in the subsonic region of the graph. Conversely given a specified pair of inlet and outlet pressures in that region we may, from (2.4) and

(2.5), determine the form of nozzle that will admit such a subsonic flow.

If the entry mass flow rate, Q_e^c, is increased to a value such that the critical rate of mass flow is attained at the throat, i.e. $Q_T = Q_*$, then one of two possible flow types may result in the diffuser. Placing an ordinate at Q_e^c will again determine the inlet pressure, p_e^c, but now an ordinate at the outlet value, Q_o^c, will provide a choice of two outlet pressures (see FIG.1). The prescription of the pressure value in the subsonic region, p_o^{cs}, will result in a subsonic critical flow and that in the supersonic region, p_o^{ct}, a transition flow (or ideal flow), in which the flow becomes 'sonic at the throat' and subsequently supersonic in the diffuser (see [4]). As above on assigning a suitable pair of pressure conditions we may again, from FIG.1, define boundary values of mass flow and hence, from (2.4) and (2.5), a nozzle that will admit either form of critical flow

In the present work the interest lies in the case where the flow is critical at the throat, i.e. $Q_e = Q_e^c$, but it is stipulated that an outlet pressure, p_o^{sf}, lower than the subsonic critical value, p_o^{cs}, must be attained (see FIG.2). The flow will behave as for transition flow up until a point in the diffuser where it must adjust somehow so as to attain the outlet pressure. This is achieved by the intervention of a stationary shock front, described in §1.2, over which the fluid is compressed (1.18) and slowed from supersonic to subsonic speed (see (1.27)). The position and strength of the shock front is automatically adjusted so as to give the correct outlet pressure (see [2]).

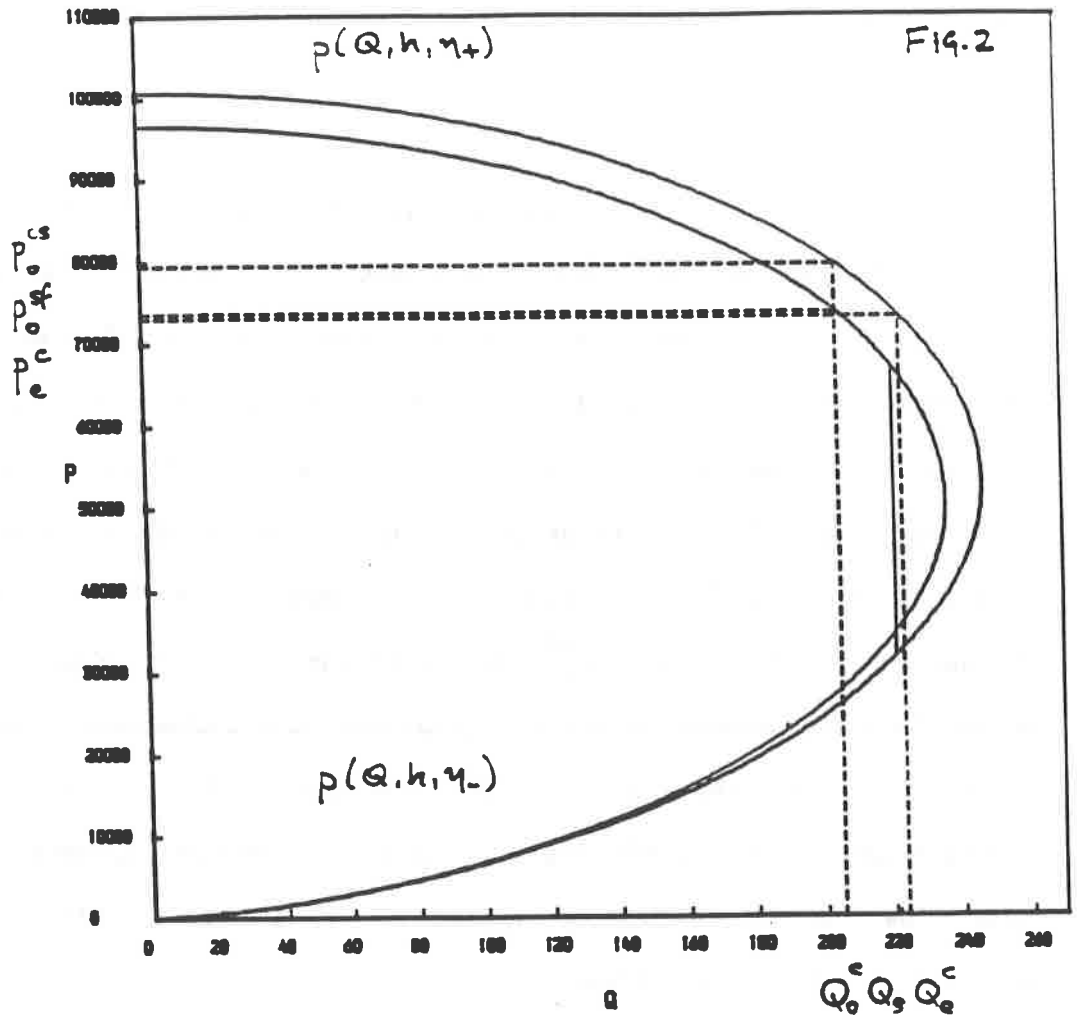

In accordance with the jump conditions (1.14) - (1.16) the mass flow rate, flow stress and total energy will be conserved across the shock front and from condition (1.17), unless it is a zero shock, there will be a positive jump in entropy; the remaining flow variables will then jump in a manner defined by (1.18), (1.23) and (1.25).

Therefore in terms of the quasi one-dimensional model a nozzle transition flow, defined by the inlet flow constants h and η_+, will shock to a subsonic flow in the exhaust section, defined (consistent with the jump condition (1.16)) by the outlet flow constants h and η_-. This process may be represented graphically and is illustrated in FIG.2. The shock front can be seen to intervene at a shock value of mass flow rate, Q_s, and the intersection of an ordinate placed at the critical outlet mass flow rate, Q_o^c, and an abscissa placed at p_o^{sf} will lie on the graph $p(Q,h,\eta_-)$, lying wholly inside $p(Q,h,\eta_+)$ in the p x Q plane.

2.3 QUASI ONE-DIMENSIONAL SHOCK FLOW IN A DE-LAVAL NOZZLE

On the basis of the qualitative definition in §2.2 we may now define, in terms of the conservation equations governing the fluid motion, quasi one-dimensional shock flow in a nozzle; this may be divided into three distinct regions:

1. The continuous flow prior to the shock front

$$\frac{d}{dx}(Q\,A) = 0 \,, \tag{2.6}$$

$$Q = \rho\, v \,, \tag{2.7}$$

$$h = \text{CONSTANT} \,, \tag{2.8}$$

$$\eta = \eta_+ = \text{CONSTANT} \,, \tag{2.9}$$

2. Across the shock front

$$[Q] = 0 \,,$$

$$[P] = 0 \,, \tag{2.10}$$

$$[h] = 0 \,,$$

3. The continuous flow subsequent to the shock front

$$\frac{d}{dx}(Q\,A) = 0 \,, \tag{2.11}$$

$$Q = \rho\, v \,, \tag{2.12}$$

$$h = \text{CONSTANT} \,, \tag{2.13}$$

$$\eta = \eta_- = \text{CONSTANT} \,, \tag{2.14}$$

where the square brackets indicate a jump in the enclosed quantity. The complete solution of the flow, for all the flow variables is again possible on using the total energy equation (1.3). Furthermore note that by assigning the total energy to be the same constant value in both regions of the continuous flow, as indicated by (2.4) and (2.13), the jump condition (2.10c) is inherently satisfied. Quasi one-dimensional shock flow is therefore completely defined by (2.6) - (2.14); the appropriate equation of state again being (1.7).

A particular nozzle shock flow may be considered on satisfying the conservation of mass equation throughout the complete flow by (2.2) with, from §2.2, the particular entry mass flow rate Q_e^c assigned so that

$$Q_T = \frac{C\, A_e}{A_T} = Q_* \; ; \tag{2.15}$$

the outlet boundary condition, Q_o^c, may then be found from (2.4). Hence, with the shock front being defined in the present case to be normal to the x-axis (see §1.2) at a position x_s and Q(x) being uniquely defined by (2.2) for all x, the mass flow jump condition (2.10a) is now also automatically satisfied in the definition of the flow.

2.4 THE SHOCK FLOW LIMITS

The relationship between the prescribed outlet pressure, p_o^{sf}, and the resulting shock position, x_s, in a particular nozzle may be theoretically investigated by the gradual reduction of the outlet pressure from the subsonic critical value p_o^{cs}, for which a theoretical zero shock occurs at the nozzle throat (see [2]). It is found that the resulting shock position will lie progressively further down the diffuser until for a particular value p_o^{so} a shock front will lie at the nozzle outlet station. Thus for a particular nozzle flow that is critical at the throat there will exist a range of outlet pressures that may actually result in a shock flow, namely

$$p_o^{cs} \leq p_o^{sf} \leq p_o^{so} \ . \tag{2.16}$$

In terms of the quasi one-dimensional approximation to shock flow, consistent with (1.17), there will exist a corresponding increasing set of outlet entropy values

$$\eta_T \leq \eta_- \leq \eta_D \ , \tag{2.17}$$

where $\eta_- = \eta_T = \eta_+$ corresponds to a shock of zero strength at the nozzle throat and $\eta_- = \eta_D$ corresponds to a shock at the nozzle outlet. Qualitatively the upper limit on the range of outlet entropy values, η_D, may be obtained by using the graph between flow stress and mass flow for the motion of a fluid particle on a streamline defined by the inlet flow constants, i.e. $P(Q,h,\eta_+)$ (see FIG.3).

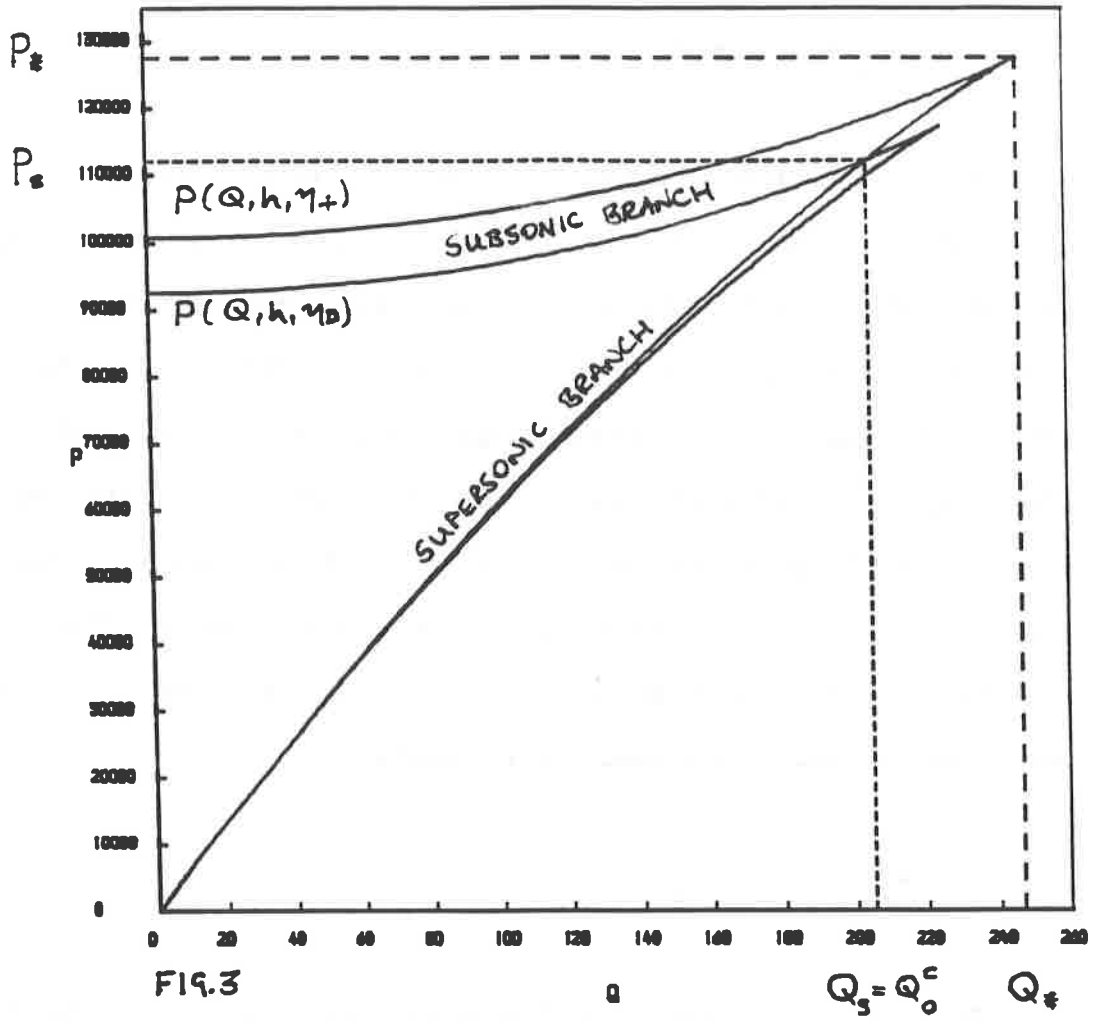

FIG.3

For any entropy value greater than that at inlet, η_+, there will exist a unique flow stress vs mass flow graph, similar in shape to those in FIG.3, in the P x Q plane. The conservation of mass flow and flow stress across a shock front (2.10ab) means that the supersonic branch of $P(Q,h,\eta_+)$ and the subsonic branch of $P(Q,h,\eta_-)$ will intersect at the shock values of these quantities, denoted Q_s and P_s (see [1] or [3]). In the present situation the mass flow shock value is known to be that at outlet, i.e. $Q_s = Q_o^c$, and hence by placing an ordinate at this value in the P x Q plane one of the family of mass flow vs flow stress graphs, namely $P(Q,h,\eta_D)$, will intersect with both this ordinate and $P(Q,h,\eta_+)$, thus providing the required limit η_D.

Subsequently we may now compute the lower limit, p_o^{so}, of the pressure range (2.16) that will result in a shock flow. The graph $p(Q,h,\eta_D)$ may be derived in the manner outlined previously (see §2.2); an ordinate placed at the outlet shock value, $Q_s = Q_o^c$, will then intersect with this graph at the required pressure value (see FIG.4).

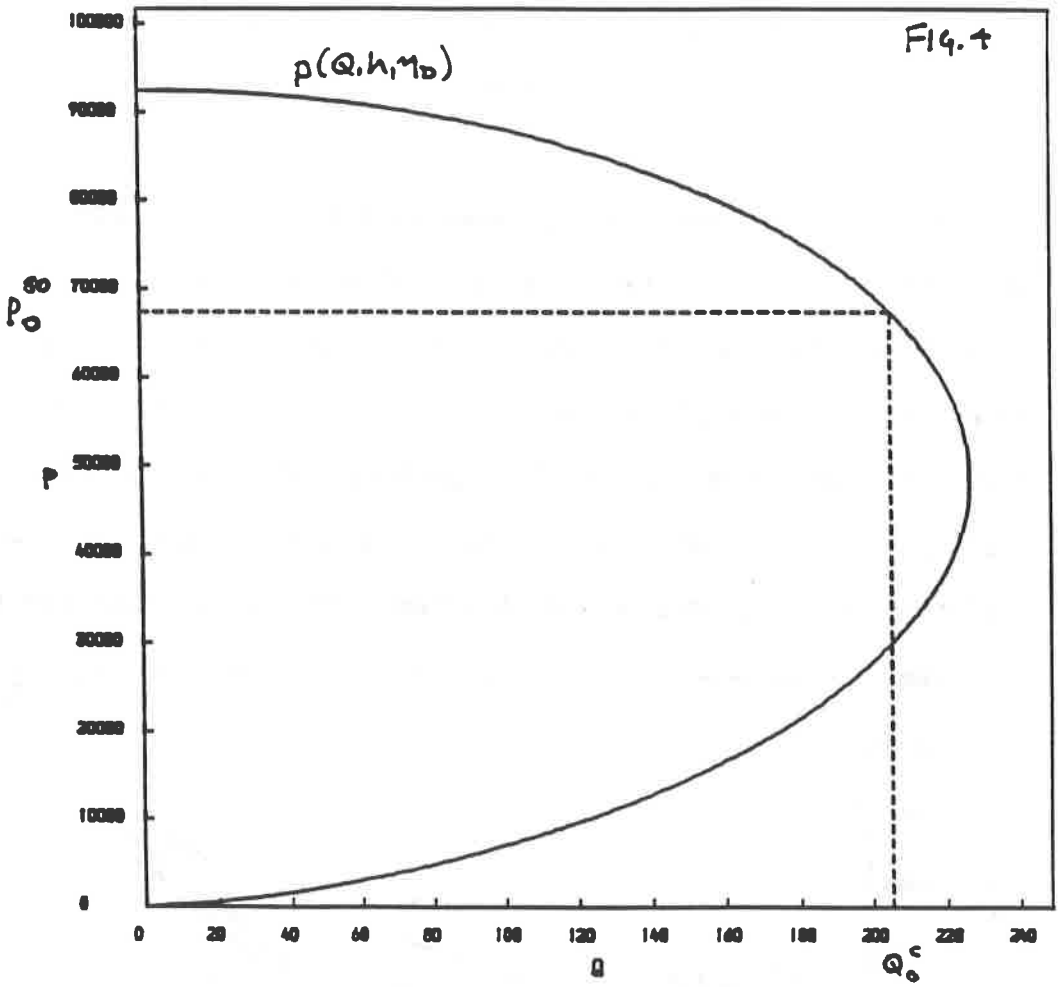

It may also be noted that on the definition of a particular quasi one-dimensional shock flow in terms of the entropy values at inlet (2.9) and, in the range (2.17), at outlet (2.14) the corresponding inlet and outlet pressures may also be determined from the associated $p(Q,h,\eta)$ graphs by placing ordinates at Q_e^c and Q_o^c respectively.

2.5 GRAPHS RELATING THE FLOW VARIABLES IN A SHOCK FLOW

In §2.2 it is stated that the graphs relating the variables in a continuous nozzle flow are segments of each of the full graphs defined by the flow constants h and η; in that case these are found by the positioning of ordinates at the mass flow boundary values, (2.3) and (2.4), and also the throat value (2.5) (see [3] and [4]).

This principle may now be extended (see [3]) to obtain the graphs between the flow variables in a particular quasi one-dimensional nozzle shock flow subsequent to obtaining the shock value of mass flow rate. Recall from §2.4 that on deriving the full flow stress vs mass flow graphs corresponding to the flow constants at inlet, $P(Q,h,\eta_+)$, and at outlet, $P(Q,h,\eta_-)$, on a common axis the intersection of these graphs will then give the required shock values (this is illustrated in FIG.5).

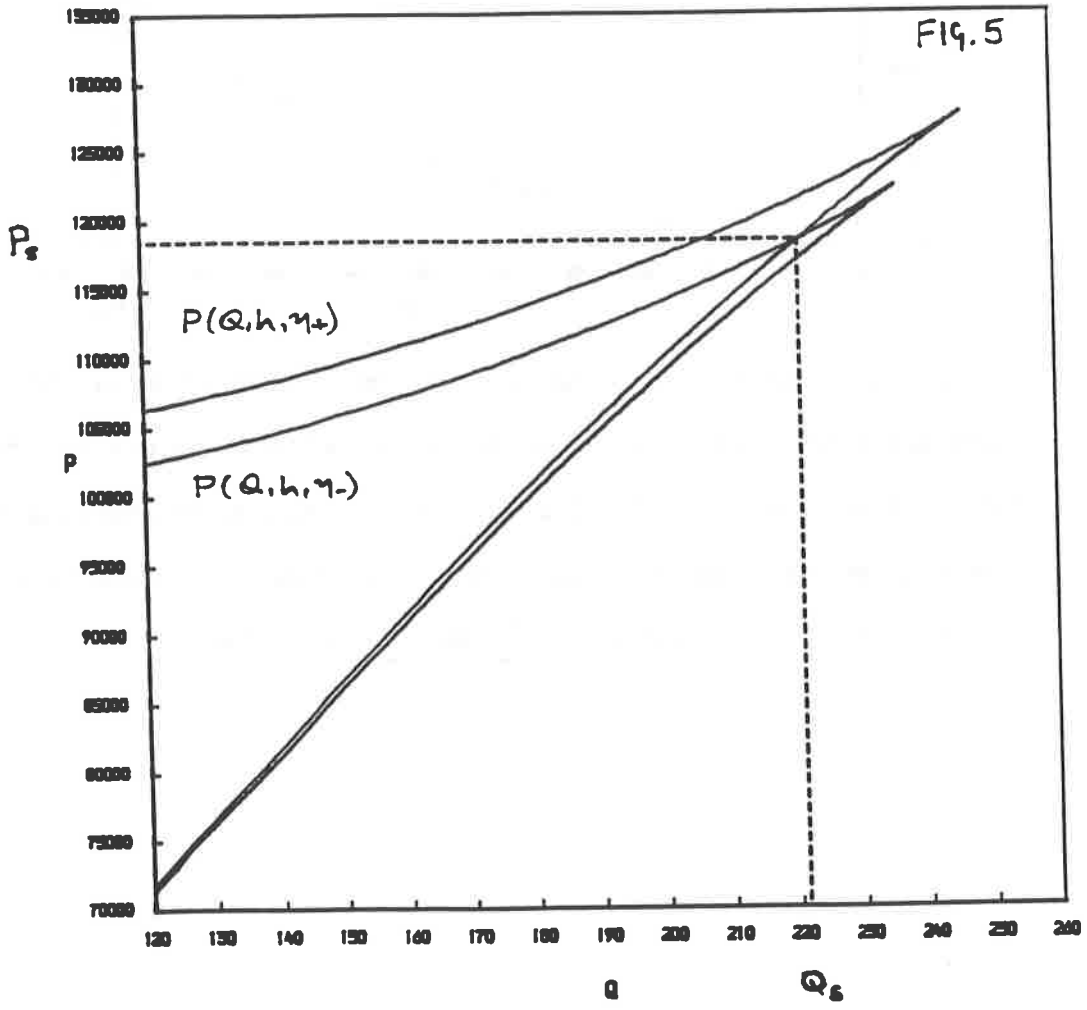

In the same way as for the determination of Q_s each of the full set of inter-variable graphs are derived for the motion of a fluid particle on a general streamline, defined in turn by the inlet and outlet flow constants, on a common axis. Ordinates are then placed, on the graphs involving mass flow as a dependent variable, at the values

$$Q_e,\ Q_T,\ Q_s,\ Q_o\ , \tag{2.18}$$

A graph, for an illustrative set of h, η_+, and η_- values, between the mass flow rate and the second dependent flow variable in the shock flow may then be explained, with reference to each of FIG.6, by

a → b → c : THE TRANSITION FLOW PRIOR TO THE SHOCK FRONT ,

c → d : THE TRAVERSAL OF THE SHOCK FRONT ,

d → e : THE SUBSONIC DIFFUSER FLOW SUBSEQUENT TO THE SHOCK .

(2.19)

Subsequently the boundary, throat and shock values of each of the remaining flow variables may be obtained by inspection of each of FIG.6 and hence the full set of graphs for the shock flow are now available (see FIG.7), where a, b, c, d and e are again explained by (2.19).

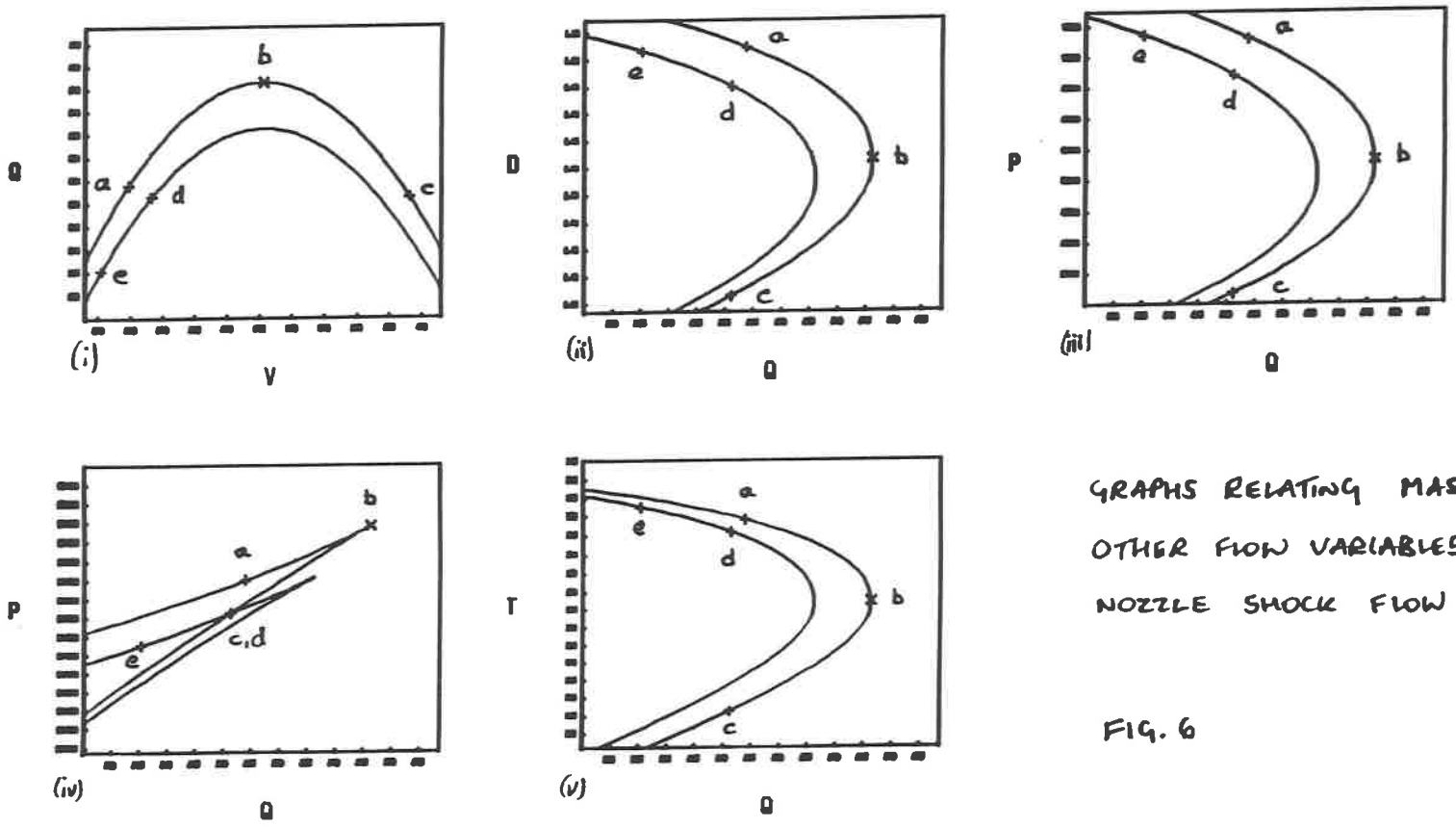

GRAPHS RELATING MASS FLOW AND OTHER FLOW VARIABLES IN A NOZZLE SHOCK FLOW

FIG. 6

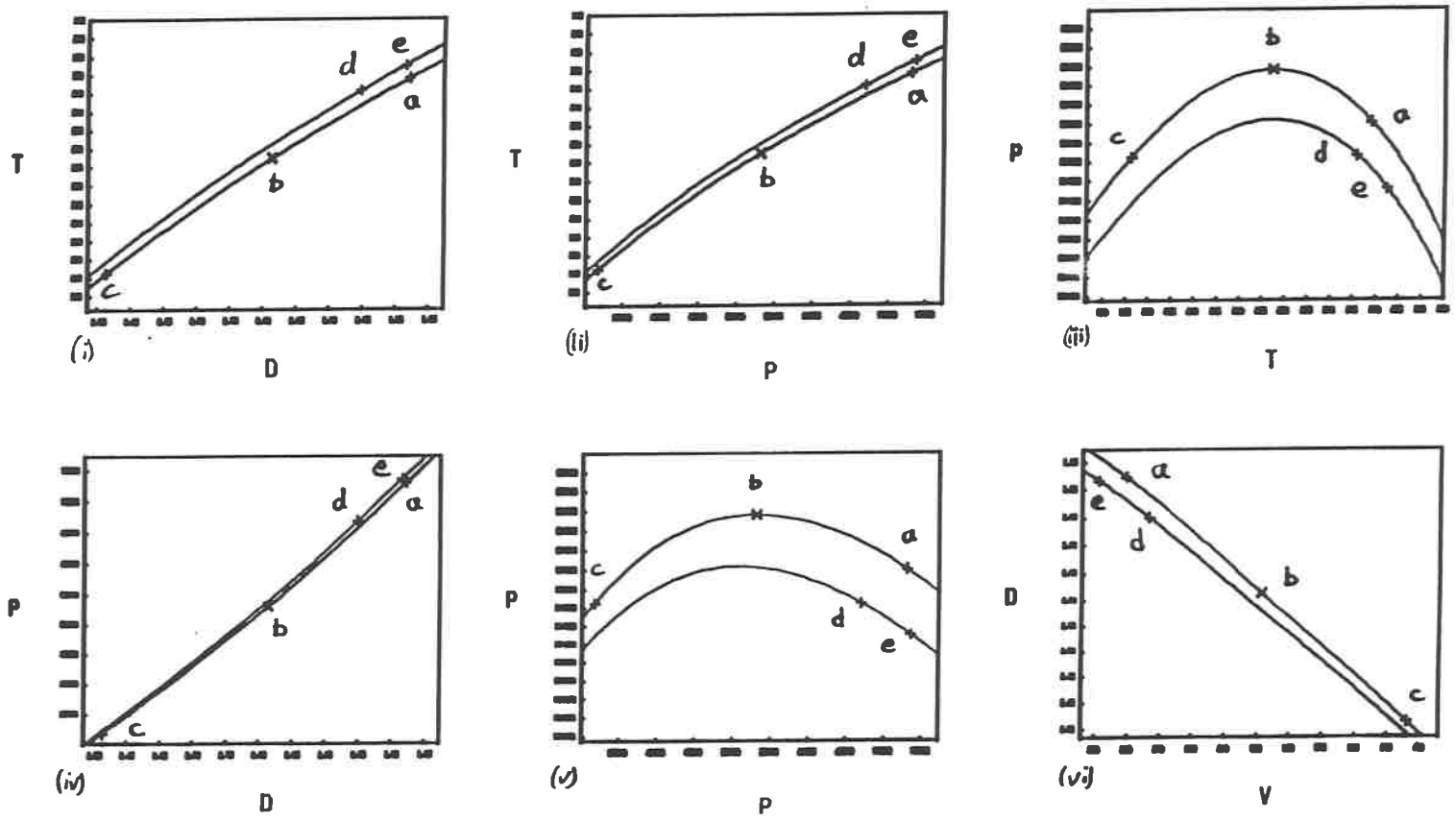

GRAPHS RELATING THE FLOW VARIABLES IN A NOZZLE SHOCK FLOW

FIG. 7

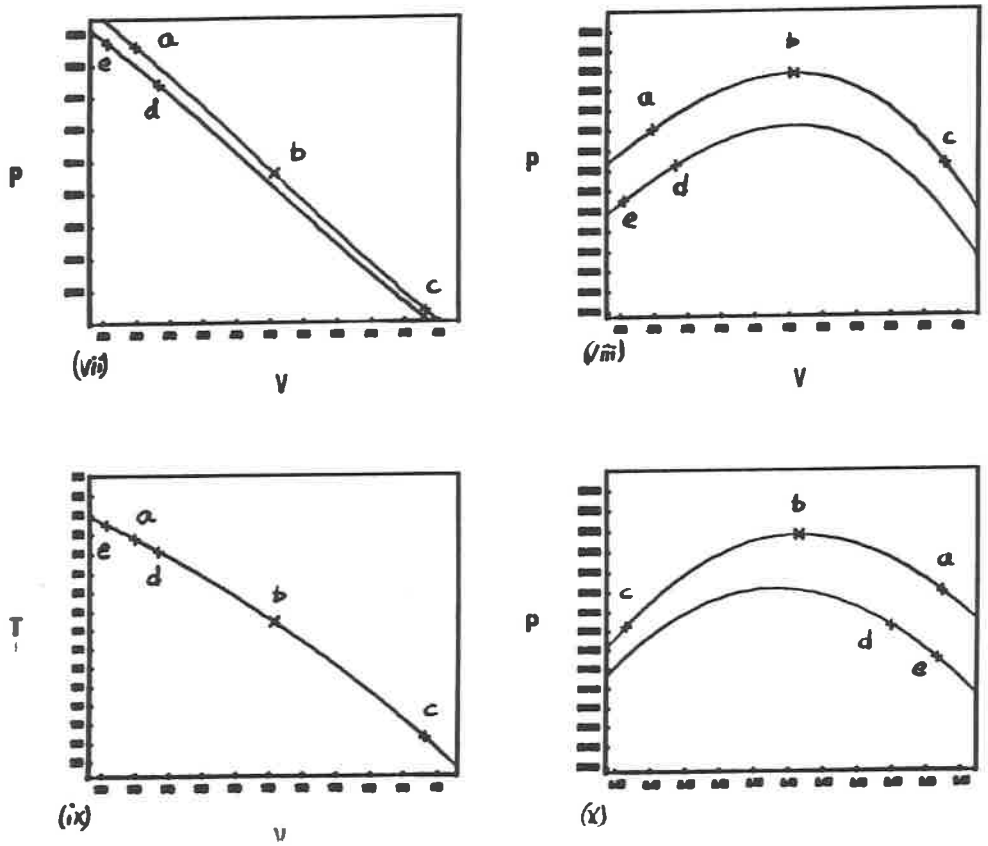

GRAPHS RELATING THE FLOW VARIABLES IN A NOZZLE SHOCK FLOW

FIG. 7

SECTION THREE : AN ALGEBRAIC PARAMETERIZATION OF SHOCK FLOW IN A DE-LAVAL NOZZLE

In this section a particular quasi one-dimensional shock flow in a nozzle is defined, which by necessity includes the derivation of the range of conditions that will result in such a flow. An algebraic parameterization of shock flow is then used to determine the variation of each variable in the flow in terms of the spatial distance, x, along the nozzle axis. The properties of the flow variables on traversal of the shock front, with reference to the definitions of the previous sections, are then discussed. This will provide a basis for comparison with the numerical solution of quasi one-dimensional shock flow in a nozzle to be presented in Section Four.

3.1 A PARTICULAR QUASI ONE-DIMENSIONAL SHOCK FLOW IN A NOZZLE

The quasi one-dimensional approximation to shock flow is defined by (2.6) - (2.14) which are considered to hold in a fixed domain, D, representing the nozzle axis

$$0.0 \leq x \leq 2.0 \ . \tag{3.1}$$

The total energy in both regions of continuous flow, (2.8) and (2.13), is specified as

$$h = 2.74 \times 10^{5} \ \text{Jmol}^{-1}\text{Kg}^{-1} \tag{3.2}$$

thus satisfying the jump condition (2.10c); the inlet entropy (2.9) is

assigned to be

$$\eta_+ = 7.08 \times 10^4 \text{ (SI UNITS)} . \qquad (3.3)$$

The limit speed in the flow may now, from (1.13), be computed

$$v_L = 740.3 , \qquad (3.4)$$

and subsequently, by (1.12), the critical fluid speed is then

$$C_* = 302.5 . \qquad (3.5)$$

The corresponding critical values of the remaining flow variables may be obtained from the algebraic relationships in [1] and for a flow defined by (3.2) and (3.3) may be found in [4]; in particular the maximum critical mass flow rate is

$$Q_* = 246.31124 . \qquad (3.6)$$

The linear area variation of the nozzle, in each of its composite sections, is defined by

$$\begin{aligned} &\text{ENTRY SECTION} \quad : A(x) = 1.1 - (x/8) \qquad [0.0 \leq x \leq 0.8] \\ &\text{EXHAUST SECTION} \quad : A(x) = (2.6/3.0) + (x/6) , \quad [0.8 \leq x \leq 2.0] \end{aligned} \qquad (3.7)$$

and therefore

$$A_e = 1.1 \ ,$$
$$A_T = 1.0 \qquad (3.8)$$
and $$A_o = 1.2 \ ,$$

where recall A_T is the cross-sectional area at the throat location, x_T, which from (3.7) is

$$x_T = 0.8 \ . \qquad (3.9)$$

The conservation of mass equation is satisfied by (2.2), hence in turn the jump condition (2.10a), and the entry mass flow rate is assigned by

$$Q_e = Q_e^c = 223.919 \ , \qquad (3.10)$$

such that condition (2.15) is upheld and (3.6) is attained at the throat. The outlet boundary condition, from (2.4), is then

$$Q_o = Q_o^c = 205.259 \ . \qquad (3.11)$$

The upper limit, η_D, on the range of outlet entropy values (2.17) that may result in a shock flow is obtained qualitatively in the manner outlined in §2.4, where note $P(Q,h,\eta_+)$ in FIG.3 is derived for a total energy value (3.2) and an entropy value (3.3), also the ordinate at Q_o^c on the graph is that defined in (3.11). The analagous numerical process must however take account of the fact that a graph between flow stress and mass flow rate is obtained by using an intermediate range of fluid speed values; we require two quantities, the shock value of mass flow at outlet, known to be (3.11), and additionally the corresponding magnitude of the flow stress P_s.

The algebraic relationship $Q(v_o^{sp},h,\eta_+)$ (from [1])

$$Q_o = Q(v_o^{sp},h,\eta_+) = \eta_+^{(1/1-\gamma)}\ v_o^{sp}\ [\ ((\gamma - 1)/\gamma)\ (h - ((v_o^{sp})^2/2))\ ]^{(1/\gamma-1)}, \tag{3.13}$$

must first be solved for the supersonic outlet fluid speed, v_o^{sp}, by Newton's single variable method, with the initial value (see [4])

$$v_o^{sp}(o) = 500.0\ , \tag{3.14}$$

giving in the present case

$$v_o^{sp} = 418.801\ . \tag{3.15}$$

The substitution of (3.15) into the algebraic relationship $P(v_o^{sp},h,\eta_+)$ (from [1])

$$P_s = P(v_o^{sp},h,\eta_+) = \eta_+^{(1/1-\gamma)}\ [\ ((\gamma - 1)/\gamma)\ (h - ((v_o^{sp})^2/2)) + (v_o^{sp})^2\ ]$$
$$[\ ((\gamma - 1)/\gamma)\ (h - ((v_o^{sp})^2/2))\ ]^{(1/\gamma-1)}\ , \tag{3.16}$$

then provides the required shock value of flow stress at outlet, here

$$P_s = 112051.201\ . \tag{3.17}$$

The continuity of the flow stress and the mass flow rate across the shock front means that the limit η_D may now be found by solving $Q(v_s,h,\eta_D)$ and $P(v_s,h,\eta_D)$, of the form (3.13) and (3.16), using a bisection method, where v_s is the subsonic fluid speed magnitude for a shock at outlet. The algebraic relationships $Q(v_1,h,\eta_1)$ and $Q(v_2,h,\eta_2)$ are first solved at (3.11), where η_1 and η_2 are the initial guesses to

η_D which are chosen here to be

$$\eta_1 = 7.08 \times 10^4$$

and (3.18)

$$\eta_2 = 7.4 \times 10^4 ,$$

for the corresponding fluid speeds v_1 and v_2. Then, by using the relevant form of (3.16), the suitability of the initial data may be verified by ensuring that

$$P(v_1,h,\eta_1) > P_s$$

and (3.19)

$$P(v_2,h,\eta_2) < P_s ,$$

where P_s is defined in the present case by (3.17). The relationship $Q(v_3,h,\eta_3)$, where

$$\eta_3 = 0.5\ (\eta_1 + \eta_2) , \tag{3.20}$$

is now solved for v_3 and hence the corresponding flow stress

$$P_3 = P(v_3,h,\eta_3) . \tag{3.21}$$

Now, dependent on the magnitude of (3.21), the entropy interval containing η_D may, from initially $\eta_1 \leq \eta_D \leq \eta_2$, be reduced to

$$P_3 > P_s \ : \ \eta_3 \leq \eta_D \leq \eta_2$$

or (3.22)

$$P_3 < P_s \ : \ \eta_1 \leq \eta_D \leq \eta_3 .$$

The continuation of this process, by definition of an entropy value η_3', using (3.20), inside the appropriate interval in (3.22), will result in a continual reduction of the interval containing η_D; this is said to of converged when

$$| P_3 - P_S | \leq 0.0001 , \tag{3.23}$$

and the magnitude of η_D is then defined to be, in the present case

$$\eta_D = \eta_3 = 7.32455 \times 10^4 . \tag{3.24}$$

Note that inherent in this process is the derivation of v_S, here this being

$$v_S = v_3 = 218.083 . \tag{3.25}$$

The range of outlet entropy values resulting in shock flow in the nozzle (3.7), with inlet flow constants (3.2) and (3.3), now becomes

$$7.08 \times 10^4 \leq \eta_- \leq 7.32455 \times 10^4 . \tag{3.26}$$

The upper and lower bounds on the corresponding range of pressure values (2.16) may be found by deriving $p(Q,h,\eta_+)$ (see FIG.2, which is derived for the flow constants (3.2) and (3.3)) and $p(Q,h,\eta_D)$ (see FIG.4, which is derived for the flow constants (3.2) and (3.24)) and computing their respective intersection with an ordinate erected at Q_o (3.11) in the p x Q plane. Recall though that a relation $p(Q,h,\eta)$ is actually given in terms of a parameterization by the fluid speed (see [4]) in the algebraic relationships $Q(v,h,\eta)$ (of the form (3.13)) and $p(v,h,\eta)$, where

$$p(v,h,\eta) = \eta^{(1/1-\gamma)} \left[((\gamma - 1)/\gamma) (h - (v^2/2)) \right]^{(\gamma/\gamma-1)} , \quad (3.27)$$

(from [1]). Therefore numerically the subsonic critical pressure, p_o^{cs}, in (2.16) must be obtained by first solving (3.13) for the subsonic outlet fluid speed, v_o^{sb}, by Newton's method with initial data (see [4])

$$v_o^{sb}(o) = 200.0 , \quad (3.28)$$

giving in the present case

$$v_o^{sb} = 188.935 , \quad (3.29)$$

and then substituting into $p(v_o^{sb},h,\eta_+)$ (from (3.27). In a similar manner we may compute the pressure corresponding to a shock at outlet, p_o^{so}, by the substitution of (3.25) into $p(v_s,h,\eta_D)$. The computed pressure range resulting in a shock flow is then

$$7.95095 \times 10^4 \geq p_o^{sf} \geq 6.72877 . \quad (3.30)$$

The definition of the quasi one-dimensional shock flow may now be completed by assigning, from (3.26), the outlet entropy value (2.14)

$$\eta_- = 7.2 \times 10^4 \text{ (SI UNITS)} . \quad (3.31)$$

The corresponding outlet pressure value may be obtained by an analagous process to that used to compute p_o^{so}, whence

$$p_o = p_o^{sf} = 7.35966 \times 10^4 ; \quad (3.32)$$

this process is shown qualitatively in FIG.2, where $p(Q,h,\eta_-)$ is

derived for the flow constants (3.2) and (3.31) and Q_o^c is defined by (3.11). The inlet pressure may of course also be found by substituting the subsonic entry velocity, v_e^{sb}, obtained by solving (3.13) at (3.10), into $p(v_e^{sb},h,\eta_+)$, this being

$$p_e = p_e^c = 7.30433 \times 10^4 \tag{3.33}$$

(again qualitatively this is shown in FIG.2, in which $p(Q,h,\eta_+)$ is defined by (3.2) and (3.3), with Q_e^c from (3.10)).

3.2 A PARAMETERIZATION OF SHOCK FLOW

An algebraic parameterization of quasi one-dimensional continuous duct flow is presented in [4] by the derivation of a non-linear relationship between the fluid speed and the distance from inlet along the duct axis. In the present case of air flow this takes the form

$$v^2 + 7\,\eta \left[\frac{C\,A_e}{v\,A(x)} \right]^{0.4} = 2\,h\,v^{0.4} , \tag{3.34}$$

which is dependent on the particular flow definition. The fluid speed variation for a duct flow is then obtained by employing Newton's single variable method in the solution of (3.34), with appropriate initial data, at each of a specified range of axial locations, x_i, in the domain representing the duct axis (see [4]).

In §2.2 we have stated that in terms of the quasi one-dimensional approximation to shock flow in a nozzle, in the present case defined by (3.1) - (3.11) and (3.31), the flow will shock from a transition flow

defined by the inlet flow constants (3.2) and (3.3) to a subsonic flow defined by (3.2) and (3.31). The parameterization of the shock flow is therefore obtained by combining the parameterization of transition flow in the full nozzle with the parameterization of the subsonic flow in the diffuser, about the computed shock position.

The transition flow parameterization

The appropriate form of the non-linear relationship (3.34) is obtained by the substitution of the flow constants (3.2) and (3.3) together with (3.7), (3.8a) and (3.10). This is solved at each location x_i in the domain (3.1) uniformly spaced such that

$$| x_i - x_{i+1} | = 0.001 . \qquad [i = 1(1)2000] \qquad (3.35)$$

The computed parameterization is shown in FIG.8 (from [4]) and denoted 'TF'.

The subsonic cone section flow parameterization

An algebraic parameterization of the subsonic flow in the diffuser may be obtained on definition of the relationship (3.34). The flow itself is independent of the nozzle flow in the sense that it is really a flow through a diverging cone section of the form (3.7b) which is defined by the flow constants (3.2) and (3.31).

As no transition from subsonic to supersonic flow may occur in a cone section (see [2]) the upper bound on the fluid speed in the subsonic flow is given by the critical speed (3.5). The algebraic relationship between mass flow and fluid speed (3.13) may be used, by

substitution of (3.2), (3.5) and (3.31), to obtain a corresponding upper limit on the mass flow, and in the present case

$$Q_{LIM} = 236.18 \ . \tag{3.36}$$

The subsonic cone section flow may therefore only exist in a portion of the complete nozzle diffuser defined to be

$$x_{LIM} \leq x \leq 2.0 \ , \tag{3.37}$$

where in the present case from (2.2) and (3.7b)

$$x_{LIM} = 6.0 \left[\frac{C \, A_e}{Q_{LIM}} - \frac{2.6}{3.0} \right] = 1.0575 \ . \tag{3.38}$$

It is essential when we progress to the consideration of the shock position in the diffuser that the axial locations in the domain representing the cone section flow lie at the same position as those in the corresponding portion of the domain associated with the full nozzle axis. Thus in the present case the cone section flow is defined on the reduced domain

$$1.058 \leq x \leq 2.0 \ , \tag{3.39}$$

and the range of axial locations is specified so as to be compatible with (3.35)

$$| \, x_i - x_{i+1} \, | = 0.001 \ . \qquad [\ i = 1(1)942 \ ] \tag{3.40}$$

The area variation of the cone section, $A^{CS}(x)$, is from (3.7b)

$$A^{cs}(x) = (2.6/3.0) + (x/6) \ , \tag{3.41}$$

where x lies in the domain (3.39) and therefore

$$A_e^{cs} = (2.6/3.0) + (1.058/6.0) = 1.043$$

and (3.42)

$$A_o^{cs} = 1.2 \ ,$$

where A_e^{cs} and A_o^{cs} are the cone section entry and outlet cross-sectional areas respectively. The mass flow boundary condition at inlet, Q_e^{cs}, from (3.42a) and (2.2) is

$$Q_e^{cs} = \frac{C\ A_e}{A_e^{cs}} = 236.157 \tag{3.43}$$

and, from (3.11), at outlet

$$Q_o^{cs} = 205.25 \ . \tag{3.44}$$

The subsonic cone section flow is thus defined by (3.2), (3.31) and (3.39) - (3.44) and therefore the appropriate form of (3.34) may now be found by substitution of (3.41), (3.42a) and (3.43). The domain on which the flow is defined (3.39) and the computed parameterization, denoted 'DF', are shown in FIG.8.

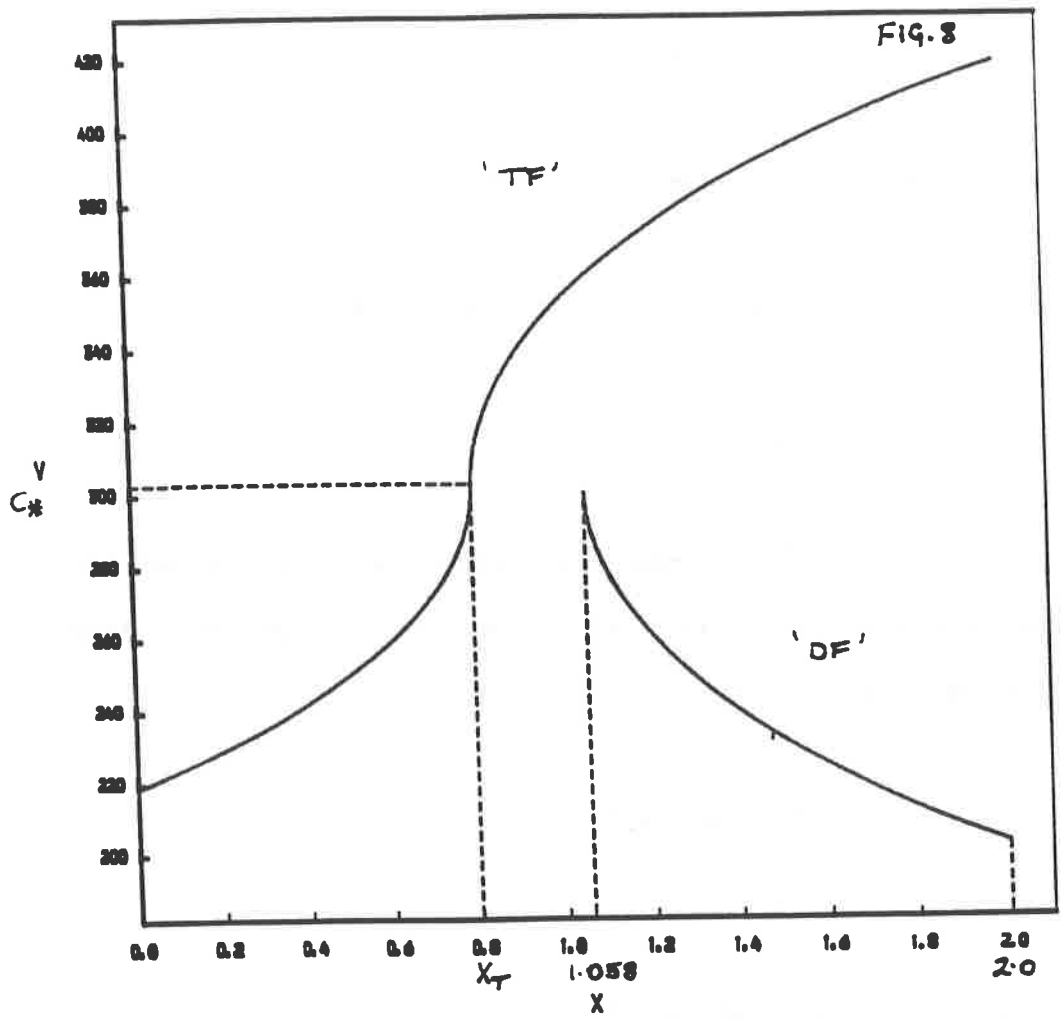

The shock position in the diffuser

The principle behind obtaining the shock value of mass flow rate has been presented in §2.5. In that case the parameterization of a $P(Q,h,\eta)$ graph was obtained by using a uniformly increasing range of fluid speed values as intermediate parameters in the relationships $Q(v,h,\eta)$ (3.13) and $P(v,h,\eta)$ (3.16). The graphs shown in FIG.5 were in fact computed for a total energy value (3.2) and entropy values at inlet of (3.3) and at outlet of (3.31) respectively, thus their intersection provides the mass flow shock value required at present.

It is convenient though, as a general algorithm, to use the computed fluid speed parameterizations of the particular transition flow and the particular subsonic cone section flow (see FIG.8) to obtain the

required $P(Q,h,\eta)$ graphs (see FIG.9). The supersonic branch of $P(Q,h,\eta_+)$, associated with the transition flow, and $P(Q,h,\eta_-)$, for the subsonic cone flow, will again theoretically intersect at the shock value of mass flow rate.

The manner in which the axial locations in the domains (3.1) and (3.39) were specified means that at each particular position common to both the mass flow rate, from (2.2) with (3.7b) or (3.41), will be the same in either flow, i.e.

$$Q(x_i) = \frac{C\,A_{e_-}}{A(x_i)} = \frac{C\,A_{e_-}}{A^{cs}(x_i)} \quad . \tag{3.45}$$

Therefore numerically the intersection of the $P(Q,h,\eta)$ graphs, and thus the shock value of mass flow rate, will be found when

$$\left| P(Q_s,h,\eta_+) - P(Q_s,h,\eta_-) \right| = \text{MIN} \left| P(Q(x_i),h,\eta_+) - P(Q(x_i),h,\eta_-) \right| , \tag{3.46}$$

where x_i are the axial locations common to both domains; thus in the present case

$$Q_s = 221.205 \quad . \tag{3.47}$$

The position of the shock in the diffuser, x_s, may then be obtained by using (2.2) with either (3.7b) or (3.41) giving

$$x_s = 6.0 \left[\frac{C\,A_e}{Q_s} - \frac{2.6}{3.0} \right] = 1.481 \quad , \tag{3.48}$$

which will lie at one of the specified axial locations common to both the nozzle and cone section axes. Therefore we may state by (3.35) and (3.40) that the error of the computed shock position is at most

$$| \text{ERROR IN } x_s | < 0.001 \ . \tag{3.49}$$

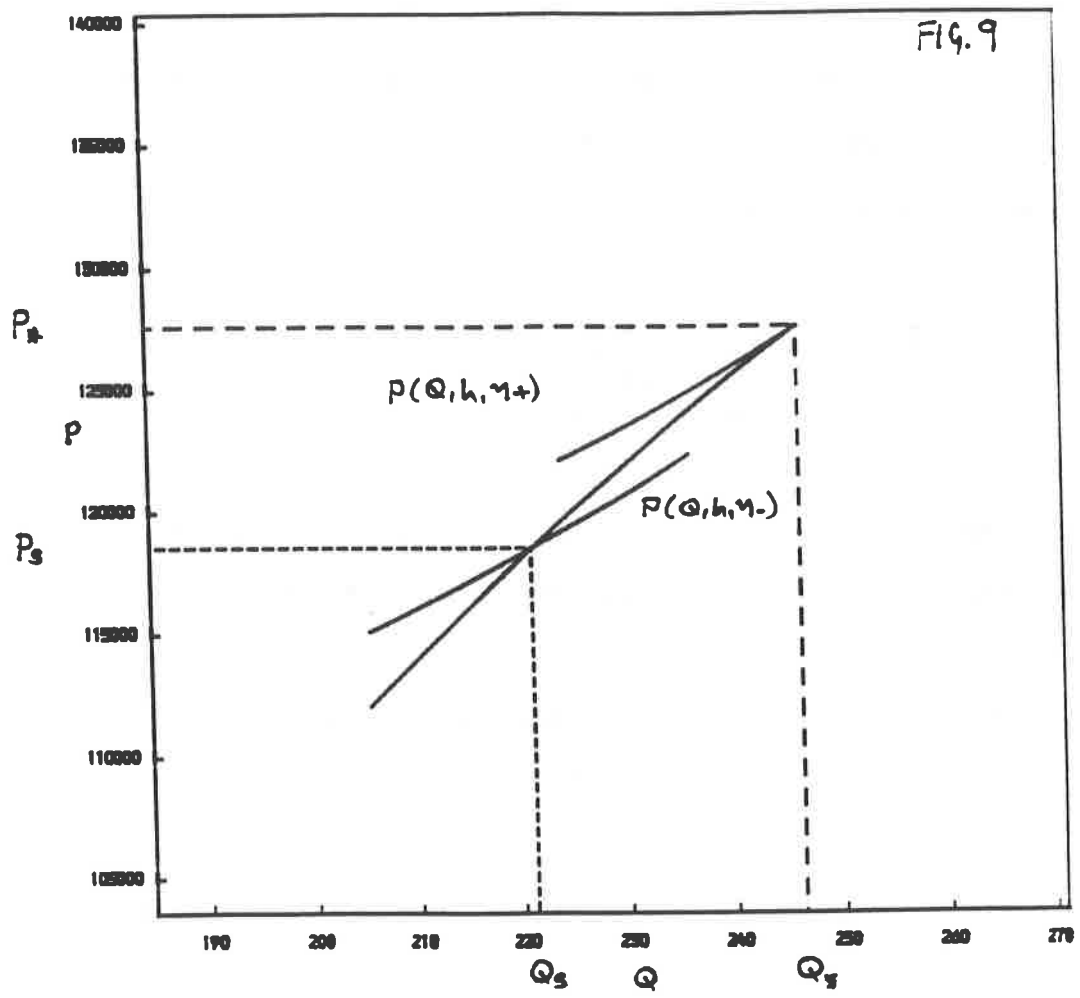

The shock flow parameterization

As stated previously the fluid speed parameterization may now be simply computed by combining the parameterization of the transition flow from inlet, up to and including the shock position (3.48), and the subsonic cone section flow from the shock position to outlet (see FIG.10). Note the jump in fluid speed magnitude across the shock front, and in particular the de-acceleration from supersonic to subsonic speed as predicted by Prandtl (1.27).

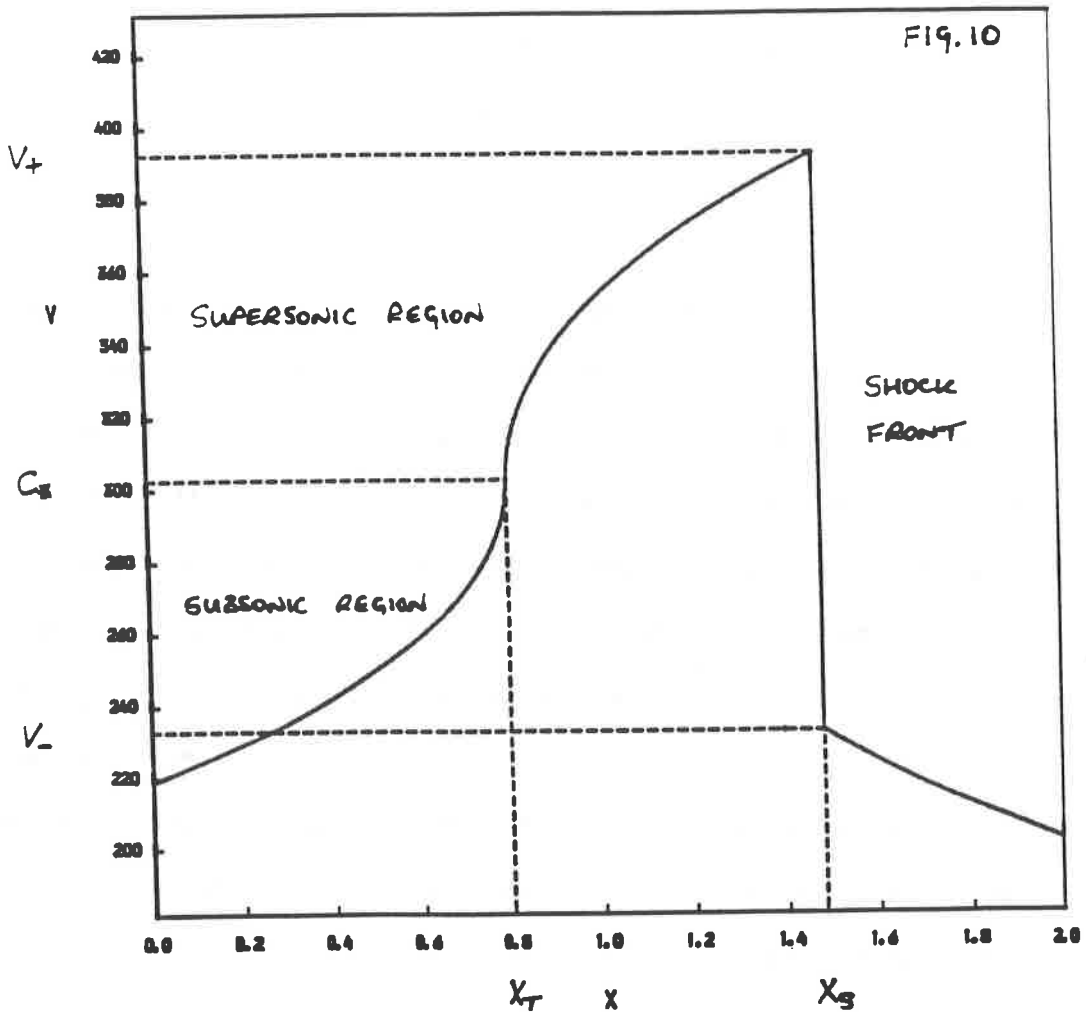

Subsequently the fluid speed parameterization may be used in the algebraic relationships (see [1]) to provide the variation of the remaining flow variables with repect to the axial location (see FIG.11). Note, consistent with the jump condition (1.15), the continuity of the flow stress in the domain (FIG.11*iii*); the discontinuity in the gradient at the shock position may be explained on considering the implications of

$$\left[\frac{\partial P}{\partial x}\right] = \left[\frac{dP}{dQ}\right]\left[\frac{\partial Q}{\partial x}\right], \tag{3.50}$$

at that location (recall the square brackets indicate a jump in the enclosed quantity), where although in accordance with (1.14) the mass flow gradient, from FIG.11*ii*, is continuous, from FIG.9 the flow stress

gradient with respect to mass flow is not. Additionally we may note that the flow variables that do jump do so in the direction established in (1.18), (1.23b) and (1.24).

Furthermore using the fluid speed variation as a set of intermediate numerical parameters in the algebraic relationships will determine the full set of inter-variable graphs in the shock flow (see FIG.12). These are simply the segments that were indicated on FIGS.6,7, computed using (3.2) and the inlet and outlet entropy values (3.3) and (3.31) respectively, by the mass flow shock value and boundary conditions. A particularly interesting feature in the graph between temperature and fluid speed (FIG.12*xiv*) is the jump subsequent to the shock front back onto the portion of the same graph representing the subsonic region of the transition flow. This is because the algebraic relationship used (see [1])

$$T(v) = \frac{m\,(\gamma - 1)\,(h - (v^2/2))}{R_o\,\gamma}\,, \qquad (3.51)$$

where the thermodynamic constants are defined in (1.2), can be seen to be independent of entropy. Note also the continuity of the flow stress vs mass flow graph (FIG.12*iv*) which is simply a truncated version of FIG.9.

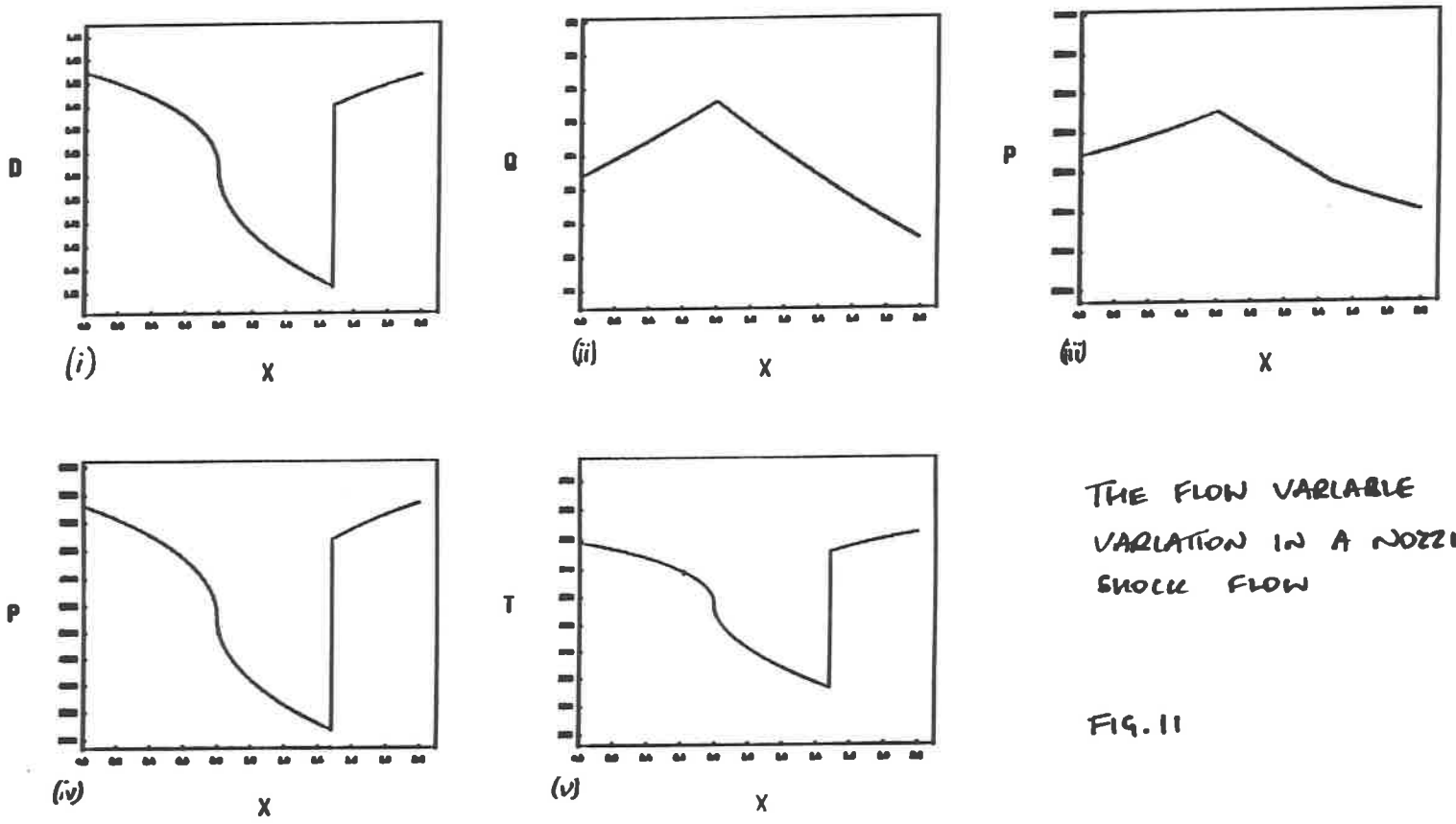

THE FLOW VARIABLE VARIATION IN A NOZZLE SHOCK FLOW

FIG. 11

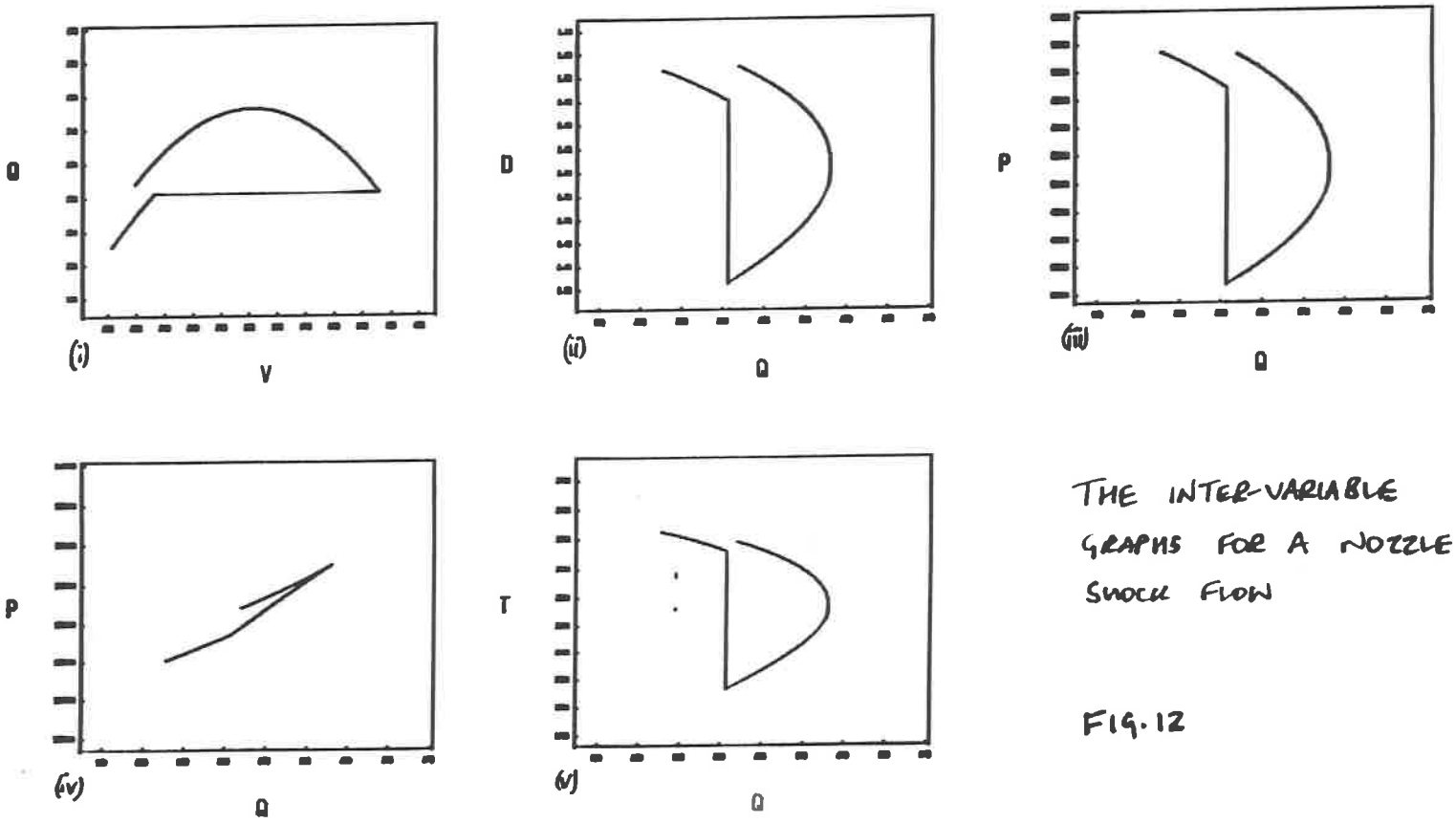

THE INTER-VARIABLE GRAPHS FOR A NOZZLE SHOCK FLOW

FIG. 12

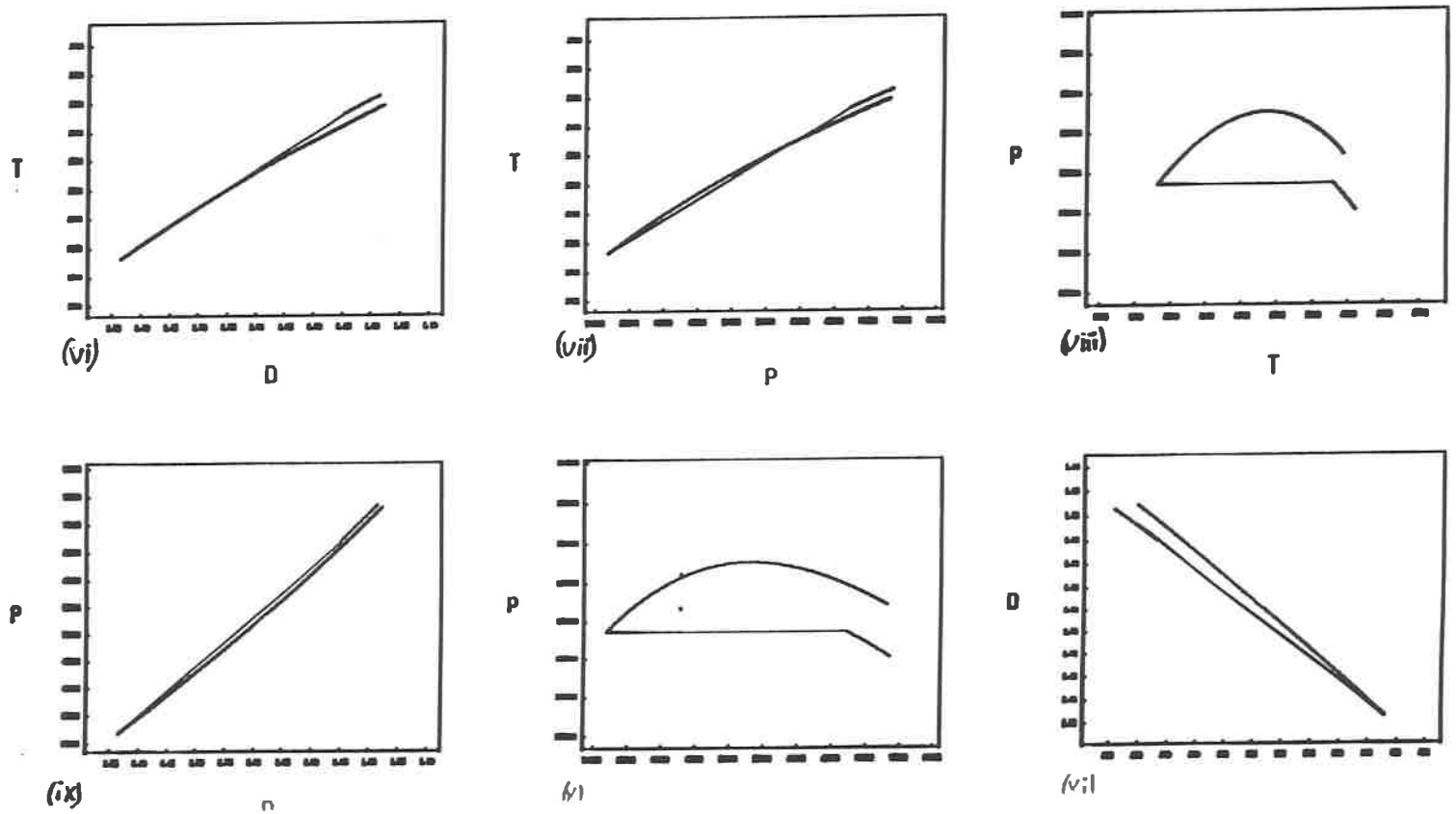

THE INTER-VARIABLE GRAPHS FOR A NOZZLE SHOCK FLOW

FIG. 12

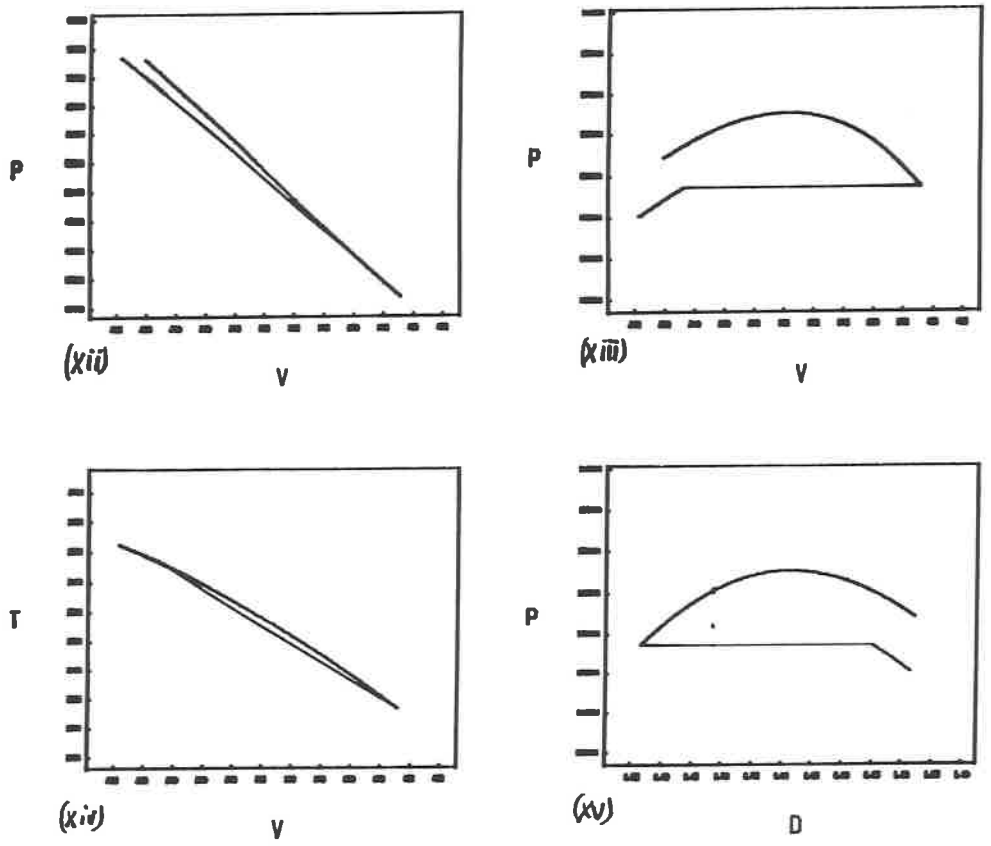

THE INTER-VARIABLE GRAPHS FOR A NOZZLE SHOCK FLOW

FIG. 12

3.3 THE SHOCK FRONT

The magnitude of the jump in the fluid speed across the shock front may be found from the value at entry, v_+, and at exit, v_-, computed in the parameterization of the flow

$$\text{FLUID SPEED JUMP} \quad : \quad v_- - v_+ = -\ 159.513 \ . \tag{3.52}$$

Subsequently in deriving FIG.11 we have also computed, by using the algebraic relationships, the quantities necessary to find the jump in the remaining flow variables

$$\begin{aligned} &\text{PRESSURE JUMP} && : \quad p(v_-) - p(v_+) = +\ 3.52858 \times 10^4 \ , \\ &\text{DENSITY JUMP} && : \quad \rho(v_-) - \rho(v_+) = +\ 0.386 \\ \text{and} \quad &\text{TEMPERATURE JUMP} && : \quad T(v_-) - T(v_+) = +\ 49.643 \ . \end{aligned} \tag{3.53}$$

The jump in entropy may be found from (3.3) and (3.31) to be

$$\text{ENTROPY JUMP} \quad : \quad \eta_- - \eta_+ = +\ 1200.0 \ . \tag{3.54}$$

The compression of the shock, by (1.19), is

$$C_{shk} = \rho(v_-)/\rho(v_+) = 1.685 \ , \tag{3.55}$$

which may be seen to lie within (1.20), and also the shock strength in terms of the excess pressure ratio (1.28) is

$$\text{SHOCK STRENGTH} = \frac{p(v_-) - p(v_+)}{p(v_+)} = 1.111 \ . \tag{3.56}$$

3.4 A COMPARISON OF SHOCK FLOWS

The notion of shock strength is of course at present meaningless because its role is as a comparative quantity between shock flows. Hence we now investigate, as suggested in §2.4, the relationship between the nozzle outlet entropy value and the resulting shock strength and position.

The prescibed η_- values in the range (3.26), with the corresponding outlet pressures, and the necessary position and strength of the shock front in the diffuser are shown in TABLE.1.

OUTLET CONDITIONS		INTERVENING SHOCK	
ENTROPY x 10^4	PRESSURE x 10^4	SHK POSITION	SHK STRENGTH
7.080	7.95095	0.800	0.000
7.082	7.94114	0.836	0.211
7.084	7.93131	0.858	0.273
7.086	7.92150	0.876	0.316
7.088	7.91168	0.893	0.352
7.090	7.90186	0.909	0.385
7.092	7.89204	0.925	0.415
7.094	7.88222	0.939	0.440
7.096	7.87240	0.953	0.465
7.098	7.86258	0.966	0.486
7.100	7.85276	0.979	0.507
7.120	7.75451	1.097	0.678
7.140	7.65613	1.201	0.809
7.160	7.55758	1.299	0.921
7.180	7.45878	1.391	1.020
7.200	7.35966	1.481	1.111
7.220	7.26012	1.568	1.196
7.240	7.16007	1.653	1.276
7.260	7.05941	1.737	1.353
7.280	6.95802	1.819	1.425
7.300	6.85576	1.901	1.496
7.320	6.75245	1.982	1.564
7.3245	6.72877	2.000	1.579

TABLE.ONE

The qualitative relationships between the quantities in TABLE.1 can be seen if they are presented graphically. The shock position ('XS') is plotted as a function, first of the outlet entropy ('ENT') in FIG.13*i*, and then of the outlet pressure ('p') in FIG.13*ii*; the shock strength ('SS') is similarly given as a function of these two variables in FIGS.14*i*,*ii* (each graph denoted by the continuous line).

The shock position is clearly seen to lie at the nozzle throat location (3.9) for $\eta_- = \eta_+$ (FIG.13*i*) or $p_o^{sf} = p_o^{cs}$ (FIG.13*ii*), the shock strength being zero (FIGS.14*i*,*ii*), and at outlet for $\eta_- = \eta_D$ or $p_o^{sf} = p_o^{so}$, with the shock strength then a maximum. The rate of change of the shock position (FIGS.13*i*,*ii*) and shock strength (FIGS.14*i*,*ii*), with respect to either outlet variable, is seen to be significantly large in the vacinity of the throat but becomes virtually constant towards outlet. Note finally the qualitative similarity in shape of the graphs in either FIG.13 or FIG.14, the opposite gradient being due only to the opposite variation in magnitude in the range (3.26) of outlet entropy and (3.30) of outlet pressure.

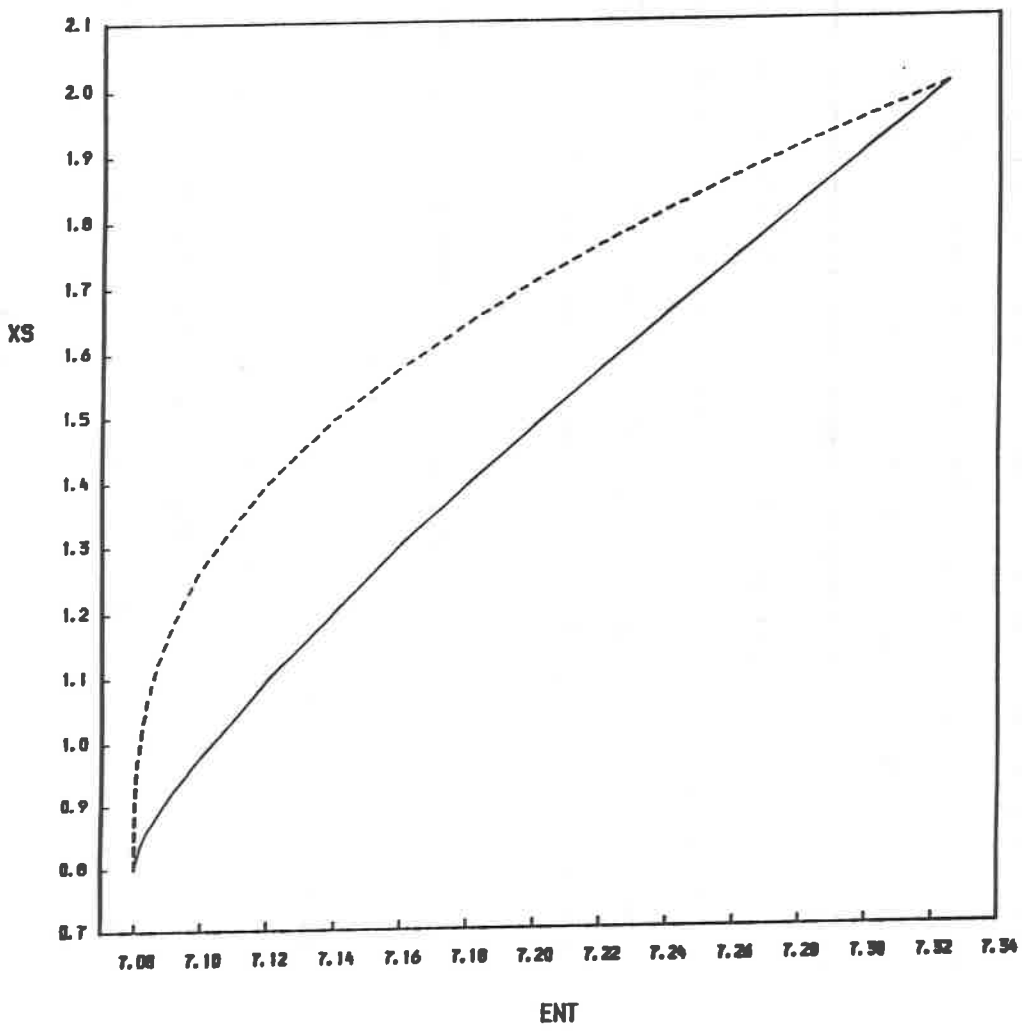
XS
2.1
2.0
1.9
1.8
1.7
1.6
1.5
1.4
1.3
1.2
1.1
1.0
0.9
0.8
0.7
7.08
7.10
7.12
7.14
7.16
7.18
7.20
7.22
7.24
7.26
7.28
7.30
7.32
7.34
ENT

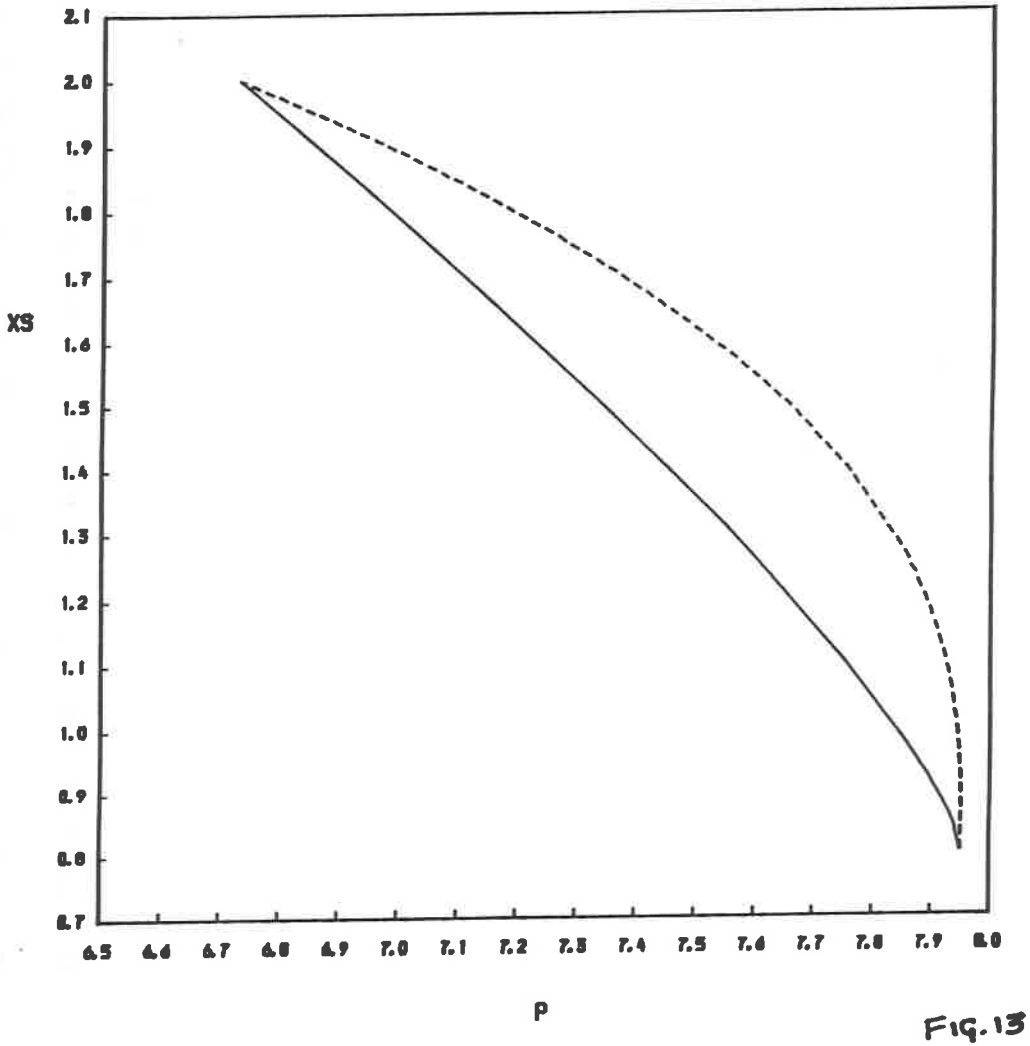
XS
2.1
2.0
1.9
1.8
1.7
1.6
1.5
1.4
1.3
1.2
1.1
1.0
0.9
0.8
0.7
6.5
6.6
6.7
6.8
6.9
7.0
7.1
7.2
7.3
7.4
7.5
7.6
7.7
7.8
7.9
8.0
P

Fig. 13

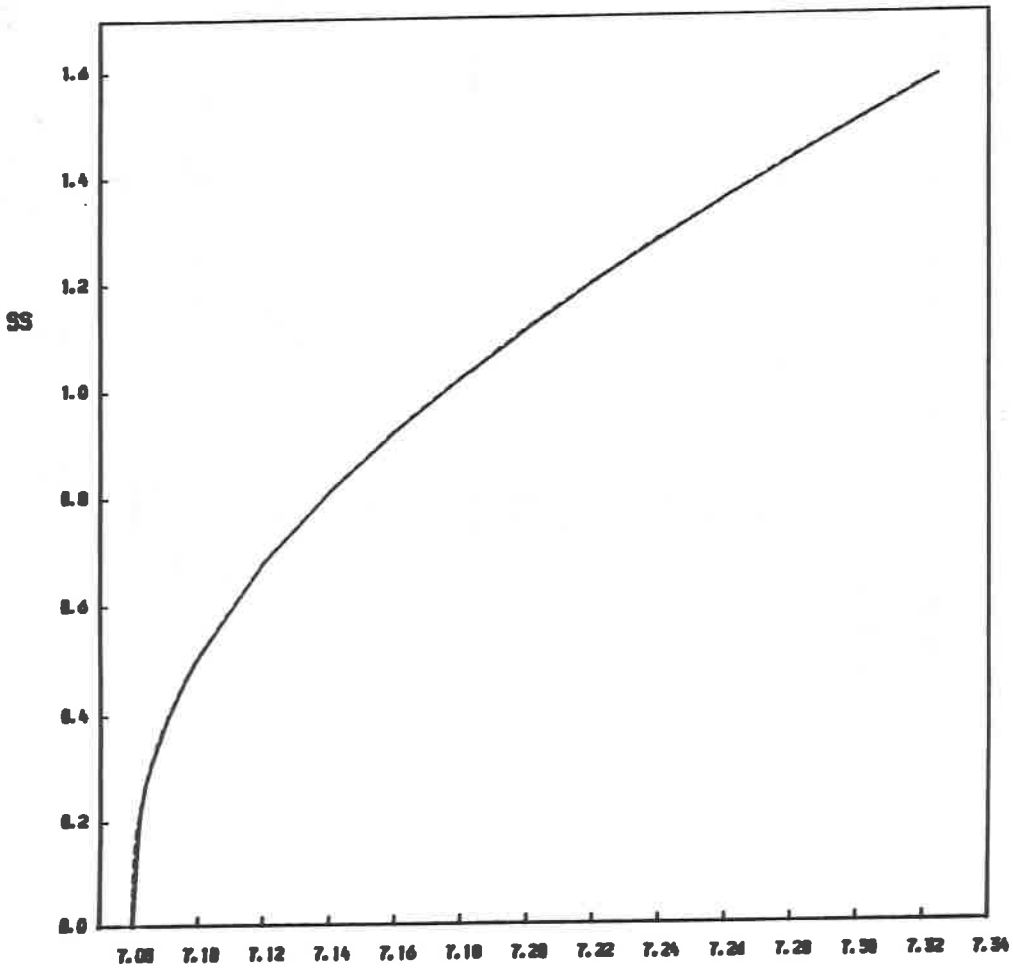
SS
1.6
1.4
1.2
1.0
0.8
0.6
0.4
0.2
0.0
7.08
7.10
7.12
7.14
7.16
7.18
7.20
7.22
7.24
7.26
7.28
7.30
7.32
7.34

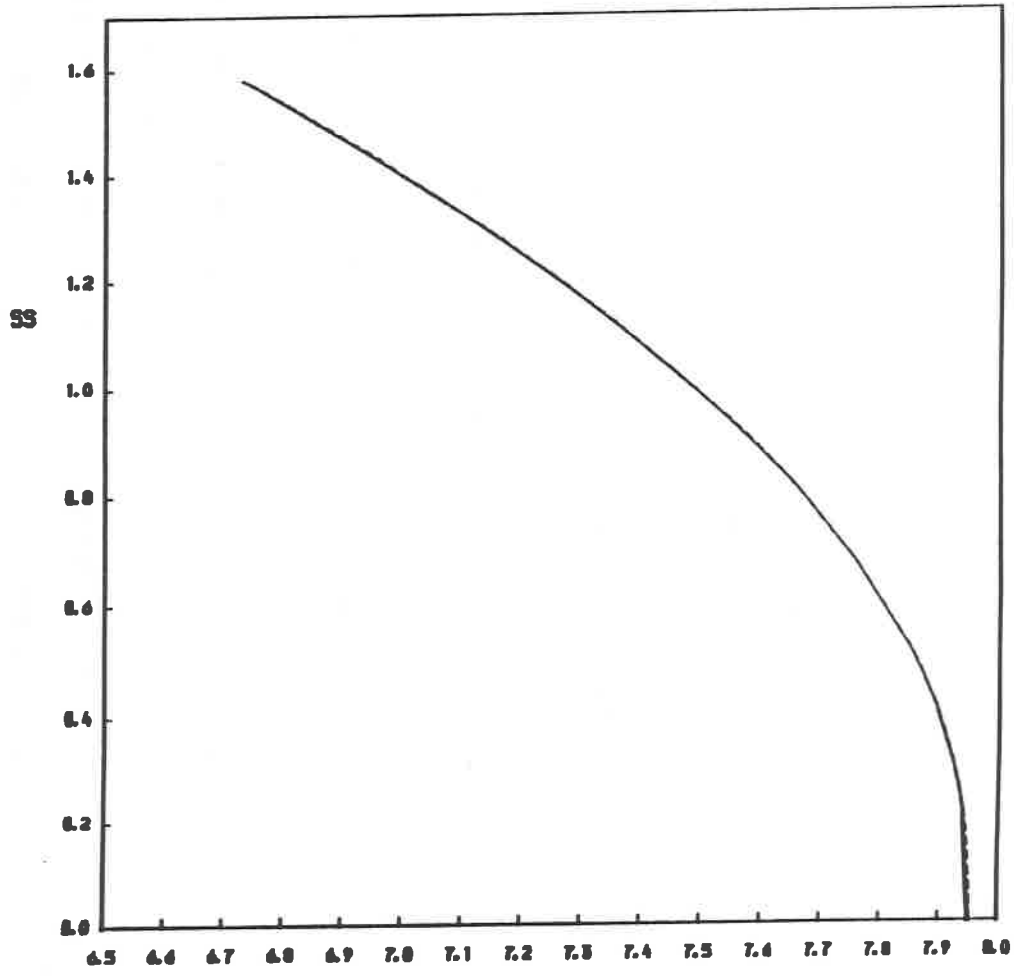
SS
1.6
1.4
1.2
1.0
0.8
0.6
0.4
0.2
0.0
6.5
6.6
6.7
6.8
6.9
7.0
7.1
7.2
7.3
7.4
7.5
7.6
7.7
7.8
7.9
8.0

A quadratic diffuser

The relationship between the nozzle outlet entropy, thus pressure, and the resulting shock position and strength is now investigated for shock flow through a nozzle as before consisting of a linear entry section (3.7a) but now with a quadratically varying diffuser, i.e.

$$\text{ENTRY SECTION} \quad : \quad A(x) = 1.1 - (x/8) \qquad [0.0 \leq x \leq 0.8] \tag{3.57}$$

$$\text{EXHAUST SECTION} \quad : \quad A(x) = (0.1/0.72)\,(x - 0.8)^2 + 1.0 \;, \quad [0.8 \leq x \leq 2.0]$$

(see FIG.15). The quasi one-dimensional approximation to a shock flow is now defined by (3.1) - (3.6), (3.57) and (3.8) - (3.11) together with the outlet entropy value which, as (3.57) is defined such that (3.8) and thus (3.10) and (3.11) still hold, lies in the range (3.26); the corresponding pressure range is then again (3.30). The relationships between the above quantities are shown in FIGS.13,14 but are now denoted by the broken line.

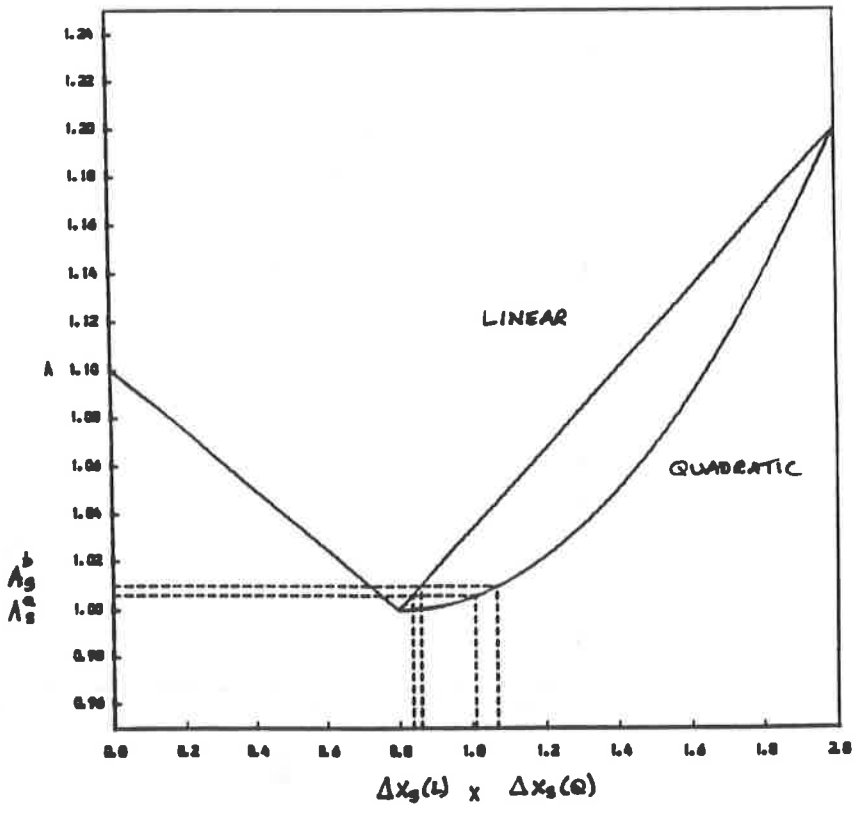

FIG. 15

The shock position will, by definition of the flow, lie at the same location as for the linear diffuser at the limits of the outlet entropy range (3.26) (see FIG.13*i*) and pressure range (3.30) (see FIG.13*ii*).

There is though a noticeably large increase in the rate of change of the position of the shock front, with respect to either flow variable, near the throat. This may be explained on first noting that the mass flow shock value Q_s is fixed for given flow constants at inlet, h and η_+, and outlet, h and η_-, being simply the intersection of the respective $P(Q,h,\eta)$ graphs. Hence, from (2.2), there exists a corresponding unique cross-sectional area, A_s, in a diffuser at which the shock must lie

$$A_s = \frac{C\, A_e}{Q_s} \,. \tag{3.58}$$

Then on considering a suitable pair of outlet entropy values, from (3.26), that are close to η_+, here

$$\eta^a = 7.082 \times 10^4$$

and (3.59)

$$\eta^b = 7.084 \times 10^4 \,,$$

then for each the resulting shock must, from (3.58), lie at the locations where

$$A_s^a = 1.006$$

and (3.60)

$$A_s^b = 1.01 \,.$$

The placing of ordinates on FIG.15, for each diffuser shape, at both of (3.60) then clearly shows the increase in the rate of change of the shock position near the throat in the quadratic diffuser, $\Delta x_s(Q)$, compared to that for the linear form, $\Delta x_s(L)$, i.e.

$$\Delta x_s(Q) >> \Delta x_s(L) \ . \qquad (3.61)$$

Note that the same argument may be applied, by assigning a pair of η_- values close to η_D, to explain the reduction in the positional rate of change of the shock on approaching the nozzle outlet.

Now, having established that for a given value η_- (thus pressure p_o^{sf}) the shock value Q_s is fixed, we may deduce that the corresponding shock strength (1.28), as shown by FIGS.14*i*,*ii*, is also fixed. This is because the quantities required to define (1.28), i.e. the pressures p_+ and p_-, may be found from Q_s alone by deriving the full graphs $p(Q,h,\eta_+)$ and $p(Q,h,\eta_-)$ on a common axis (see FIG.16) and placing an ordinate at this value; this process being independent of a particular flow.

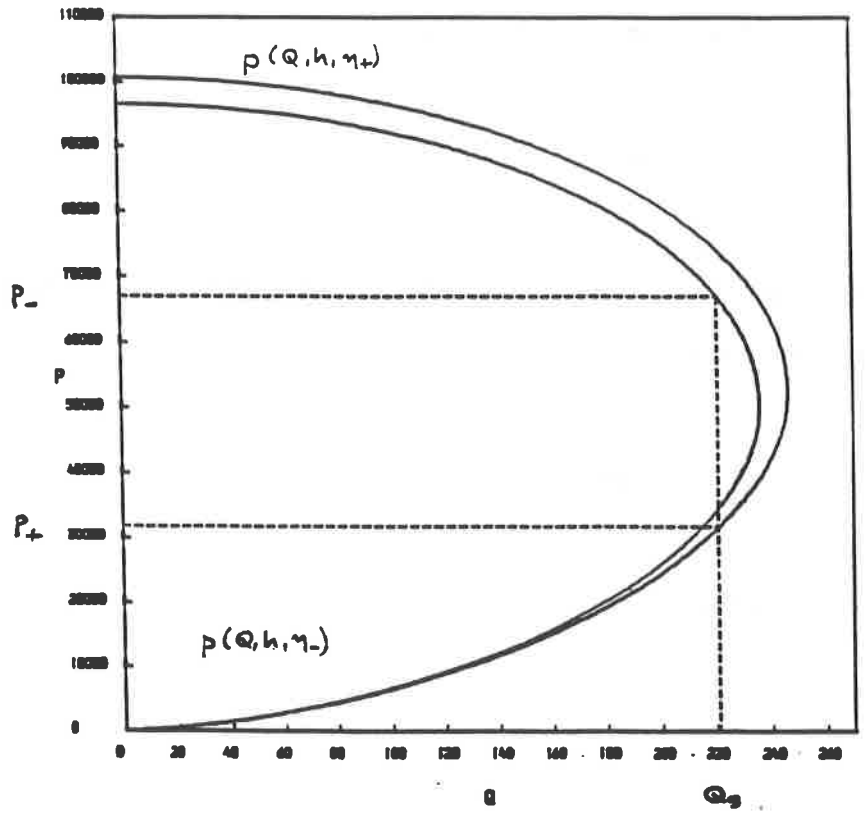

FIG.16

SECTION FOUR : A NUMERICAL FORMULATION OF SHOCK FLOW IN A DE-LAVAL NOZZLE

In this section a stationary principle is derived that is equivalent to the conditions (2.6) - (2.14) defining quasi one-dimensional shock flow in a de-Laval nozzle. A numerical 'shock fitting' method is then formulated from the stationary principle for the approximate solution on an adaptive grid of the fluid speed in a shock flow.

The particular shock flow to be considered is that defined by (3.1) - (3.11) and (3.31). This will allow a comparison between the numerical solution with the 'exact' parameterization that has been determined for this flow in §3 and thus give an idea of the relative accuracy of the numerical method. It is hoped that the solution obtained will possess two qualities. The position of the shock front in the diffuser must be accurately located and the representation of the continuous flow in the remainder of the solution domain, in particular around the nozzle throat, must also be sufficiently accurate. It is found that the critical factor in achieving these aims is the development of an efficient algorithm to determine an initial approximation to the shock flow.

4.1 A STATIONARY PRINCIPLE FOR SHOCK FLOW

The equations defining the quasi one-dimensional approximation to shock flow in the nozzle are, recall, considered to hold in a fixed domain, D, which represents the nozzle axis. Let ϕ and ψ be undetermined functions of position and define a functional $I = I(\underline{z})$ by

$$I = \int_0^{x_s} [\, Q\, v + p(v,h,\eta_+) + \phi \frac{d}{dx}(Q\, A)\,]\, dx +$$

$$\int_{x_s}^{d} [\, Q\, v + p(v,h,\eta_-) + \psi \frac{d}{dx}(Q\, A)\,]\, dx\ , \qquad (4.1)$$

where

$$\underline{z} = (\, Q\ ,\ v\ ,\ \phi\ ,\ \psi\,)\ , \qquad (4.2)$$

and $x_s \in (0,d)$ for the present case is considered as fixed, d being the domain length. The function $p(v,h,\eta)$ is that given by (3.27), in which here the flow constants h, η_+ and η_- have been retained for clarity.

Now consider small, arbitrary variations of the arguments of I. The functional (4.1) is stationary with respect to the variations if and only if its first variation, δI, is zero, i.e.

$$\delta I = \delta \left[\int_0^{x_s} [\, Q\, v + p(v,h,\eta_+) + \phi \frac{d}{dx}(Q\, A)\,]\, dx + \right.$$

$$\left. \int_{x_s}^{d} [\, Q\, v + p(v,h,\eta_-) + \psi \frac{d}{dx}(Q\, A)\,]\, dx \right] = 0\ , \qquad (4.3)$$

which may, by extending the theory of [5], be written explicitly as

$$\delta I = \int_0^{x_s} \left[\delta Q \left(v - A \frac{d\phi}{dx} \right) + \delta v \left(Q + \frac{dp}{dx} \right) + \delta\phi \left(\frac{d}{dx} (Q\ A) \right) \right] dx +$$

$$\int_{x_s}^{d} \left[\delta Q \left(v - A \frac{d\psi}{dx} \right) + \delta v \left(Q + \frac{dp}{dx} \right) + \delta\psi \left(\frac{d}{dx} (Q\ A) \right) \right] dx = 0, \tag{4.4}$$

where it is assumed that at $x = 0$, $x = x_s$ and $x = d$ we have $\delta Q = 0$. The natural conditions of the stationary principle (4.3) are therefore, on the domain $[0\ ,\ x_s]$

$$\delta Q \ : \ v = A \frac{d\phi}{dx} , \tag{4.5}$$

$$\delta v \ : \ Q = - \frac{dp}{dv} , \tag{4.6}$$

$$\delta\phi \ : \ \frac{d}{dx} (Q\ A) = 0 , \tag{4.7}$$

and on the domain $[x_s\ ,\ d]$

$$\delta Q \ : \ v = A \frac{d\psi}{dx} , \tag{4.8}$$

$$\delta v \ : \ Q = - \frac{dp}{dv} , \tag{4.9}$$

$$\delta\psi \ : \ \frac{d}{dx} (Q\ A) = 0 , \tag{4.10}$$

where (4.6) and (4.9) may be written in the form

$$Q = \rho\, v \ , \tag{4.11}$$

by definition of the pressure gradient

$$p'(v) = - \rho\, v \ . \tag{4.12}$$

We now consider allowing x_s in (4.1) to vary, giving an additional contribution to the first variation (4.4), and therefore a corresponding natural condition of (4.3) which arises from

$$\int_{x_s}^{x_s + \delta x_s} [\, Q\, v + p(v,h,\eta_+) + \phi\, \overline{\frac{d}{dx}}\, (Q\, A)\,]\, dx +$$

$$\int_{x_s + \delta x_s}^{x_s} [\, Q\, v + p(v,h,\eta_-) + \phi\, \overline{\frac{d}{dx}}\, (Q\, A)\,]\, dx \ , \tag{4.13}$$

where δx_s denotes the variation in x_s. By the (first) mean value theorem for integrals the natural condition arising from the variation δx_s is easily seen to be

$$[Q\, v + p(v,h,\eta_+) + \phi\, \overline{\frac{d}{dx}}\, (Q\, A)]\, \Big|_{x_s^+} - [Q\, v + p(v,h,\eta_-) + \phi\, \overline{\frac{d}{dx}}\, (Q\, A)]\, \Big|_{x_s^-} = 0, \tag{4.14}$$

where the superscripts '+' and '−' denote the shock when approached from the front and back respectively. The full set of natural conditions of the principle $\delta I = 0$, when x_s is varied in addition to the other

variables, therefore consists of (4.5) - (4.10) and (4.14).

The natural conditions (4.7) and (4.10) may be imposed as constraints on the variations in (4.3) on ensuring that mass conservation is satisfied by assigning

$$Q(x)\, A(x) = \text{CONSTANT} = C\, A_e \ , \tag{4.15}$$

which in the present case is chosen in accordance with (2.2). The new stationary principle obtained is therefore

$$\delta J \equiv \delta \left[\int_0^{x_s} \left[\frac{C\, A_e}{A(x)}\, v + p(v,h,\eta_+) \right] dx + \int_{x_s}^{d} \left[\frac{C\, A_e}{A(x)}\, v + p(v,h,\eta_-) \right] dx \right] = 0 \tag{4.16}$$

with the natural conditions of (4.16) being (4.5), (4.6), (4.8), (4.9) and from (4.14)

$$\left[\frac{C\, A_e}{A(x)}\, v + p(v,h,\eta_+) \right] \Big|_{x_s^+} - \left[\frac{C\, A_e}{A(x)}\, v + p(v,h,\eta_-) \right] \Big|_{x_s^-} = 0 \ . \tag{4.17}$$

Then, from the definition of flow stress (1.10)

$$P = p + \rho\, v^2 = p + Q\, v \ , \tag{4.18}$$

in magnitude (4.17) may be written

$$P(v,h,\eta_+) \Big|_{x_s^+} - P(v,h,\eta_-) \Big|_{x_s^-} = [P]_-^+ = 0 \ , \tag{4.19}$$

which is the shock condition (2.10b).

Hence, having satisfied the conservation of mass by (2.2) and of total energy by definition of (4.16), we may conclude that the stationary principle δJ is equivalent to the conditions defining the quasi one-dimensional approximation to shock flow. The principle δJ may be applied to the present motion by substitution of the nozzle area variation (3.7), the entry mass flow rate to the central streamline (3.10), the entry nozzle cross-sectional area (3.8a) and the flow constants at inlet, (3.2) and (3.3) and at outlet, (3.2) and (3.31). Note finally that J depends only on the fluid speed and the position of the shock front and may now be used to develop a numerical method for the approximate fluid speed variation in the shock flow.

4.2 THE NUMERICAL FORMULATION

A numerical method is now formulated on an adaptive grid. The nodal amplitudes $a_i = a_i(k)$, $i = 1(1)N$, with a_{M+} and a_{M-} the amplitudes of the node, M, representing the shock front, when approached from the front and the back respectively, and the corresponding nodal positions $s_i = s_i(k)$, $i = 1(1)N$, are unknown at each iteration level, k, towards the final approximate solution. A semi-discrete approximation to the fluid speed is now sought

$$\bar{v}(x,k) = \sum_{i=1}^{N} a_i(k)\, \alpha_i(x,\underline{s}(k)) \ , \qquad (4.20)$$

where $\underline{s}(k)$ is the nodal position vector and $\alpha_i = \alpha_i(x,\underline{s}(k))$, $i = 1(1)N$, are piece-wise linear basis functions of local compact support (see

[6]). In particular

$$\alpha_M = \begin{cases} \alpha_{M+} = \dfrac{x - s_{M-1}}{s_M - s_{M-1}} & [\ s_{M-1} \leq x \leq s_M\ ] \\ \alpha_{M-} = \dfrac{s_{M+1} - x}{s_{M+1} - s_M} & [\ s_M \leq x \leq s_{M+1}\ ] \end{cases} . \qquad (4.21)$$

The substitution of the approximation to the fluid speed (4.20), in which nodes are constrained to remain fixed at the domain extremes

$$s_1 = 0.0$$

and (4.22)

$$s_N = d\ ,$$

into the functional, J, underlying the stationary principle (4.16) yields now a function, L, of the unknown coefficients

$$L = L(\ a_1 \ \ldots\ a_N\ ,\ s_2 \ \ldots\ s_{N-1}\ )\ , \qquad (4.23)$$

where $L = J(\bar{v})$ is defined by

$$L = \int_0^{s_M} [\ \frac{C\ A_e}{A(x)}\ \bar{v} + p(\bar{v},h,\eta_+)\ ]\ dx + \int_{s_M}^{d} [\ \frac{C\ A_e}{A(x)}\ \bar{v} + p(\bar{v},h,\eta_-)\ ]\ dx\ . \qquad (4.24)$$

Therefore making the function (4.24) stationary gives an approximation to the stationary point of the functional J; the conditions for this are simply

$$\frac{\partial L}{\partial a_i} = 0 , \qquad [i = 1(1)N] \tag{4.25}$$

and

$$\frac{\partial L}{\partial s_i} = 0 \qquad [i = 2(1)N-1] \tag{4.26}$$

The partial derivatives (4.25) may be written, using (4.12), as

$$\int_D \left[\frac{C A_e}{A(x)} - \rho \bar{v} \right] \alpha_i \, dx = 0 , \qquad [i = 1(1)N, \; i \neq M] \tag{4.27}$$

and

$$\left.\begin{aligned} &\int_0^{s_M} \left[\frac{C A_e}{A(x)} - \rho \bar{v} \right] \alpha_{M+} \, dx = 0 \\ &\int_{s_M}^{d} \left[\frac{C A_e}{A(x)} - \rho \bar{v} \right] \alpha_{M-} \, dx = 0 \end{aligned}\right] ; \tag{4.28}$$

similarly those in (4.26) become

$$\int_D \left[\frac{C A_e}{A(x)} - \rho \bar{v} \right] \beta_i \, dx = 0 , \qquad [i = 1(1)N, \; i \neq M] \tag{4.29}$$

and

$$\left[\frac{C A_e}{A(x)} \bar{v} + p(\bar{v},h,\eta_+) \right] \Big|_{M^+} - \left[\frac{C A_e}{A(x)} \bar{v} + p(\bar{v},h,\eta_-) \right] \Big|_{M^-}$$

$$\int_0^{s_M} \left[\frac{C A_e}{A(x)} - \rho(v,h,\eta_+) \bar{v} \right] [a_{M+} - a_{M-1} / s_M - s_{M-1}] \alpha_{M+} \, dx -$$

$$\int_{s_M}^{d} \left[\frac{C A_e}{A(x)} - \rho(v,h,\eta_-) \bar{v} \right] [a_{M+1} - a_{M-} / s_{M+1} - s_M] \alpha_{M-} \, dx = 0 . \tag{4.30}$$

where $\vartheta_i = \vartheta_i(x, \underline{a}(k), \underline{s}(k))$ is a second type of basis function (see [6]), $a(\underline{k})$ being the vector of unknown nodal amplitudes. The pressure function in (4.30) is, recall, defined by (3.27) and to enable the solution for the approximate fluid speed in the nozzle to be found the density term in (4.27) - (4.29) is replaced by (see [1])

$$\rho(v,h,\eta) = \eta^{(1/1-\gamma)} \left[((\gamma - 1)/\gamma) \left(h - (v^2/2) \right) \right]^{(1/\gamma-1)} . \quad (4.31)$$

Now by noting (4.28) and also that

$$\bar{v} \Big|_{M^+} = a_{M+}$$

and (4.32)

$$\bar{v} \Big|_{M^-} = a_{M-} ,$$

then (4.30) may be written as

$$\left[\frac{C\, A_e}{A(x)}\, a_{M+} + p(a_{M+},h,\eta_+) \right] - \left[\frac{C\, A_e}{A(x)}\, a_{M-} + p(a_{M-},h,\eta_-) \right] = 0 , \quad (4.33)$$

which is the discrete form of the shock condition $[P]_-^+ = 0$.

The conditions (4.25) - (4.26) then take the form of a system of non-linear equations, at each iteration level k, for the unknown parameters; the system may be written in the form of the inner products

$$\langle \varphi , \psi \rangle_1 = \int_0^{s_M} \phi \, \psi \, dx$$

and (4.34)

$$\langle \phi , \psi \rangle_2 = \int_{s_M}^{d} \phi \, \psi \, dx ,$$

as

$$\left\langle \frac{C A_e}{A(x)} - \rho(\bar{v},h,\eta_+) \, \bar{v} , \alpha_1 \right\rangle_1 = 0 ,$$

$$\left.\begin{aligned} \left\langle \frac{C A_e}{A(x)} - \rho(\bar{v},h,\eta_+) \, \bar{v} , \alpha_i \right\rangle_1 &= 0 \\ \left\langle \frac{C A_e}{A(x)} - \rho(\bar{v},h,\eta_+) \, \bar{v} , \beta_i \right\rangle_1 &= 0 \end{aligned}\right\} , \quad [i = 2(1)M-1]$$

$$\left\langle \frac{C A_e}{A(x)} - \rho(\bar{v},h,\eta_+) \, \bar{v} , \alpha_{M+} \right\rangle_1 = 0 ,$$

$$\left[\frac{C A_e}{A(x)} a_{M+} + p(a_{M+},h,\eta_+) \right] - \left[\frac{C A_e}{A(x)} a_{M-} + p(a_{M-},h,\eta_-) \right] = 0 ,$$

$$\left\langle \frac{C A_e}{A(x)} - \rho(\bar{v},h,\eta_-) \, \bar{v} , \alpha_{M-} \right\rangle_2 = 0 ,$$

$$\left.\begin{aligned} \left\langle \frac{C A_e}{A(x)} - \rho(\bar{v},h,\eta_-) \, \bar{v} , \alpha_i \right\rangle_2 &= 0 \\ \left\langle \frac{C A_e}{A(x)} - \rho(\bar{v},h,\eta_-) \, \bar{v} , \beta_i \right\rangle_2 &= 0 \end{aligned}\right\} , \quad [i = M+1(1)N-1]$$

$$\left\langle \frac{C A_e}{A(x)} - \rho(\bar{v},h,\eta_-) \, \bar{v} , \alpha_N \right\rangle_2 = 0 . \qquad (4.35)$$

On solution of the system (4.35) the function (4.24) has been made stationary with respect to its parameters, representing the given shock flow discretely, and determining an approximation to the fluid speed in the motion.

4.3 THE SOLUTION ALGORITHM

The solution algorithm to be presented here is a direct extension, modified for shock flow, of that used for the numerical solution of a continuous quasi one-dimensional nozzle flow on an adaptive grid found in [6].

1. The preliminary solution stage

In terms of the quasi one-dimensional approximation to shock flow it is stated in §2.4, and employed in the shock flow parameterization of §3.2, that a shock front intervenes between a nozzle transition flow, defined by (3.2) and (3.3), and an independent subsonic cone section flow defined by (3.2) and (3.31). In this stage of the solution process a piece-wise linear approximation to the fluid speed in each of these flows is obtained on a fixed uniform grid (the full formulation may be found in [5]).

The approximation to the nozzle transition flow

The approximation to the fluid speed in a nozzle transition flow, $\underline{a}_T^*$, defined by (3.1) -(3.11), when solving on the numerical grid found in TABLE 2, is shown in FIG.17 (from [5]) and denoted 'TF'. Note that there are twenty-one nodes employed in the discrete solution and that

the amplitude of the node at the nozzle throat location (3.9) has been overwritten by the critical fluid speed value (3.5).

TRANSITION FLOW IN A DE-LAVAL NOZZLE			
FIXED UNIFORM GRID - TWENTY ONE NODES			
NODE NUMBER	NODE POSITION	NODE NUMBER	NODE POSITION
1	0.0	11	1.0
2	0.1	12	1.1
3	0.2	13	1.2
4	0.3	14	1.3
5	0.4	15	1.4
6	0.5	16	1.5
7	0.6	17	1.6
8	0.7	18	1.7
9	0.8	19	1.8
10	0.9	20	1.9
		21	2.0

TABLE TWO

The approximation to the subsonic cone section flow

It has been established in §3.2 that the subsonic cone section flow defined by (3.2) and (3.31) may only exist in a portion of the complete nozzle diffuser (3.7b), in the present case from (3.37) and (3.38) this being

$$1.0575 \leq x \leq 2.0 \ . \tag{4.36}$$

To enable the definition of an initial shock position in the numerical method the cone section flow is therefore solved on a fixed uniform grid defined by the portion of the grid in TABLE 2 that lies in the domain (4.36) (see TABLE 3).

SUBSONIC FLOW IN A DIVERGING CONE SECTION			
FIXED UNIFORM GRID - TEN NODES			
NODE NUMBER	NODE POSITION	NODE NUMBER	NODE POSITION
1	1.1	6	1.6
2	1.2	7	1.7
3	1.3	8	1.8
4	1.4	9	1.9
5	1.5	10	2.0

TABLE THREE

The cone section flow to be solved numerically is therefore defined on the domain

$$1.1 \leq x \leq 2.0 \ , \tag{4.37}$$

with the area variation, $A^{cn}(x)$, from (3.7b), being

$$A^{cn}(x) = (2.6/3.0) + (x/6) \ , \tag{4.38}$$

where x lies in (4.37). The cross-sectional area of the cone at entry, A_e^{cn}, is therefore

$$A_e^{cn} = (2.6/3.0) + (1.1/6.0) = 1.05 \ , \tag{4.39}$$

and at exit, A_o^{cn} where

$$A_o^{cn} = 1.2 \ . \tag{4.40}$$

The mass flow boundary condition at inlet, from (2.2) and (4.39), is now

$$Q_e^{cn} = \frac{C\ A_e}{A_e^{cn}} = 234.582 \ , \qquad (4.41)$$

and, from (3.11), at outlet

$$Q_o^{cn} = 205.259 \ . \qquad (4.42)$$

The approximation to the fluid speed in the subsonic cone section flow, $\underline{a}_C^*$, defined by (4.37) - (4.42) is shown in FIG.17 and is denoted 'DF'.

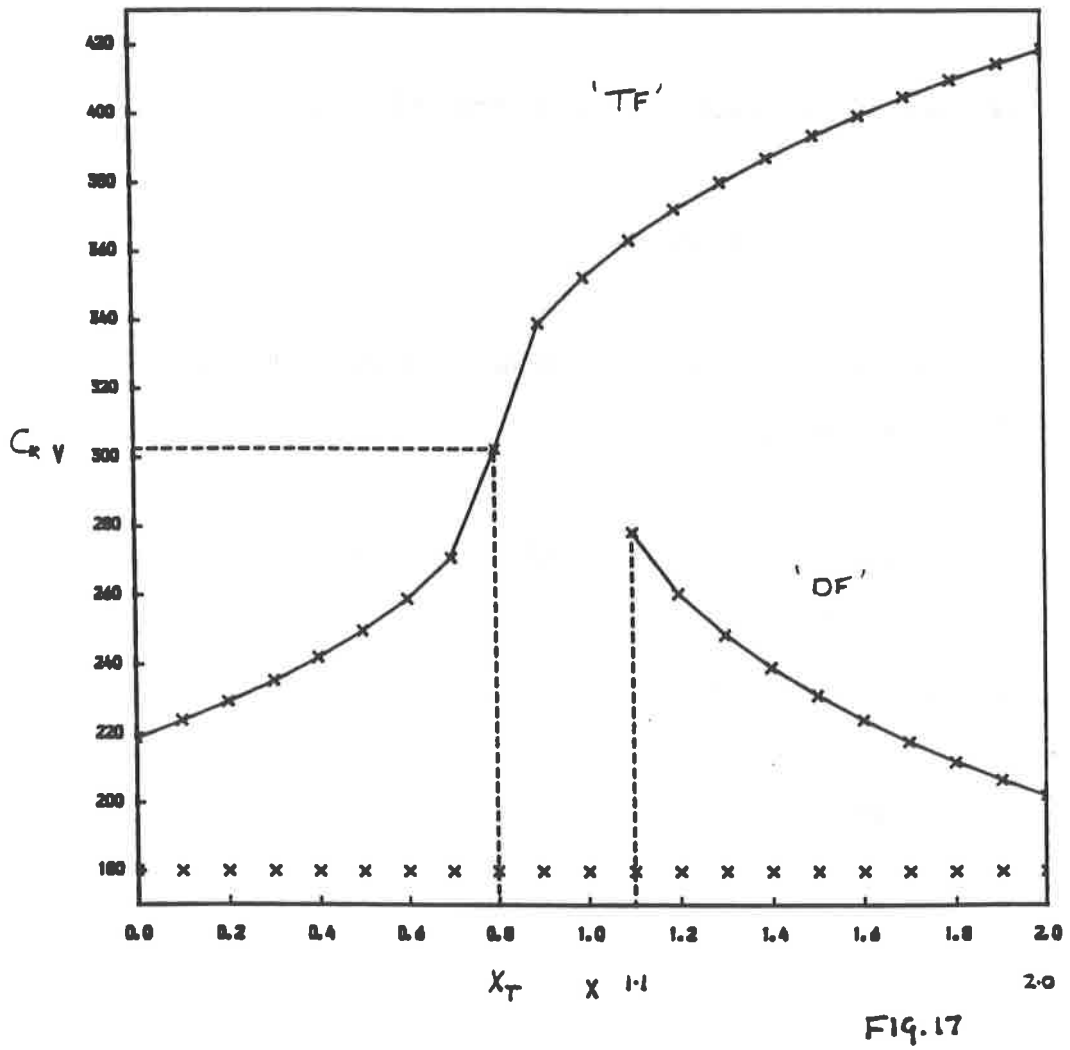

FIG.17

2. The initial shock flow approximation

The aim of this stage of the solution is to determine an initial position for the shock front in the diffuser, and thus subsequently to obtain an initial numerical approximation to the shock flow. The equation system (4.35) is first de-coupled and reformulated in a local manner.

The local formulation

A set of local basis functions

$$\phi_{iL} = \phi_{iL}(x,\underline{s}(k)) \qquad [\ i = 2(1)N\ ]$$

and (4.43)

$$\phi_{iR} = \phi_{iR}(x,\underline{s}(k)) \qquad [\ i = 1(1)N-1\ ]$$

are defined in a node-wise manner (see [6]), where note

$$\phi_{ML} = \phi_{ML}(x,\underline{s}(k)) = \alpha_{M+}$$

and (4.44)

$$\phi_{MR} = \phi_{MR}(x,\underline{s}(k)) = \alpha_{M-} \ .$$

The resulting system of equations, in terms of the inner products (4.34) is now

$$\left\langle \frac{C\,A_e}{A(x)} - \rho(\bar{v},h,\eta_+)\,\bar{v}\ ,\ \varphi_{1R} \right\rangle_1 = 0\ . \tag{4.45}$$

$$\underline{F}_i = \begin{cases} F_{iL} \equiv \left\langle \dfrac{C\,A_e}{A(x)} - \rho(\bar{v},h,\eta_+)\,\bar{v}\ ,\ \varphi_{iL} \right\rangle_1 = 0\ , \\ \qquad\qquad [\ i = 2(1)M-1\ ] \\ F_{iR} \equiv \left\langle \dfrac{C\,A_e}{A(x)} - \rho(\bar{v},h,\eta_+)\,\bar{v}\ ,\ \phi_{iR} \right\rangle_1 = 0\ , \end{cases} \tag{4.46}$$

$$\underline{F}_s = \begin{cases} F_s^1 \equiv [C\,A_e\,a_{M+} + p(a_{M+},h,\eta_+)] - [C\,A_e\,a_{M-} + p(a_{M-},h,\eta_-)] = 0\ , \\ F_s^2 \equiv \left\langle \dfrac{C\,A_e}{A(x)} - \rho(\bar{v},h,\eta_+)\,\bar{v}\ ,\ \phi_{ML} \right\rangle_1 = 0\ , \\ F_s^3 \equiv \left\langle \dfrac{C\,A_e}{A(x)} - \rho(\bar{v},h,\eta_-)\,\bar{v}\ ,\ \phi_{MR} \right\rangle_2 = 0\ , \end{cases} \tag{4.47}$$

$$\underline{F}_i = \begin{cases} F_{iL} \equiv \left\langle \dfrac{C\,A_e}{A(x)} - \rho(\bar{v},h,\eta_-)\,\bar{v}\ ,\ \phi_{iL} \right\rangle_2 = 0\ , \\ \qquad\qquad [\ i = M+1(1)N-1\ ] \\ F_{iR} \equiv \left\langle \dfrac{C\,A_e}{A(x)} - \rho(\bar{v},h,\eta_-)\,\bar{v}\ ,\ \phi_{iR} \right\rangle_2 = 0\ , \end{cases} \tag{4.48}$$

$$\left\langle \frac{C\,A_e}{A(x)} - \rho(\bar{v},h,\eta_-)\,\bar{v}\ ,\ \phi_{NL} \right\rangle_2 = 0\ . \tag{4.49}$$

Providing that the local gradients of the approximate solution m_{i-1} and m_i, where

$$m_i = \frac{a_{i+1} - a_i}{s_{i+1} - s_i}\ , \tag{4.50}$$

are not equal then the system equations in (4.35) corresponding to the interior nodes may be written as 2 x 2 non-overlapping pairs. i.e. (4.46) and (4.48). In a similar manner the system equations corresponding to the node, M, representing the shock front may now be written as a local shock node system (4.47).

The initial location of the shock front

The manner in which the approximation to the fluid speed in both the transition flow and cone section flow has been obtained will provide, excluding that at outlet, a choice of, here nine, initial shock positions, s_M^o, (see FIG.18) lying at the grid locations in TABLE 3. Subsequent to the assignment of s_M^o the resulting initial approximation to the fluid speed in the shock flow, $\underline{w}^o$

$$\underline{w}^o = (a_1^*, s_1, \ldots, a_{M+}^*, s_M^o, a_{M-}^*, \ldots, a_N^*, s_N) \qquad (4.51)$$

will consist of the approximation to the transition flow from inlet to M^+ and to the cone section flow from M^- to outlet, i.e.

$$\underline{a}^* = \begin{bmatrix} \underline{a}_T^* & [i = 1(1)M^+] \\ \underline{a}_C^* & [i = M^-(1)N] \end{bmatrix}, \qquad (4.52)$$

where the nodal positions are defined in TABLE 2.

The local nature of the present discrete formulation allows the nodes to be updated in any order; particular use of this flexibility is made in the following algorithm to determine s_M^o.

(a) The initial solution vector, $\underline{w}^o$, resulting from assignment of a particular s_M^o is fixed except for the amplitudes, a_{M+}^o and a_{M-}^o, and position, s_M^o, of the shock node.

(b) The parameters a_{M+}^o, a_{M-}^o and s_M^o are updated once by solving the local shock node system (4.47) by a three variable form of Newton's method

$$\underbrace{\begin{bmatrix} A & B & C \\ D & 0 & E \\ 0 & F & G \end{bmatrix}}_{[J]_s} \underbrace{\begin{bmatrix} \delta a_{M+}^o \\ \delta a_{M-}^o \\ \delta s_M^o \end{bmatrix}}_{\delta \underline{w}_s} = - \underbrace{\begin{bmatrix} F_s^1 \\ F_s^2 \\ F_s^3 \end{bmatrix}}_{\underline{F}_s} , \tag{4.53}$$

where the vector of local parameter updates, $\delta \underline{w}_s$, consists of the updates in amplitude of the shock nodes, δa_{M+}^o and δa_{M-}^o, and the update in the shock position, δs_M^o; the elements of the Jacobian matrix $[J]_s$ are

$$A = \frac{\partial F_s^1}{\partial a_{M+}^o} , \quad B = \frac{\partial F_s^1}{\partial a_{M-}^o} , \quad C = \frac{\partial F_s^1}{\partial s_M^o} , \quad D = \frac{\partial F_s^2}{\partial a_{M+}^o} , \quad E = \frac{\partial F_s^2}{\partial s_M^o} , \quad F = \frac{\partial F_s^3}{\partial a_{M-}^o} , \quad G = \frac{\partial F_s^3}{\partial s_M^o} , \tag{4.54}$$

where note that δ is used here in a totally different sense to that of the variations in §4.1. The local system (4.53) is solved by forming the augmented matrix and reducing to row echelon form to give (assuming that $G \neq (A\ F/B\ D)\ (C\ D/A - E)$)

$$\delta s_M^o = \frac{(A\ F/B\ D)\ (D\ F_s^1/A - F_s^2) - F_s^3}{G + (A\ F/B\ D)(E - (C\ D/A))} , \tag{4.55}$$

and subsequently by back substitution

$$\delta a^{o}_{M-} = \frac{F^{2}_{s} - (D\, F^{1}_{s}/A) + \delta s^{o}_{M}\,(E - (C\, D/A))}{(B\, D/A)} \qquad (4.56)$$

and

$$\delta a^{o}_{M+} = -\frac{(F^{3}_{s} + \delta a^{o}_{M-}\, B + \delta s^{o}_{M}\, C)}{A} \; . \qquad (4.57)$$

The amplitudes and positions of the shock nodes may now be updated according to

$$\begin{aligned} a_{M+} &= a^{o}_{M+} + \delta a^{o}_{M+} \; , \\ a_{M-} &= a^{o}_{M-} + \delta a^{o}_{M-} \end{aligned}$$

and (4.58)

$$s^{o}_{M} = s^{o}_{M} + \delta s^{o}_{M} \; .$$

(c) The direction and magnitude of the update to the shock position (4.55) is first computed for the s^{o}_{M} closest to outlet, in the present case (see TABLE 3)

$$s^{o}_{M} = 1.9 \; , \qquad (4.59)$$

and subsequently for the remaining positions decreasing in magnitude [7] until for, say, $s^{o}_{m_1}$ and $s^{o}_{M_2}$, with $s^{o}_{M_1} > s^{o}_{M_2}$, we find that

$$\delta s^{o}_{M_1} < 0.0$$

and (4.60)

$$\delta s^{o}_{M_2} > 0.0 \; ,$$

(this process is illustrated for the present case in FIG.18)

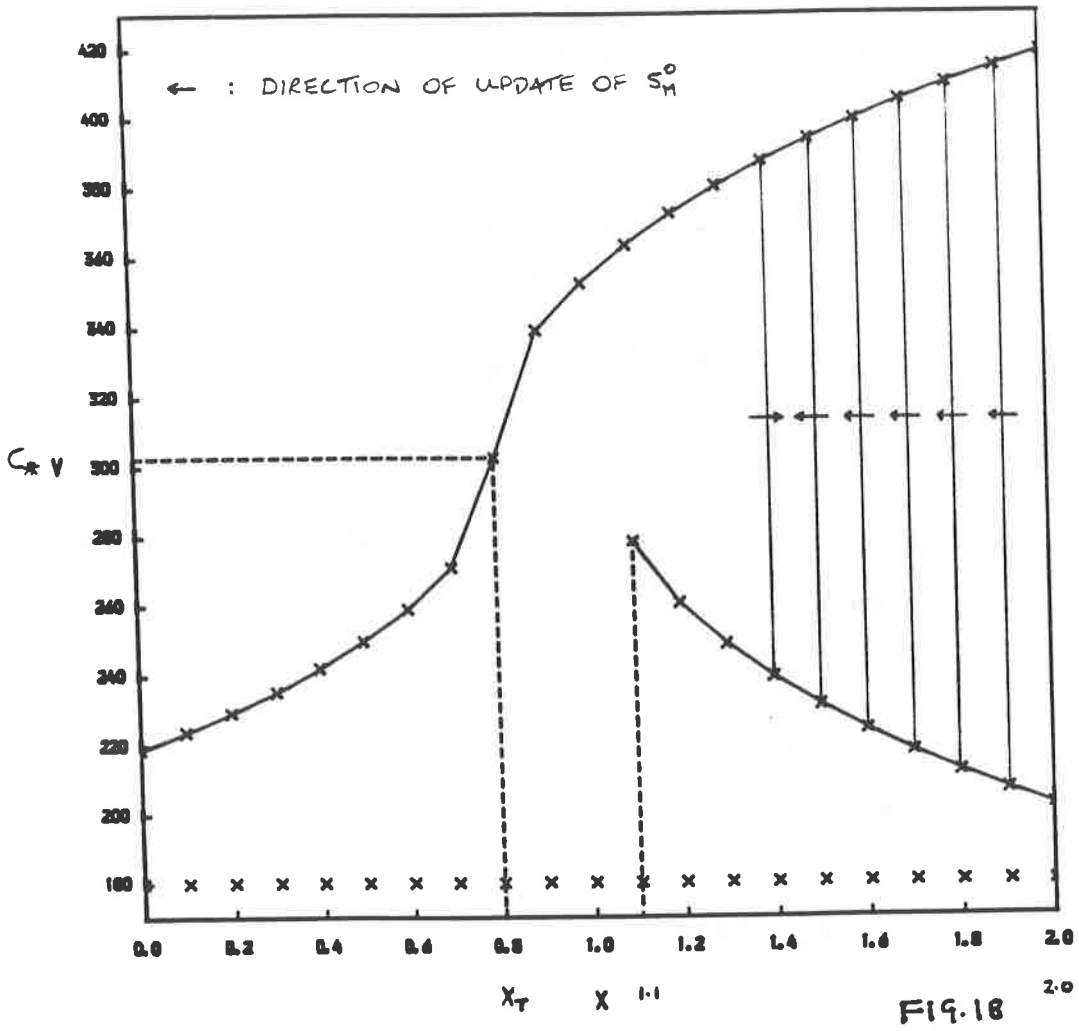

(d) The minimum absolute update of those in (4.60), $\delta s^o_{M_3}$, i.e.

$$\delta s^o_{M_3} = \text{MIN} \mid \delta s^o_{M_1} , \delta s^o_{M_2} \mid , \tag{4.61}$$

is then computed and the shock position associated with that minimum update is employed as the initial approximation to the position of the shock front in the numerical method, in the present case

$$s^o_M = 1.5 . \tag{4.62}$$

The resulting initial approximation to the fluid speed, $\underline{w}^o$, in the full shock flow may now, as stated previously, be obtained by combining the approximations to the transition flow and the cone section flow about s^o_M (see (4.51) and (4.52)), this is illustrated here in FIG.19.

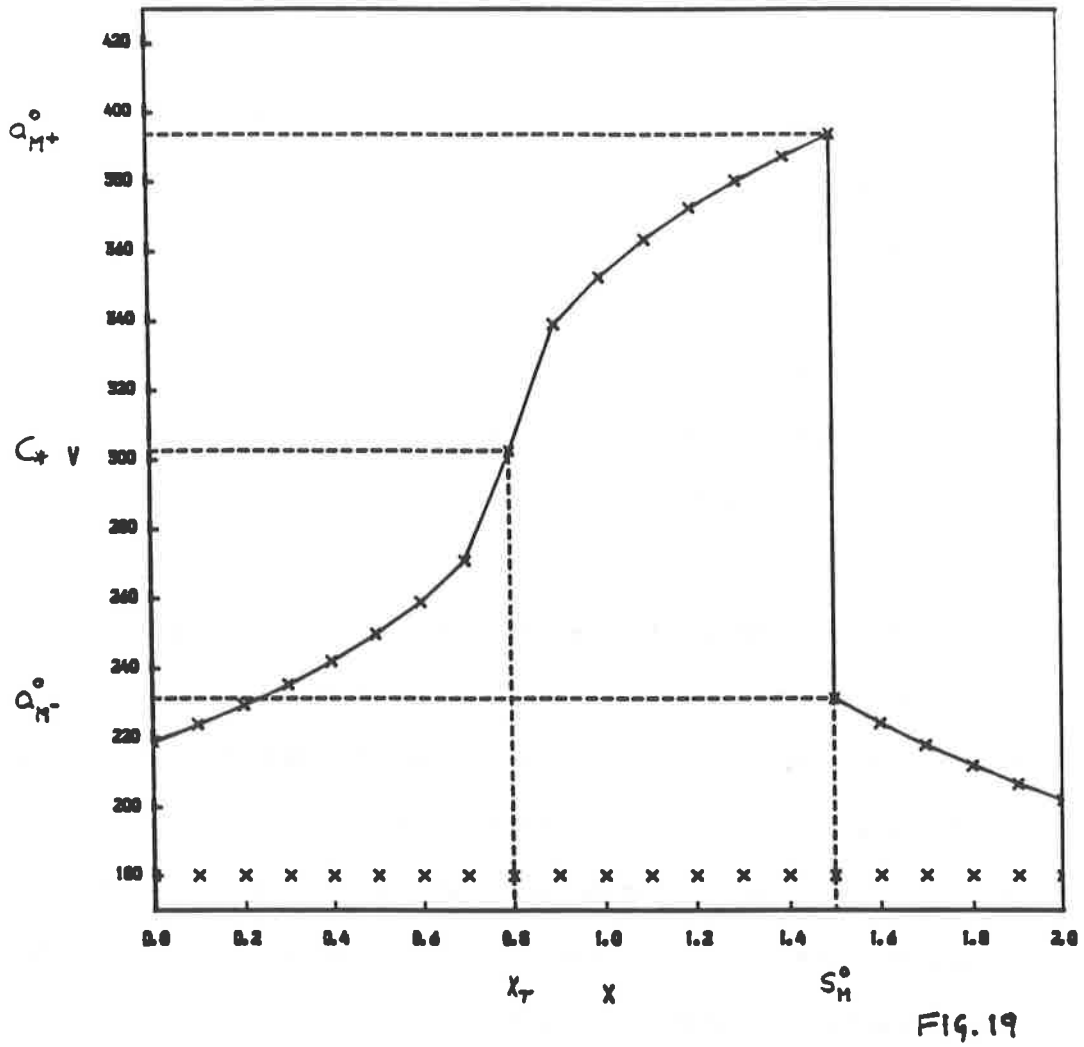

FIG. 19

3. The adaptive grid solution stage

The manner in which the initial approximation to the shock flow (4.51) has been computed means that prior to any displacement of the nodes it will contain approximately the correct solution curvature in the regions of continuous flow, which should minimize the appearance of ill-conditioning in the adaptive grid solution. The nodes throughout the complete solution domain are now updated individually, consistent with the local formulation (4.45) - (4.49), by an analagous process to that used in the adaptive grid solution of a continuous nozzle flow presented in [6].

(*i*) The amplitudes, a_1^k and a_N^k, of the nodes at the domain extremes (4.22), where here d = 2.0 (3.1), are first updated once by solving the associated equations (4.45) and (4.49) using the simple single variable Newton iterative algorithm (see [6]).

(*ii*) The amplitudes, a_{M+}^k and a_{M-}^k, and position, s_M^k, of the shock node are then updated once by solving the local shock node system (4.47) in the manner outlined in (b).

(*iii*) The remaining interior nodes, in both regions of continuous flow in the solution domain, are finally updated using a similar process to that used for (*ii*). The present solution vector, $\underline{w}^k$, is fixed except for the amplitude, $\underline{a}_i^k$, and position, $\underline{s}_i^k$, of the particular node under consideration. These parameters are then updated by solving the associated local equation system, (4.46) or (4.48), by a two variable form of Newton's method (see [6]).

Note that the node initially at the nozzle throat location is constrained to remain fixed in this position (3.9) and additionally in amplitude at the critical fluid speed (3.5); this is as a result of the comparative study of the possible treatments for this node presented in [6]. Subsequent to the above updating process it may then be said that N local iterations ('one sweep') have been performed. The adaptive grid stage of the solution is said to of converged to the final approximate solution vector, $\underline{w}^n$, when the maximum absolute nodal displacement for a complete sweep, including that of the shock node, is less than the specified tolerance

$$\text{MAX} \mid \delta s_i^k \mid < 0.0001 \ . \qquad [i = 2(1)N-1] \tag{4.63}$$

4.4 THE SHOCK FLOW SOLUTION

The approximation to the fluid speed in the shock flow defined by (3.1) - (3.11) and (3.31) is shown in FIG.20, with the final solution grid denoted on the figure by a series of x's; the exact nodal positions may be found in TABLE 4 in which the shock node is denoted †.

SHOCK FLOW IN A DE-LAVAL NOZZLE			
FINAL SOLUTION GRID - TWENTY ONE NODES			
NODE NUMBER	NODE POSITION	NODE NUMBER	NODE POSITION
1	0.0000	12	0.9166
2	0.1899	13	1.0147
3	0.3547	14	1.1415
4	0.4944	15	1.2970
5	0.6087	16	1.4808 †
6	0.6969	17	1.5685
7	0.7588	18	1.6643
8	0.7938	19	1.7681
9	0.8000	20	1.8800
10	0.8079	21	2.0000
11	0.8475		

TABLE FOUR

The numerical shock position, s_M^n, in the present case lies at

$$s_M^n = 1.4808 \ , \tag{4.64}$$

which, noting that the corresponding 'exact' shock position (3.48) is computed to within (3.49), may be said, after rounding, to be accurate to three decimal places.

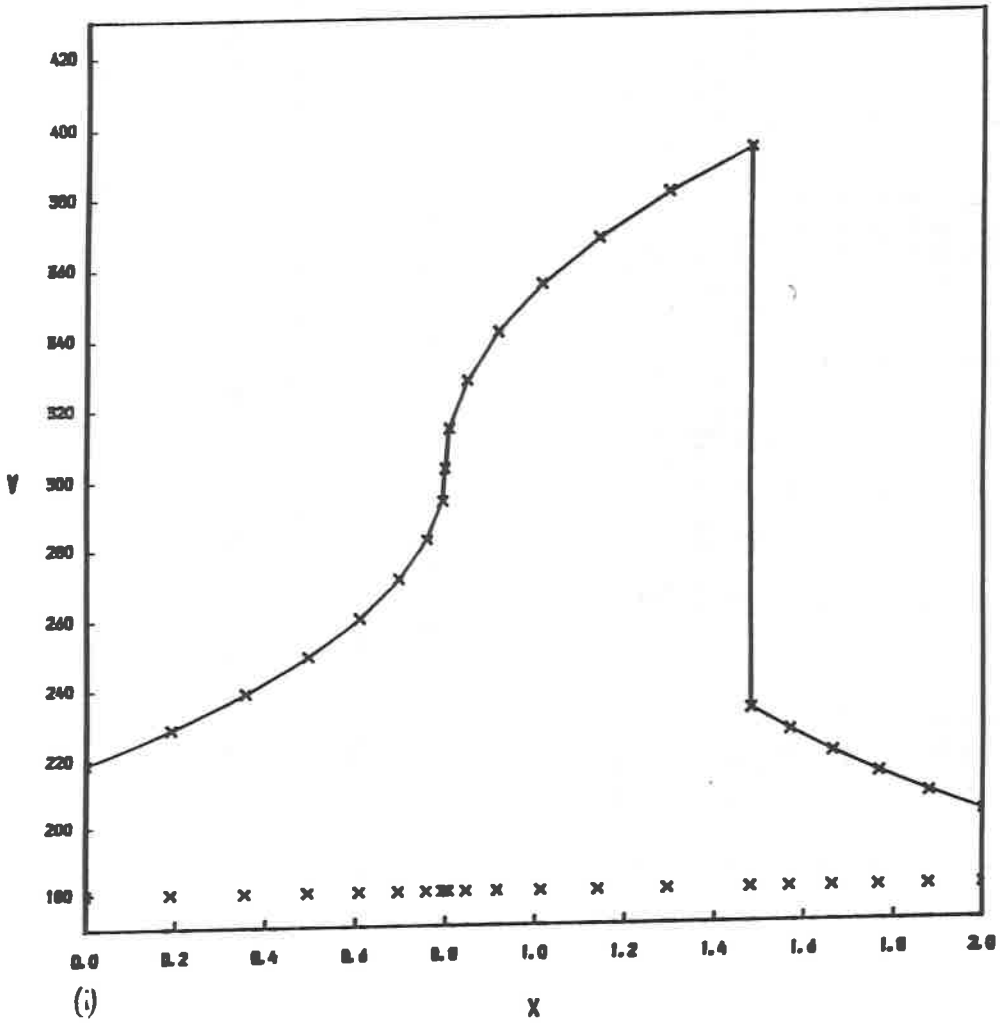
420
400
380
360
340
320
300
280
260
240
220
200
180
Y
0.0
0.2
0.4
0.6
0.8
1.0
1.2
1.4
1.6
1.8
2.0
X

(i)

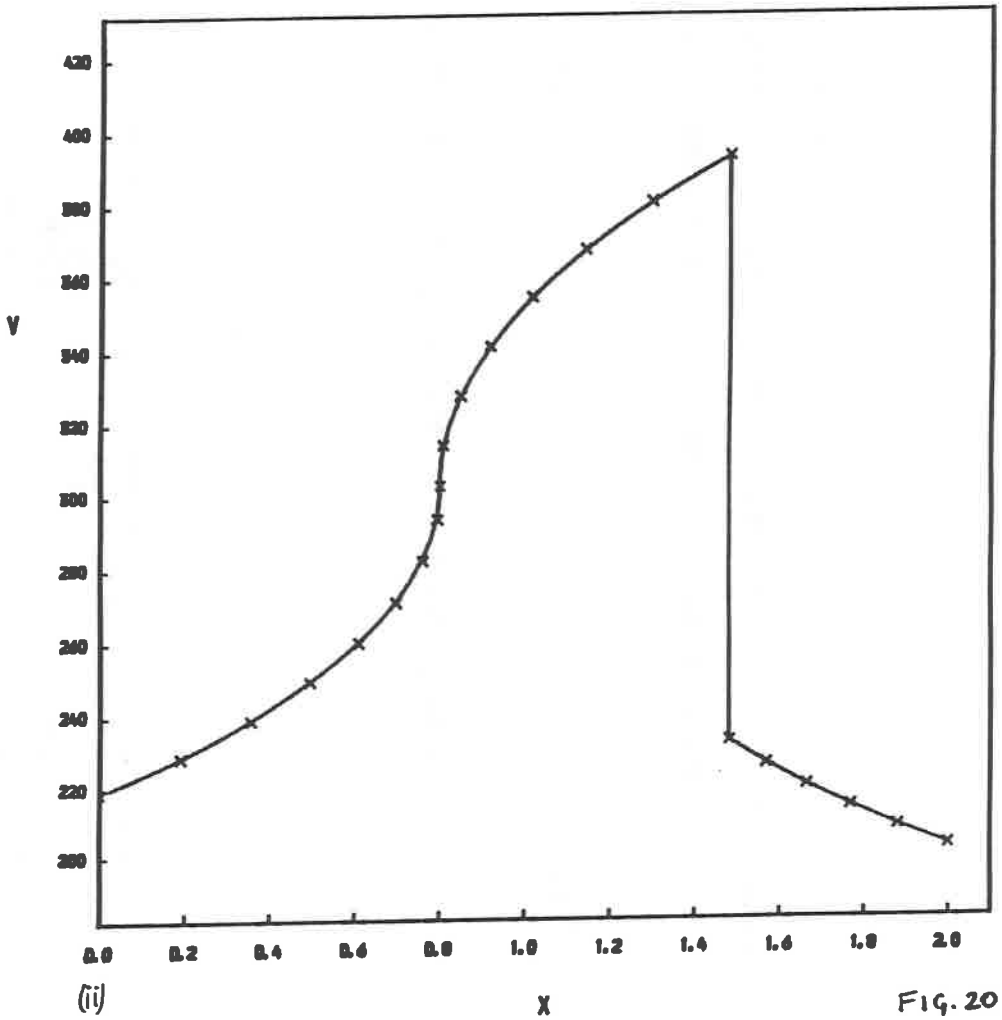
420
400
380
360
340
320
300
280
260
240
220
200
Y
0.0
0.2
0.4
0.6
0.8
1.0
1.2
1.4
1.6
1.8
2.0
X

(ii)

FIG. 20

The accuracy of the numerical solution may be examined by plotting the nodal values and the exact parameterization (FIG.10) on a common axis (see FIG.20*ii*). It is apparent that considerable accuracy has been achieved in the modeling of the present shock flow, notably in the representation of the relatively large rates of fluid speed change in the continuous flow around the throat, and of course in the fitting of the shock front.

The detailed features of the adaptive grid stage of the numerical solution may be obtained by inspection of the nodal displacements and amplitudes at the current solution vector, $\underline{w}^k$, for each level k. The trajectories of the nodes, in both cases, are thus shown in FIG.21.

The uniform displacement of the nodes in the solution domain at the initial approximation to the shock flow, $\underline{w}^o$, (from FIG.19) may be seen in FIG.21*i*. The displacement of the shock node, i.e. s_M^k, is denoted on this figure by a broken line, from which it is found that s_M^n (4.64) is attained roughly after only two sweeps; this is due to the efficiency of the algorithm used in computing the initial shock position (4.62). The total of 92 sweeps on the adaptive grid is therefore predominantly required to attain the representation of the continuous flow (as expected from [6]) to within the tolerance (4.63); note the node fixed at the nozzle throat (3.9). The amplitudes of the shock node, when approached from the front and back respectively, are indicated in FIG.21*ii* by a similar fine broken line which, corresponding to the displacements, become unchanged roughly after a couple of sweeps. The amplitude of the throat node, fixed at (3.5), is clearly shown and the coarse broken lines represent the variation in the amplitude of the nodes in the subsonic flow subsequent to the intervention of the shock front.

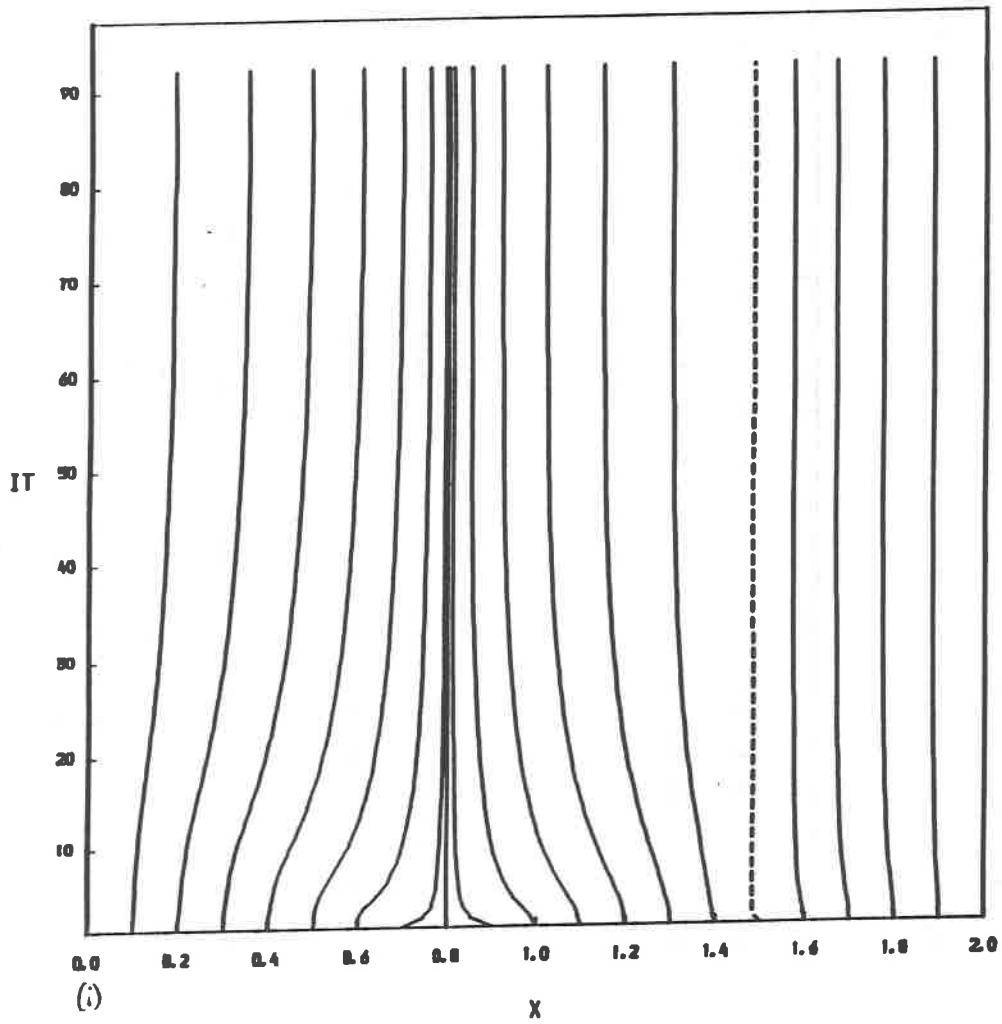
IT
X
0.0
0.2
0.4
0.6
0.8
1.0
1.2
1.4
1.6
1.8
2.0
10
20
30
40
50
60
70
80
90

(i)

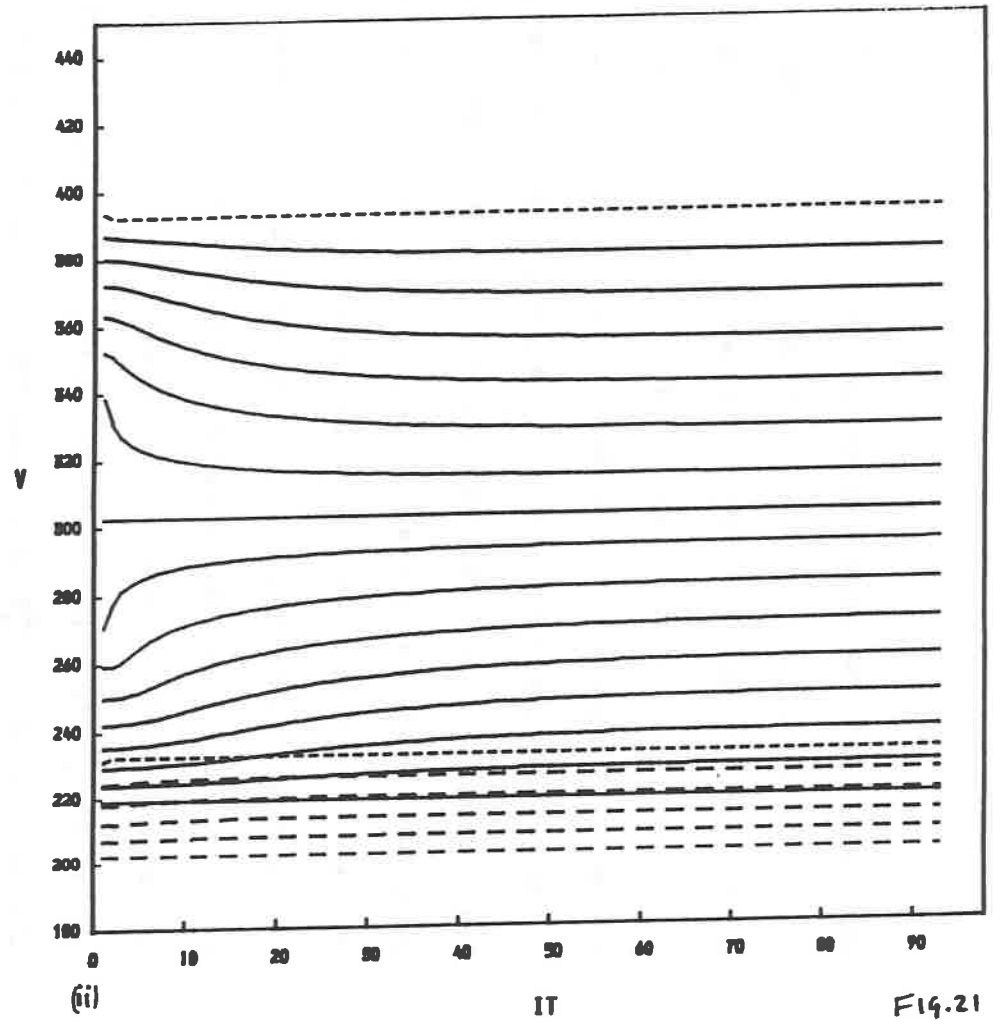
V
IT
180
200
220
240
260
280
300
320
340
360
380
400
420
440
0
10
20
30
40
50
60
70
80
90

(ii)

Fig.21

The magnitude of the jump in the fluid speed across the shock front may be computed from the amplitude of the shock node at entry to the shock front, a_{M+}, and exit, a_{M-}, in the numerical solution. Subsequently the algebraic relationships (3.27), (4.31) and (3.51) may be used to compute the jumps in the other flow variables (see TABLE 5).

THE SHOCK FRONT		
QUANTITY	JUMP MAGNITUDE	PERCENTAGE ERROR
v	- 159.731	0.137
p	+ 35334.088	0.137
ρ	+ 0.387	0.259
T	+ 49.720	0.155
	MAGNITUDE	
C_{shk}	1.687	0.119
S_{str}	1.114	0.270

TABLE FIVE

The percentage error in the fluid speed jump, between the numerical value and that in the exact parameterization (4.65), is seen (TABLE 5) to lead an error of the same order in the computed jump of the other flow variables (the imposed jump in entropy is of course exact). The magnitude of other significant quantities associated with the shock front may also be found from the algebraic relationships (see §3.3), in particular both the shock compression, C_{shk}, and strength, S_{str}, are again seen to have the same order error, in comparison with (3.55) and (3.56), as the speed jump.

4.5 THE NUMERICAL METHOD

The robustness and overall accuracy of the numerical method may be investigated by considering the relationship between the outlet entropy value and the resulting numerical shock position and strength (see TABLE 6) in comparison to the analagous relationship (TABLE 1) for the exact parameterization; these are presented graphically in FIG.22 where the numerical results are denoted by the broken graph and the 'exact' results by the full graph, the axial quantities are defined as in FIG.13.

ENTROPY $\times 10^4$	s_M^n	$s_M^n(E)$	S_{str}^n	$S_{str}^n(E)$
7.080	0.80053	0.125	0.038	-
7.082	0.83607	-	0.234	10.900
7.084	0.85830	-	0.303	10.989
7.086	0.87739	0.114	0.355	12.342
7.088	0.89474	0.224	0.398	13.068
7.090	0.91092	0.220	0.435	12.987
7.092	0.92624	0.108	0.469	13.012
7.094(*)	0.94089	0.213	0.500	13.636
7.096	0.95294	-	0.475	2.151
7.098	0.96640	-	0.498	2.469
7.100	0.97949	-	0.520	2.564
7.120	1.09714	-	0.686	1.180
7.140	1.20149	-	0.815	0.724
7.160	1.29872	-	0.925	0.434
7.180	1.39139	-	1.024	0.392
7.200	1.48084	-	1.114	0.270
7.220	1.56789	-	1.199	0.251
7.240	1.65309	-	1.279	0.235
7.260	1.73682	-	1.355	0.148
7.280	1.81936	-	1.428	0.211
7.300	1.90093	-	1.498	0.134
7.320	1.98170	-	1.566	0.128
7.3245	1.99978	-	1.581	0.127

TABLE SIX

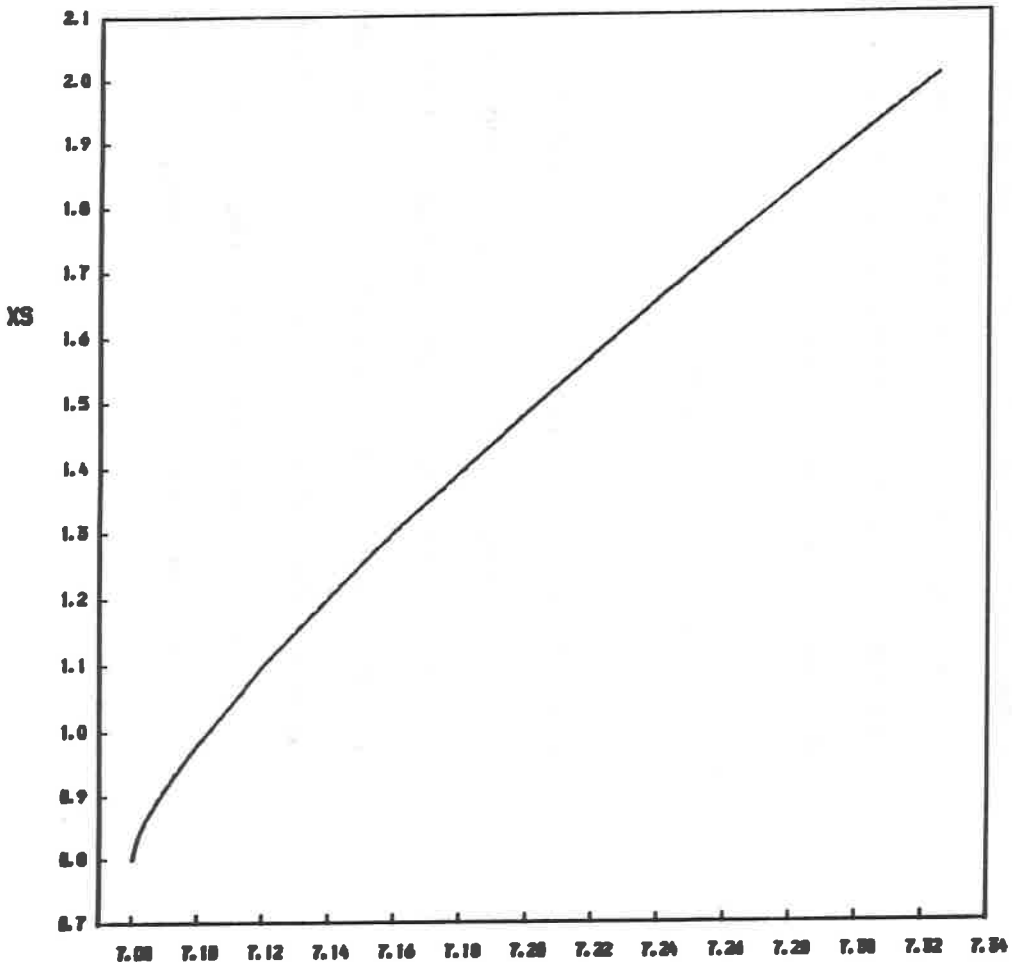
XS
2.1
2.0
1.9
1.8
1.7
1.6
1.5
1.4
1.3
1.2
1.1
1.0
0.9
0.8
0.7
7.08
7.10
7.12
7.14
7.16
7.18
7.20
7.22
7.24
7.26
7.28
7.30
7.32
7.34

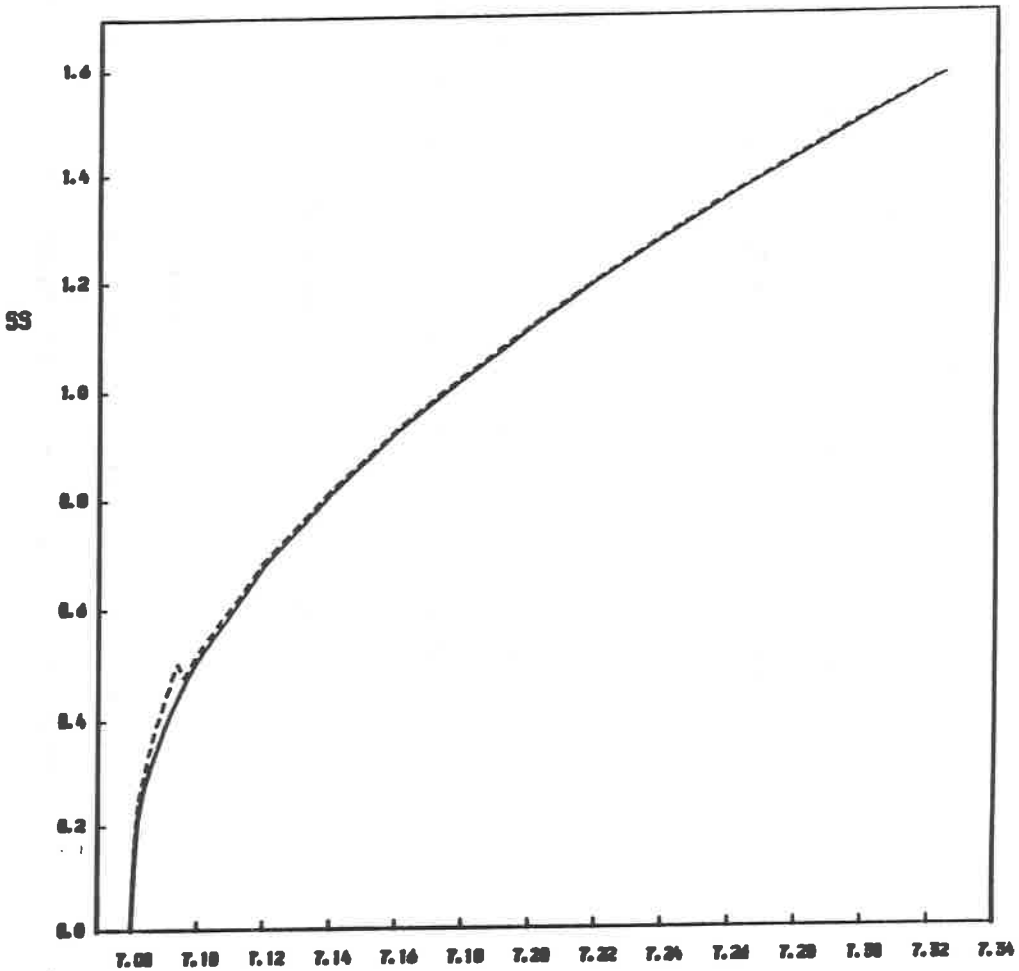
SS
1.6
1.4
1.2
1.0
0.8
0.6
0.4
0.2
0.0
7.08
7.10
7.12
7.14
7.16
7.18
7.20
7.22
7.24
7.26
7.28
7.30
7.32
7.34

A percentage error in the numerical shock position, $s_M^n(E)$, is only computed if s_M^n is not accurate to three decimal places, and it is then evaluated using the rounded value. Similarly the error in the numerical shock strength, $S_{str}^n(E)$, is computed using the value, S_{str}^n, given in TABLE 6.

The significant feature of the results in TABLE 6 and FIG.22 is the relatively poor fitting of the shock front by the numerical method if the outlet entropy value is prescribed in the range

$$7.086 \times 10^4 \leq \eta_- \leq 7.094 \times 10^4 \ . \qquad (4.65)$$

This inaccuracy is a consequence of the algorithm to determine the initial approximation to the position of the shock front (§4.3). The solution of the local shock system (4.47) in the adaptive grid stage depends directly on the neighbouring nodes to those in the shock front; if these are representative of the local curvature of the continuous flow then an accurate numerical shock position will result. In the case of an outlet entropy value of

$$\eta_- = 7.096 \times 10^4 \ , \qquad (4.66)$$

the initial shock position is assigned such that a node is always present between the shock nodes and the throat node, adequately (although note not accurately) representing the local curvature in that region throughout the adaptive grid stage (see FIG.23i), resulting in an accurate shock position (see TABLE 6). Conversely on prescription of a value η_- in the range (4.65) the initial shock position is chosen so that no such intermediate node exists, hence the continuous flow around

the throat is poorly represented (see FIG.23*ii* with η_- = 7.092), resulting in an inaccurate shock position (see TABLE 6). The inaccuracy will be reflected to a greater degree in the numerical shock strength because, due to the large rate of fluid speed change around the nozzle throat, an error in the shock position will produce considerable error in the amplitudes of the shock node, which are exactly the quantities required to compute S^n_{str} (see TABLE 6) (* note that for η_- = 7.094 a node has been deleted in the adaptive grid stage of the solution due to a linearity in the numerical approximation of the subsonic flow subsequent to the intervention of the shock front (see [6])).

Finally it is found from TABLE 6 that an accurate shock position is obtained when the expected shock is almost at the nozzle throat. This is because the shock node approached from the front and the throat node together are enough to represent adequately the intermediate fluid speed change. Note though that as a consequence of the extreme rate of fluid speed change in this region the numerical shock strength still has considerable error; in fact as a result of numerical error in the amplitudes of the shock node this occurs, although to a lesser degree, throughout the full range of shock flows in TABLE 6 (see FIG.22*ii*).

In summary an initial approximation to the shock flow is required that will consistently produce, not only a good first approximation to the position of the shock front, but more importantly an accurate representation, throughout the adaptive grid stage, of the regions of continuous flow, in particular around the nozzle throat.

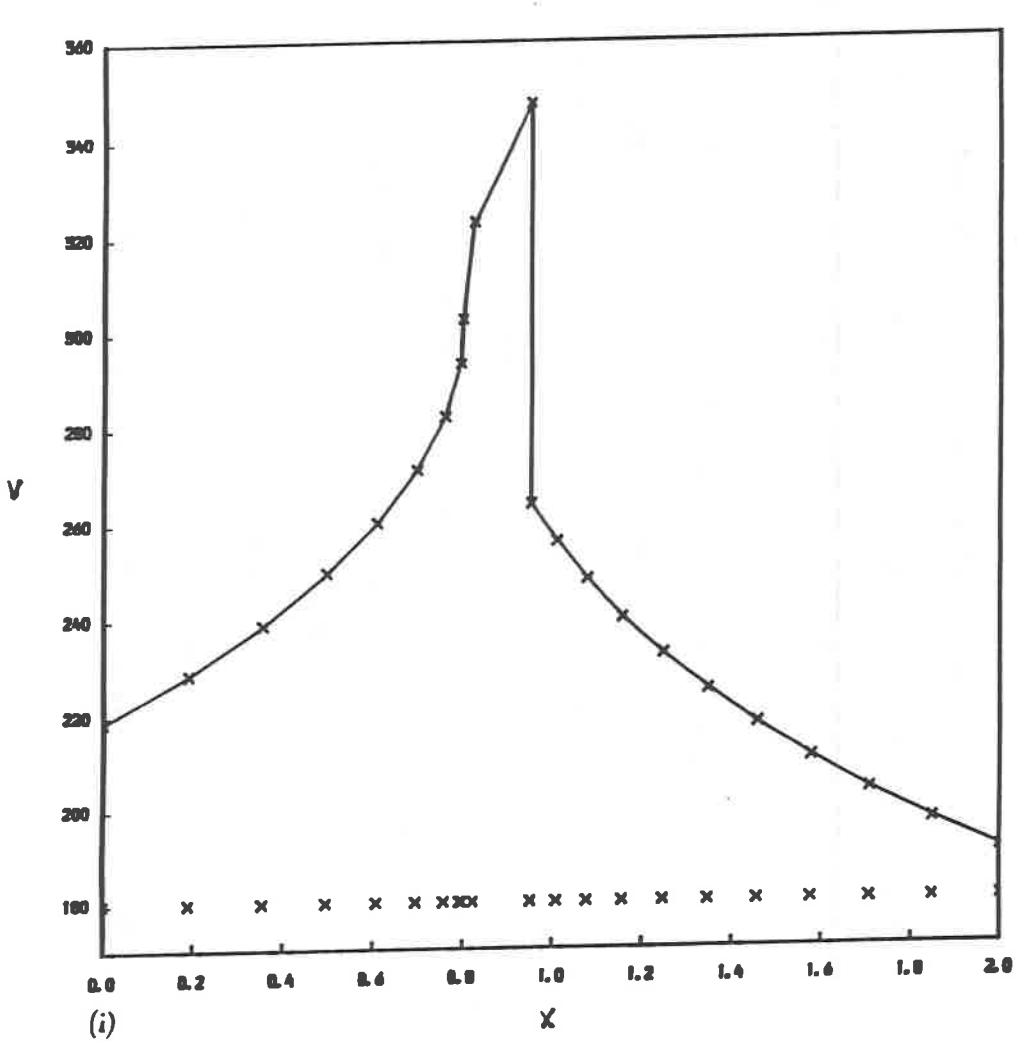

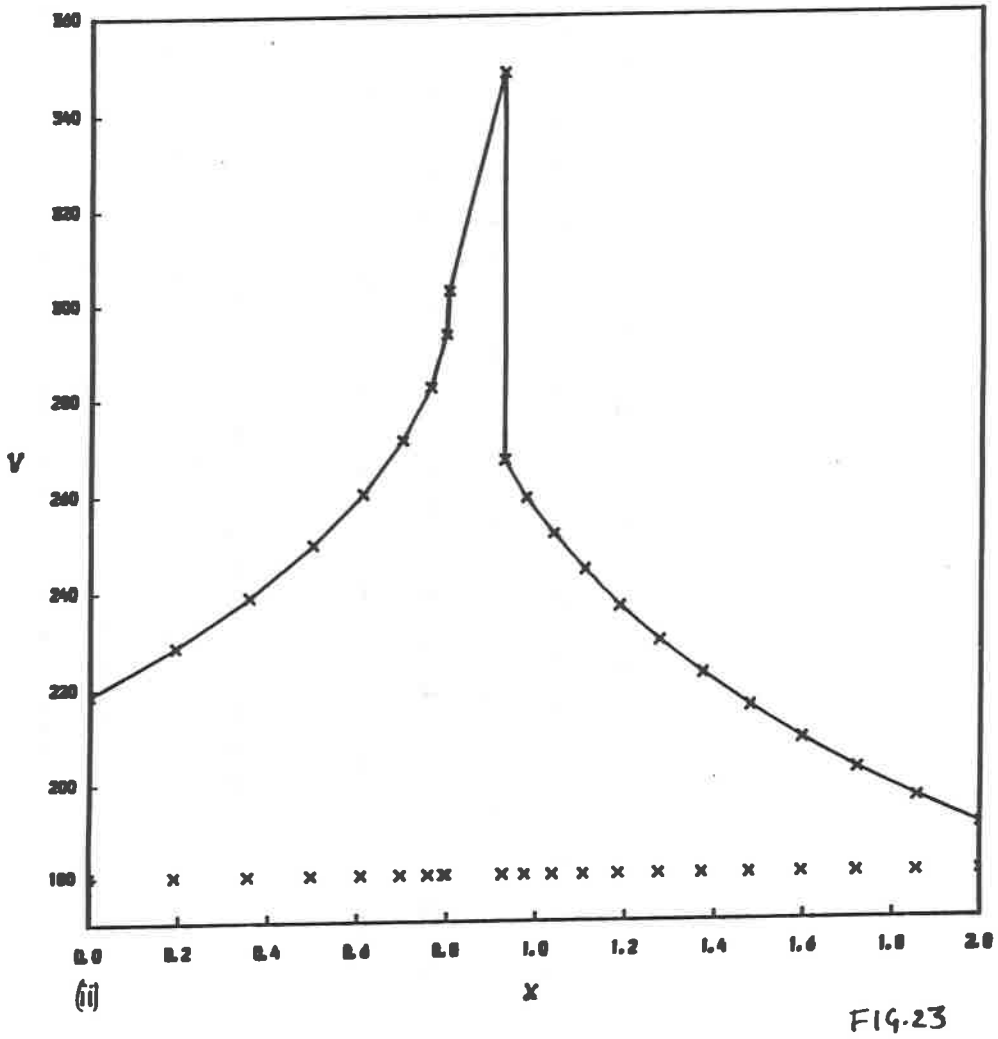

FIG.23

4.6 THE MODIFIED SOLUTION ALGORITHM

In the development of an algorithm for solution of the equation system (4.35) the numerical solution of several shock flows was obtained, again using a local reformulation, but with the initial position of the shock front lying at the diffuser outlet. The local system (4.47) was solved to update the shock nodes as in §4.3 (b), with nodes passing 'through' the shock front in a manner akin to Heath [9], and after one update a reasonable approximation to the exact shock position was consistently obtained. The frequent extreme finite jump in the shock position caused however considerable inaccuracy in the amplitudes of the shock node, leading ultimately to the merging of nodes in the adaptive grid stage.

On the basis of these observations the present algorithm §4.3 was developed to determine a sufficiently close initial approximation to the position of the shock front so as to eliminate any such potential problems. A consequence of this approach is that the number of nodes, in the diffuser, representing the continuous flow regions either side of the shock front must remain unchanged in the adaptive grid stage. This explains the problems encountered in §4.5 in which, for an initial shock position close to the throat, insufficient nodes are present prior to the shock and subsequent to it there is an abundance (see FIG.23).

The aim must therefore be to ensure, as far as possible, the optimum distribution of nodes in the initial approximation to the shock flow so as to accurately represent the regions of continuous flow wherever the initial position of the shock front.

The modified solution algorithm is presented for the particular

shock flow in §4.4 defined by

$$\eta_{-} = 7.2 \times 10^{4} \ , \tag{4.67}$$

and is applied specifically, not only in the solution of this flow, but also to the more informative case where

$$\eta_{-} = 7.092 \times 10^{4} \ . \tag{4.68}$$

The solution algorithm

The approximation to the fluid speed in the nozzle transition flow defined by (3.1) - (3.11) is first solved now on an adaptive grid (this formulation is presented in [6]), for which the final solution grid is found in TABLE 7, and is shown in FIG.24 denoted 'TF' (from [6]). Twenty one nodes are again employed in the discrete solution and the throat node is fixed throughout at a position (3.9) and amplitude (3.5).

TRANSITION FLOW IN A DE-LAVAL NOZZLE			
FINAL SOLUTION GRID - TWENTY ONE NODES			
NODE NUMBER	NODE POSITION	NODE NUMBER	NODE POSITION
1	0.0000	11	0.8336
2	0.1899	12	0.8814
3	0.3547	13	0.9479
4	0.4944	14	1.0315
5	0.6087	15	1.1306
6	0.6969	16	1.2438
7	0.7588	17	1.3701
8	0.7938	18	1.5087
9	0.8000	19	1.6595
10	0.8057	20	1.8230
		21	2.0000

TABLE SEVEN

The approximation to the subsonic cone section flow defined by (3.1) and (3.31) is obtained fundamentally as stated in §4.3. The flow, as we already know, will only exist in part of the diffuser defined by (4.36); to allow the definition of the initial numerical shock position the cone flow must now be solved on a fixed irregular grid (as formulated in [5]), obtained as in §4.3, and shown in TABLE 8.

SUBSONIC FLOW IN A DIVERGING CONE SECTION			
FIXED IRREGULAR GRID - SEVEN NODES			
NODE NUMBER	NODE POSITION	NODE NUMBER	NODE POSITION
1	1.1306	5	1.6595
2	1.2438	6	1.8230
3	1.3701	7	2.0000
4	1.5087		

TABLE EIGHT

The cone section flow to be solved numerically is now defined on the domain

$$1.1306 \leq x \leq 2.000 \ , \tag{4.69}$$

where $A^{cn}(x)$, A_e^{cn} and A_o^{cn} may be deduced from (4.38) -(4.40) and similarly the mass flow boundary conditions from (4.41) and (4.42). The present approximation to the fluid speed is shown for this flow in FIG.24 and is denoted 'DF'.

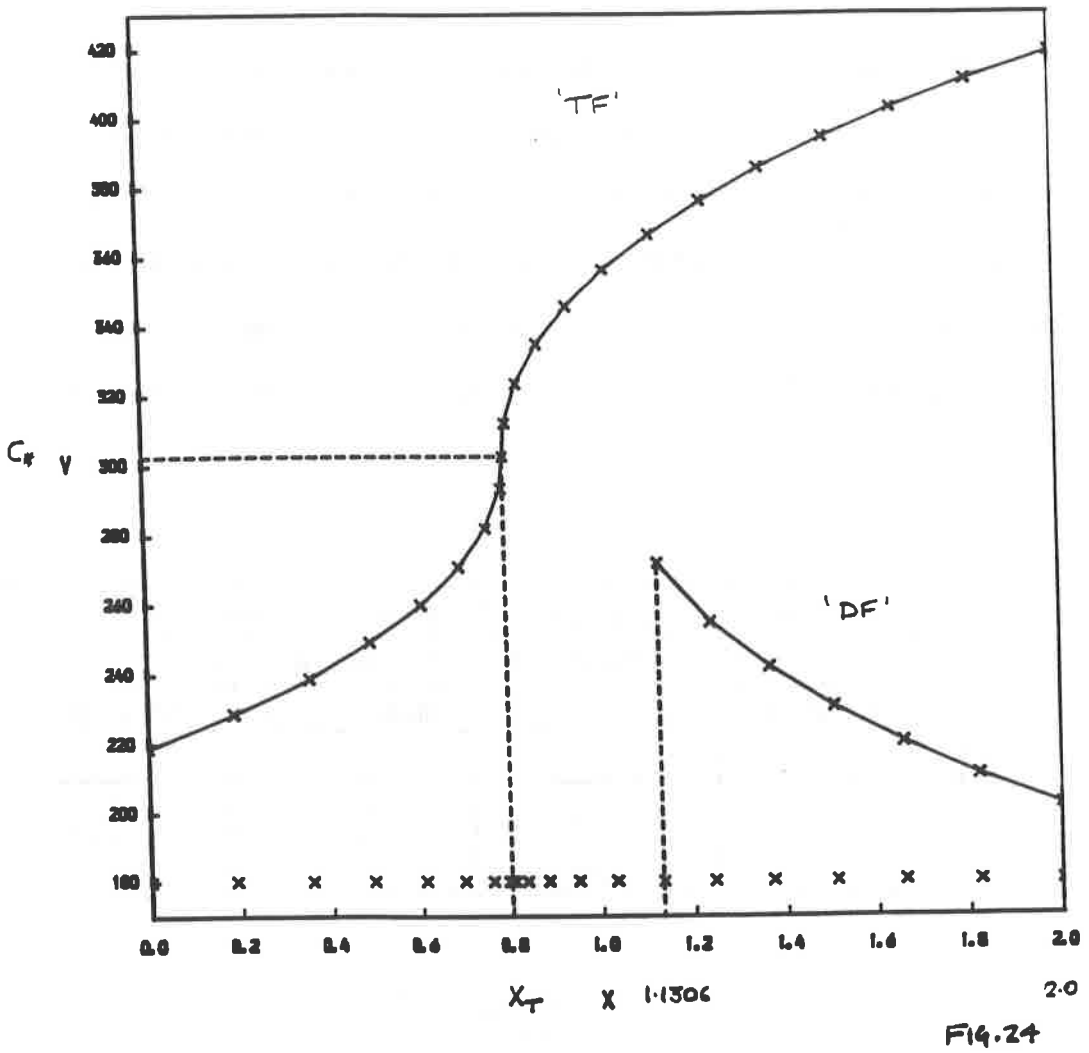

FIG.24

The initial approximation to the shock flow is obtained by the process outlined in §4.3 2. with the initial shock position now being

$$s_M^o = 1.5087 \ , \tag{4.70}$$

out of the possible locations in TABLE 8, and is shown in FIG.25*i*; this is also shown for a shock flow defined by (4.68) in FIG.25*ii*, with here

$$s_M^o = 0.9479 \ . \tag{4.71}$$

In both of these figures, and for that matter the initial approximation to any shock flow in the nozzle, the nodes in the continuous flow prior to the shock front are optimally distributed, wherever the initial shock position, because they originate from the adaptive grid solution of the

transition flow (FIG.24). Due to the qualitative similarity, subsequent to the shock front, in the absolute magnitude of the curvature of the exact parameterization of the transition flow and subsonic cone flow the nodes in this region are not adapted to the optimal distribution: this will occur anyway as a consequence of updating the shock position. Note finally that the initial shock position, although dramatically improved near the nozzle throat, will in fact be poorer on approaching the diffuser outlet; this however is not found to impair the final shock position because of the relative linearity of the fluid speed variation in this region.

The nodes are updated in the adaptive grid stage of the solution in accordance with §4.3 3.. Although obvious additional computational expense has been incurred in obtaining an initial approximation on an adaptive grid it must be noted that, due to the local formulation and the fixed throat node, the nodes prior to the throat have no influence on the subsequent numerical solution in the diffuser. Therefore, these nodes already being optimally distributed, means that they need be updated no further (this is discussed again later).

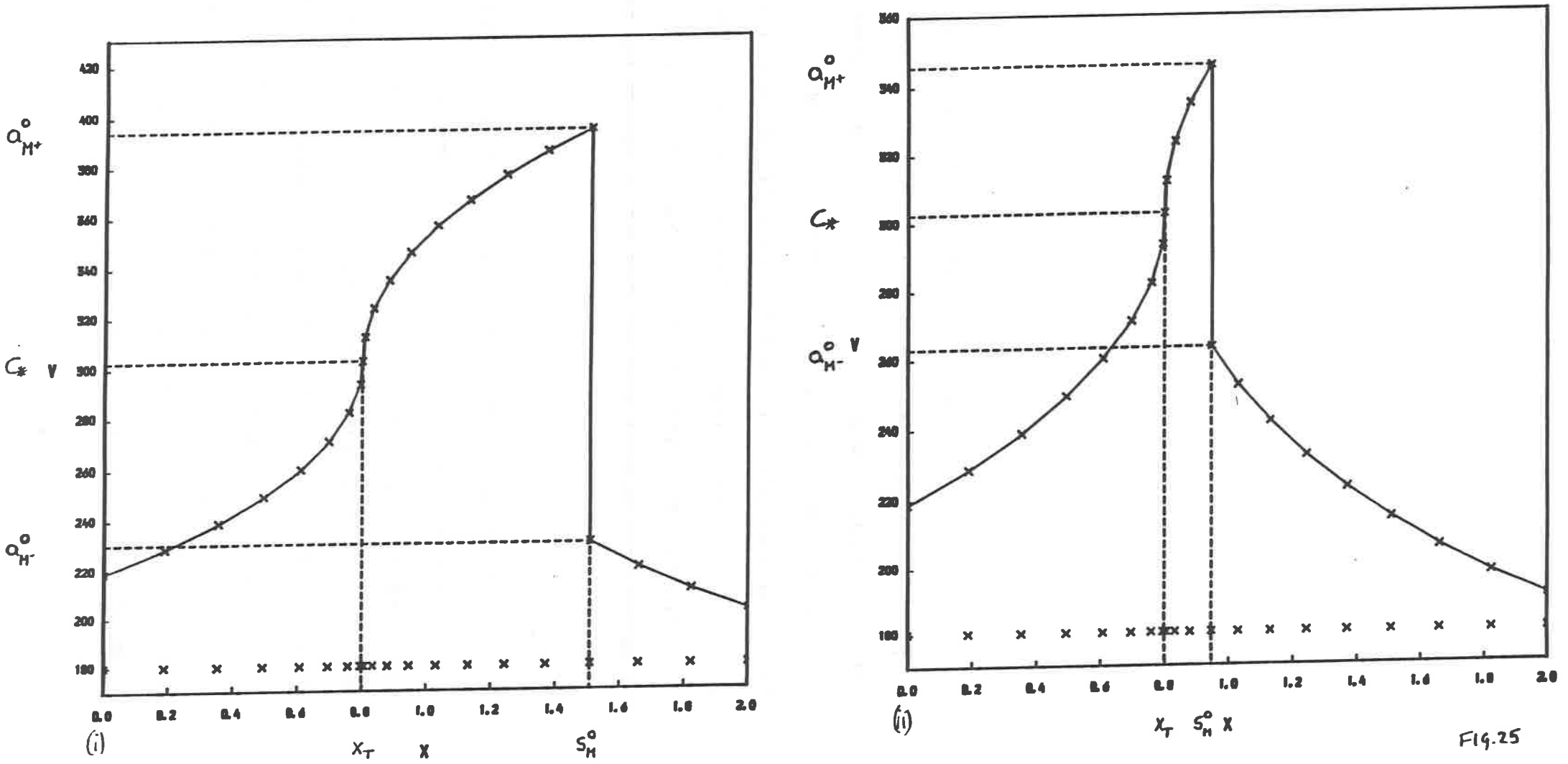
$a^{o}_{H^+}$
C_*
$a^{o}_{H^-}$
420
400
380
360
340
320
300
280
260
240
220
200
180
0.0
0.2
0.4
0.6
0.8
1.0
1.2
1.4
1.6
1.8
2.0
(i)
X_T
X
S^{o}_{H}
$a^{o}_{H^+}$
C_*
$a^{o}_{H^-}$
V
(ii)
X_T
S^{o}_{H}
X

FIG.25

The shock flow solution

The approximation to the fluid speed in the shock flows defined by (3.1) - (3.11) and the outlet entropy values (4.67) or (4.68) are shown in FIGS.26*i*,*ii* respectively along with, in each case, the final solution grid (see also TABLE 9). The numerical shock positions, for each flow, are

$$\eta_{-} = 7.2 \times 10^{4} \quad : \quad s_M^n = 1.4808$$

and (4.71)

$$\eta_{-} = 7.092 \times 10^{4} \quad : \quad s_M^n = 0.9245 \ ,$$

which may both now be said, after rounding to be accurate to three decimal places. The accuracy of (4.71), as explained in §4.5, is a direct consequence of the accurate local representation of the continuous flow in the vacinity of the shock front, in particular in the case of (4.71b) around the nozzle throat (see FIG.26*ii* compared to FIG.23*ii*).

The constraint of the nodes prior to the nozzle throat in the adaptive grid stage is apparent from TABLE.9, in which for both shock flows the final grid is that for the transition solution (TABLE 7) in that region. The superior nodal distribution for each flow when using the present initial approximation technique is highlighted by the increase in nodal numbers of the node representing the shock front, again denoted †, when compared to TABLE 4 and FIG.23*ii* repectively.

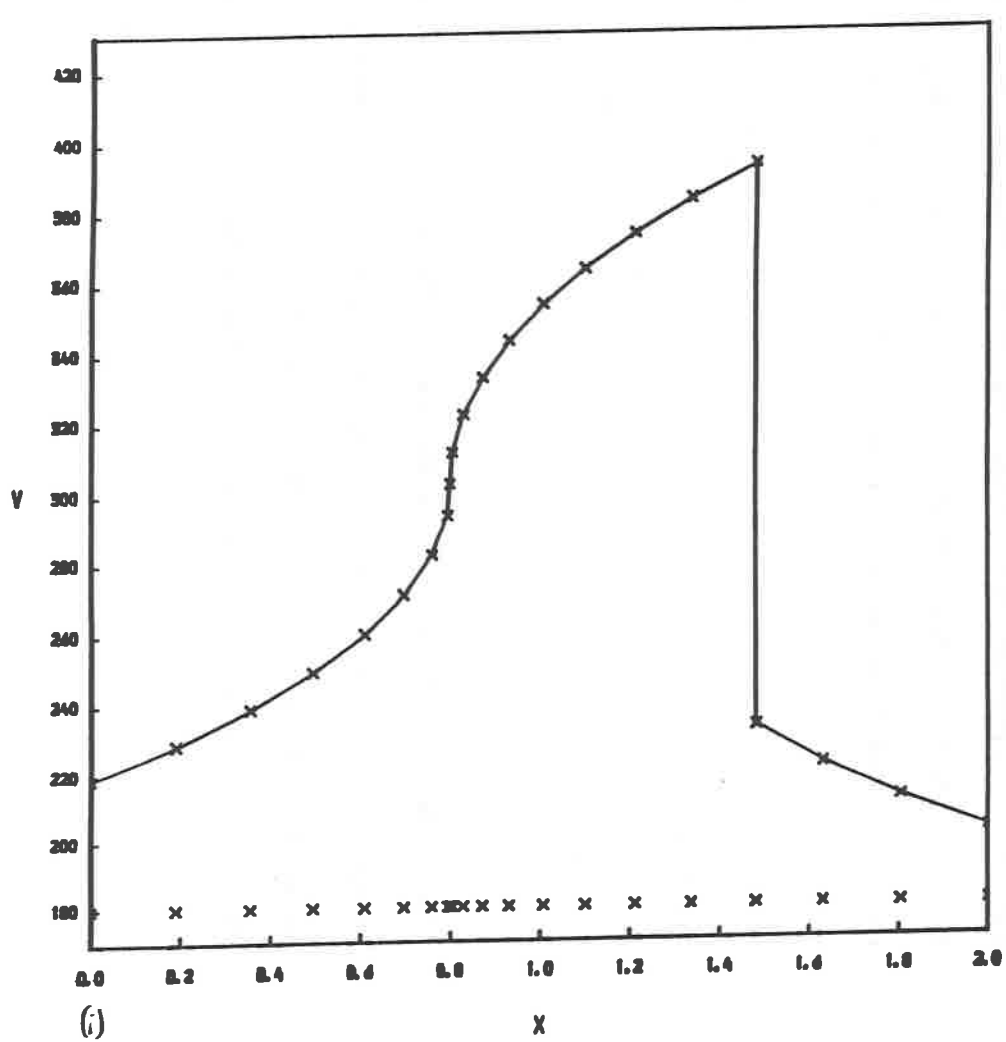
V
X
0.0
0.2
0.4
0.6
0.8
1.0
1.2
1.4
1.6
1.8
2.0
180
200
220
240
260
280
300
320
340
360
380
400
420

(i)

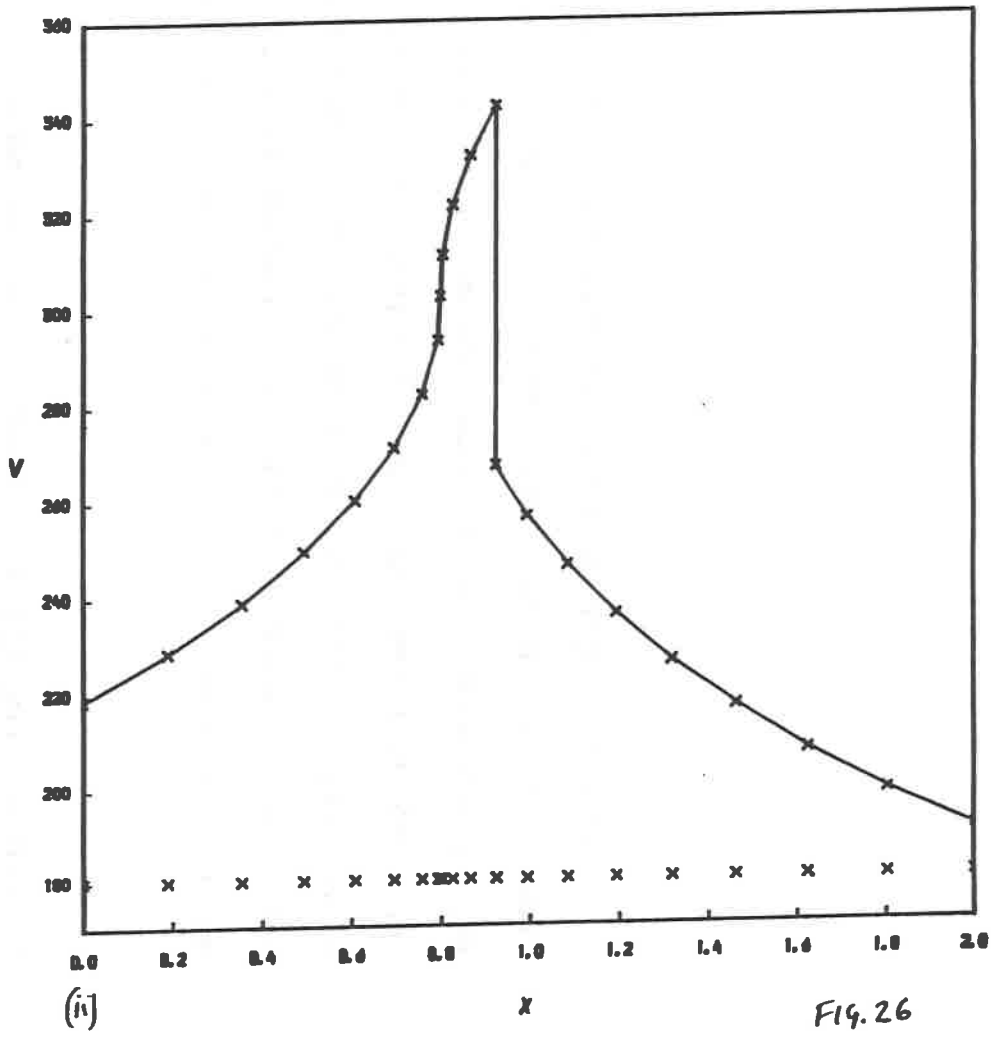
V
X
0.0
0.2
0.4
0.6
0.8
1.0
1.2
1.4
1.6
1.8
2.0
180
200
220
240
260
280
300
320
340
360

(ii)

FIG. 26

SHOCK FLOW IN A DE-LAVAL NOZZLE					
FINAL SOLUTION GRID - TWENTY ONE NODES					
NODE #	η = 7.092	η = 7.2	NODE #	η = 7.092	η = 7.2
1	0.0000	0.0000	12	0.8676	0.8710
2	0.1899	0.1899	13	0.9245 †	0.9304
3	0.3547	0.3547	14	0.9958	1.0070
4	0.4944	0.4944	15	1.0856	1.1004
5	0.6087	0.6087	16	1.1936	1.2106
6	0.6969	0.6969	17	1.3194	1.3374
7	0.7588	0.7588	18	1.4630	1.4808 †
8	0.7938	0.7938	19	1.6242	1.6315
9	0.8000	0.8000	20	1.8031	1.8046
10	0.8047	0.8047	21	2.0000	2.0000
11	0.8276	0.8276			

TABLE NINE

The nodal trajectories in the adaptive grid stage of the solution of the shock flow defined by (4.67) are shown in FIG.27, which may be compared with FIG.21. Noticeable displacement of the shock node again occurs for only a couple of sweeps (FIG.27*i*). As a result of the constraint of the nodes in the entry section, clearly seen, and also the improved nodal distribution in the diffuser, only 62 sweeps are now necessary to sweep to convergence within (4.63). This is significantly less than the 92 required previously; for the flow defined by (4.68) 70 sweeps are needed, which is actually exactly half that for the former method. The initial expense incurred in obtaining an initial approximation through the adaptive grid solution of the transition flow is therefore countered in the present case by the significant decrease in the number of sweeps in the adaptive grid stage. The corresponding features may be also seen with respect to the nodal amplitude variation in FIG.27*ii*, in which the definition of the particular trajectories is the same as for FIG.21*ii*.

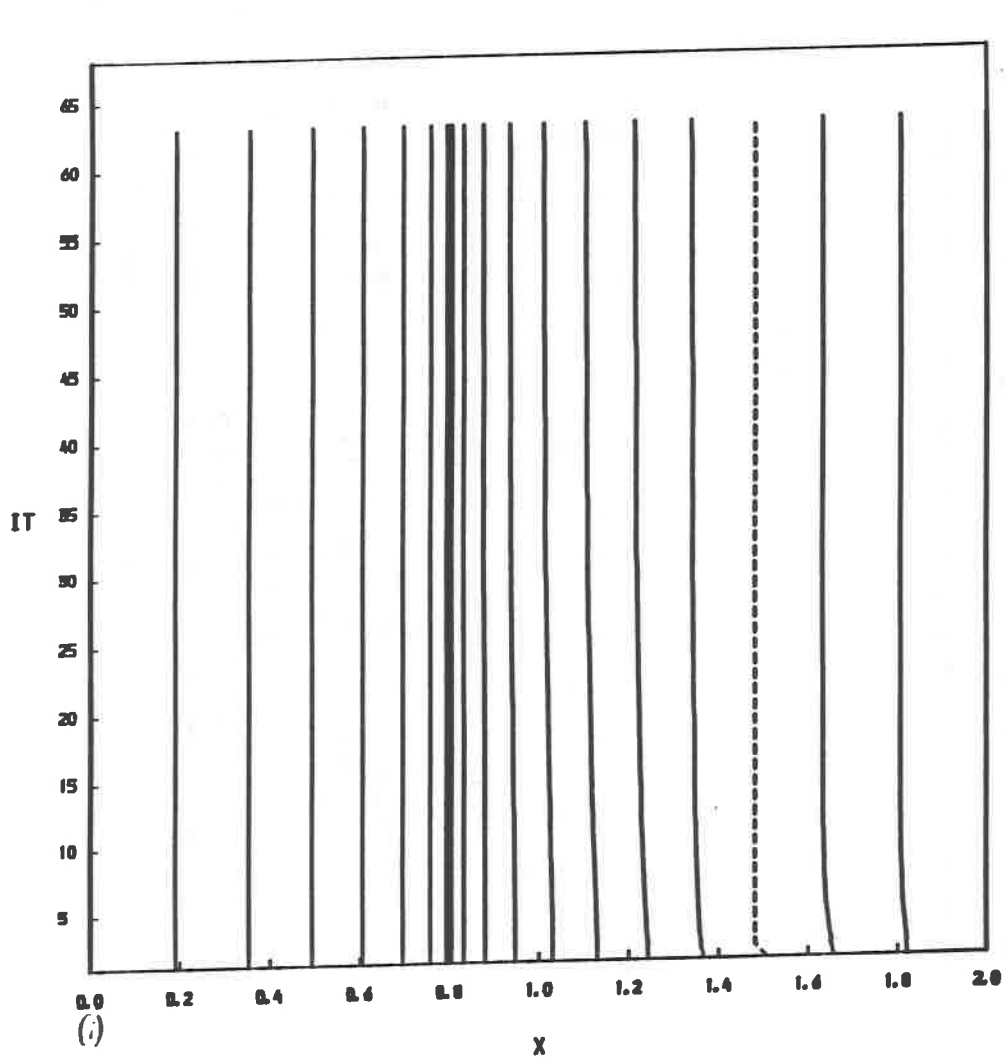
IT
X
0.0
0.2
0.4
0.6
0.8
1.0
1.2
1.4
1.6
1.8
2.0
5
10
15
20
25
30
35
40
45
50
55
60
65

(i)

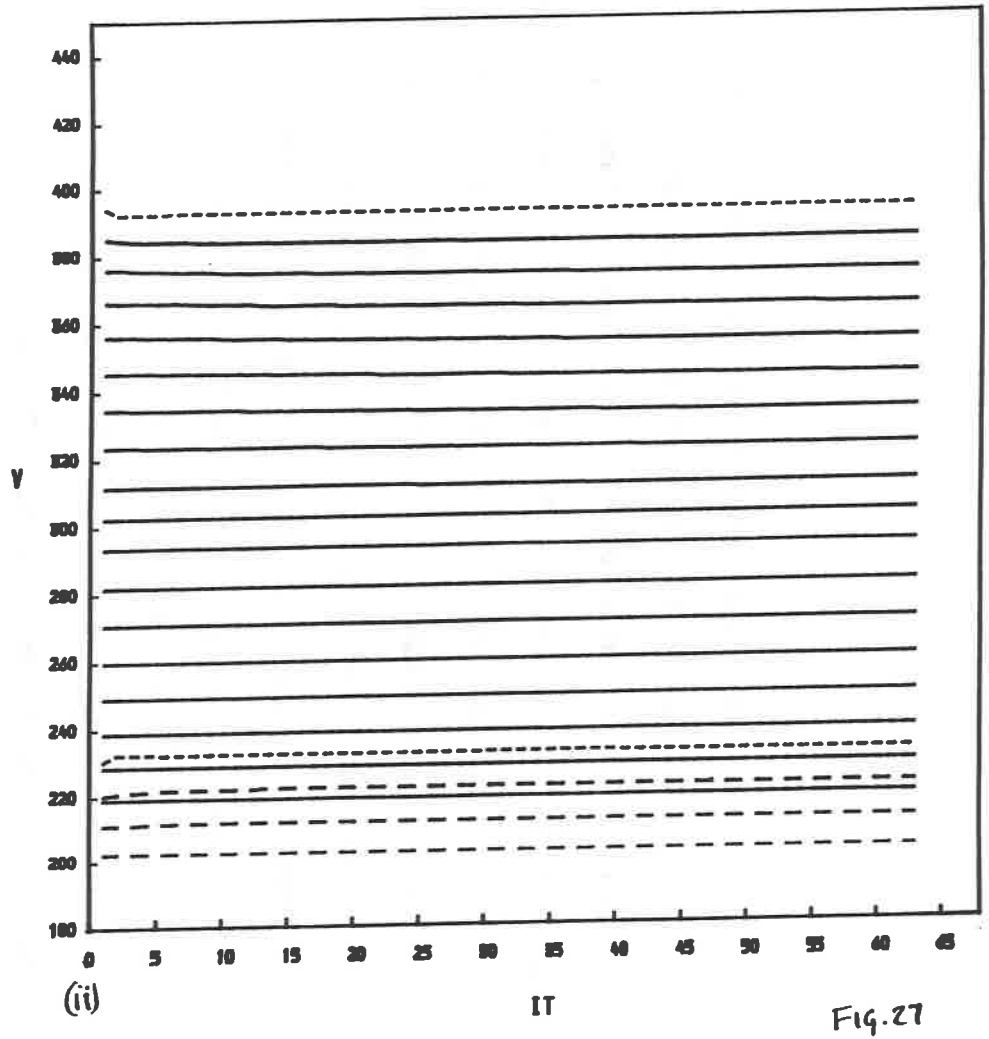
y
IT
180
200
220
240
260
280
300
320
340
360
380
400
420
440
0
5
10
15
20
25
30
35
40
45
50
55
60
65

(ii)

Fig. 27

The magnitude in the jump of the fluid speed, and the other flow variables, may again be computed from the amplitudes of the shock node; these are shown for a flow defined using (4.67) in TABLE 10, and similarly, together with the exact values, for both methods of numerical solution of a flow defined by (4.68) in TABLE 11.

THE SHOCK FRONT		
QUANTITY	JUMP MAGNITUDE	PERCENTAGE ERROR
v	- 159.767	0.159
p	+ 35342.066	0.159
ρ	+ 0.387	0.259
T	+ 49.717	0.149
	MAGNITUDE	
C_{shk}	1.687	0.119
S_{str}	1.114	0.270

TABLE TEN

THE SHOCK FRONT - JUMP MAGNITUDE					
QUANTITY	EXACT	UNIFORM I	ERROR	ADAPTIVE I	ERROR
v	- 7.780	- 81.504	8.992	- 75.144	0.487
p	+ 18044.555	+ 19661.757	8.962	+ 18132.350	0.487
ρ	+ 0198	+ 0.216	9.091	+ 0.199	0.505
T	+ 22.673	+ 24.955	10.065	+ 22.781	0.476
THE SHOCK FRONT - MAGNITUDE					
C_{shk}	1.280	1.314	10.065	1.281	0.078
S_{str}	0.415	0.469	13.012	0.418	0.723

TABLE ELEVEN

The nodal distribution in the present solution algorithm, i.e. relatively few representing the fluid speed variation near outlet, could potentially lead to inaccuracies in the numerical solution of a flow admitting a shock in this region, i.e. a flow defined using (4.67). However it is exactly because of the linearity in this region that the nodes present are able to represent the local curvature accurately and thus the shock position (4.71a) is as accurate as that obtained previously (4.64), where there were excessive nodes. The error in the shock node amplitudes and thus the quantities in TABLE 10 will, as can be seen, therefore, for the same reasons, be of the same order of accuracy as those obtained in TABLE 5. Therefore we may conclude that the numerical solutions of the shock flow defined by (4.67), using both forms of the initial approximation, are of the same degree of accuracy with regard to the shock front, but the representation of the continuous flow is superior in the present case.

The benefits of employing the modified initial approximation, when considering a flow with a shock front intervening near the throat (4.68), are conclusively illustrated, not only by the accuracy of the numerical shock position (4.71b), but also by the dramatic increase in accuracy of all of the quantities associated with the shock front (TABLE 11). In particular the numerical shock strength may be seen to be in excess of ten times more accurate than when using the previous approach.

The approximation to the fluid speed in a shock flow may now be used directly in the complete set of algebraic relationships [1] to provide the discrete axial variation of the other flow variables (see FIG.28 for (4.67)), for which an exact parameterization is given in FIG.11, and further as a set of intermediate numerical parameters to

determine the discrete form of the inter-variable graphs (FIG.12) in the shock flow.

The numerical method

The overall accuracy of the numerical method when employing the present initial approximation to a shock flow is now investigated, as previously, by considering the numerical solution of a variety of shock flows and constructing TABLE 12.

ENTROPY $\times 10^4$	s_M^n	$s_M^n(E)$	s_{str}^n	$s_{str}^n(E)$
7.080	0.80053	0.125	0.038	-
7.082	0.83563	-	0.216	2.370
7.084	0.85756	-	0.276	1.099
7.086	0.87639	-	0.321	1.582
7.088	0.89349	-	0.358	1.705
7.090(*)	0.90946	-	0.393	2.078
7.092	0.92454	-	0.418	0.723
7.094	0.93898	-	0.444	0.909
7.096	0.95288	-	0.468	0.645
7.098	0.96634	-	0.491	1.029
7.100	0.97943	-	0.512	0.977
7.120	1.09712	-	0.681	0.442
7.140	1.20148	-	0.812	0.371
7.160	1.29872	-	0.924	0.326
7.180	1.39139	-	1.023	0.294
7.200	1.48084	-	1.114	0.270
7.220	1.56789	-	1.199	0.251
7.240	1.65309	-	1.279	0.235
7.260	1.73681	-	1.355	0.148
7.280	1.81936	-	1.428	0.211
7.300	1.90093	-	1.498	0.134
7.320	1.98170	-	1.566	0.128
7.3245	1.99978	-	1.581	0.127

TABLE TWELVE

The quantities in TABLE 12 are defined exactly as in TABLE 5. It may now be seen that, except for the extreme case of a theoretical zero shock at the nozzle throat, all of the numerical shock positions are accurately located to three decimal places. There is though, as expected, an overall decrease in accuracy of the computed shock strength as the shock position lies progressively towards the nozzle throat. The only uncharacteristically large error in the shock strength occurs for a prescribed outlet entropy value of

$$\eta_{-} = 7.09 \times 10^{4} \ . \tag{4.72}$$

Although the shock position is accurately located the amplitude of the shock node at the back of the shock front is in error because, due to linearities in the numerical solution of the subsonic flow, four nodes have been deleted form the solution domain (see [6]); thus the representation of the fluid speed variation in this region is relatively inaccurate. This may be remedied by choosing the initial shock position in the opposite sense to that in §4.3 2. (d), the numerical solution then producing

$$\begin{aligned} & s_M^n = 0.90943 \ , \\ & S_{str} = 0.389 \\ \text{and} \quad & S_{str}(E) = 1.039 \ . \end{aligned} \tag{4.73}$$

The numerical shock position is again as accurate as in TABLE 12, but now no nodes need be deleted and consequently the error in the shock strength is more in keeping with the general trend

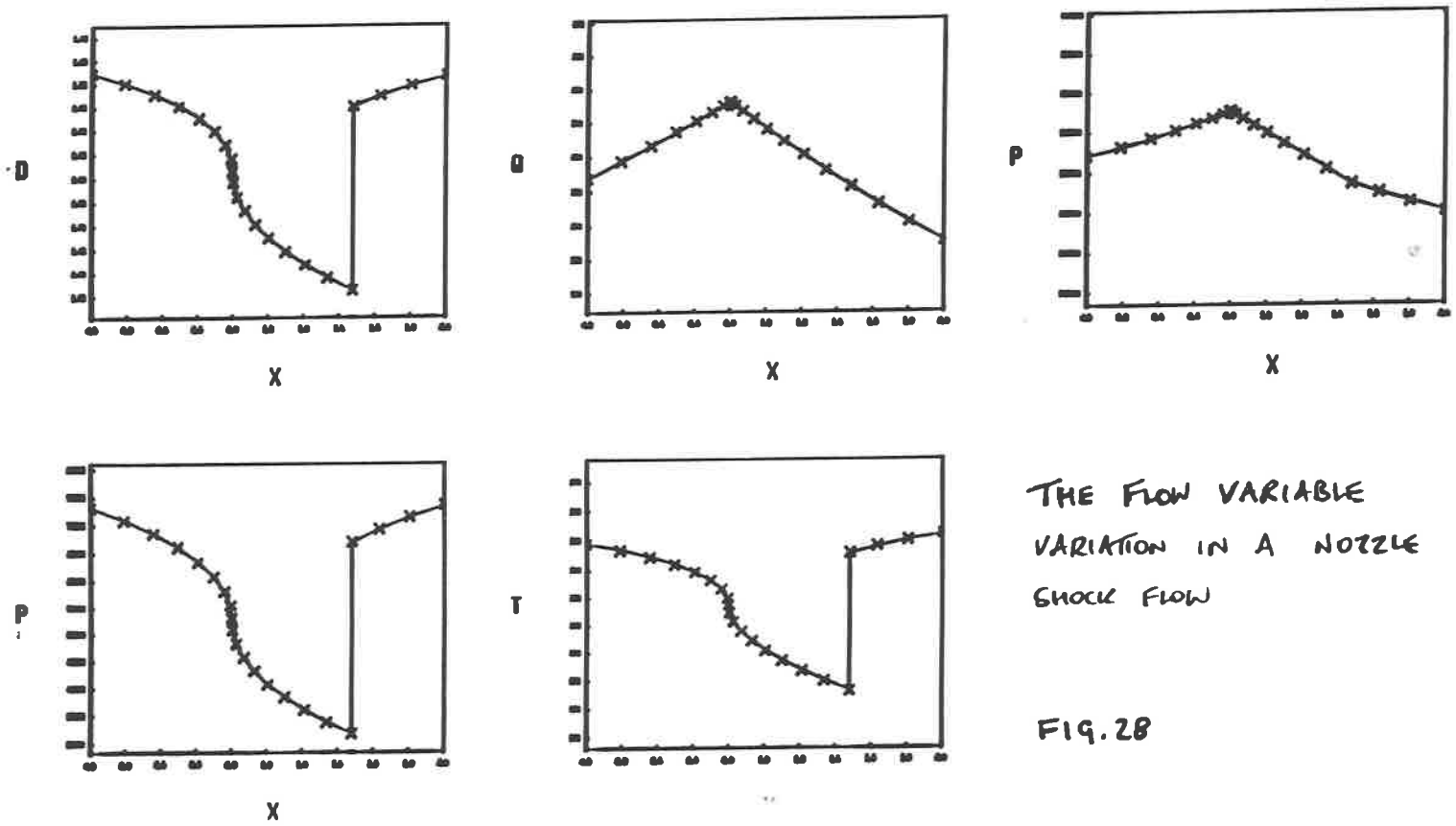

THE FLOW VARIABLE VARIATION IN A NOZZLE SHOCK FLOW

FIG. 28

CONCLUSION

A quasi one-dimensional approximation to shock flow in a nozzle has been defined. An algebraic parameterization of the flow variables with respect to the distance along the nozzle axis is then obtained. A stationary principle equivalent to the conditions defining a shock flow is constructed and is used to determine an approximate finite element solution for the fluid speed on an adaptive grid. The de-coupling of the equations allows the local update of both the nodes representing the regions of continuous flow and in particular the shock front. The numerical solution is found to be extremely accurate, when compared to the exact solution, in representing not only the fluid speed variation but also the magnitude of physical quantities associated with the shock front.

REFERENCES

[1] SEWELL. M.J. : "Properties Of A Streamline In Gas Flow", PHYS. TECHNOL. 16, (1985).

[2] COURANT, R. & FRIEDRICHS, K.O. : "Supersonic Flow And Shock Waves", INTER-SCIENCE, NEW YORK (1948).

[3] PORTER, D. & SEWELL, M.J. : Constitutive Surfaces In Fluid Dynamics", DEPT. OF MATHS., UNIV. OF READING (1979).

[4] WIXCEY, J.R. : "Compressible flow in ducts - analytic aspects", NUMER. ANAL. REPORT 12/88, DEPT. OF MATHS., UNIV. OF READING (1988).

[5] WIXCEY, J.R. : "Compressible flow in ducts - variational aspects", NUMER. ANAL. REPORT 13/88, DEPT. OF MATHS., UNIV. OF READING (1988).

[6] WIXCEY, J.R. : "Compressible flow in ducts - an adaptive grid method", NUMER. ANAL. REPORT 14/88, DEPT. OF MATHS., UNIV. OF READING (1988).

[7] BARLEY, J.J. : Private communication.

[8] HEATH, D.E. : "An Implicit Regridding Algorithm with an Underlying Fixed Grid, for Front, Shock or Boundary Tracking", NUMER. ANAL. REPORT 16/87, DEPT. OF MATHS., UNIV. OF READING (1987).